

*Synthesis and investigation of boron phases  
at high pressures and temperatures*

DISSERTATION

zur Erlangung des akademischen Grades eines  
Doktors der Naturwissenschaften (Dr. rer. nat.)  
an der Bayreuther Graduiertenschule für Mathematik und  
Naturwissenschaften (BayNAT) der Universität Bayreuth

vorgelegt von

***Gleb Parakhonskiy***

aus *Twer*

Bayreuth, 2012

# TABLE OF CONTENTS

SUMMARY .....	4
ZUSAMMENFASSUNG.....	6
1 INTRODUCTION.....	9
1.1 Motivation and background .....	9
1.2 Elemental boron modifications .....	11
1.2.1 $\alpha$ -boron .....	11
1.2.2 $\beta$ -boron .....	12
1.2.3 The controversy on the ground state of boron and a relative stability of the two modifications ( $\alpha$ -B and $\beta$ -B) at ambient conditions .....	14
1.2.4 $\gamma$ -boron .....	15
1.2.5 Tetragonal boron, T-50 and T-192 phases .....	16
1.2.6 The phase PT diagram of boron .....	18
1.3 Experimental techniques .....	20
1.3.1 High pressure techniques .....	20
1.3.1.1 Multi-anvil apparatus .....	20
1.3.1.2 Piston cylinder apparatus .....	22
1.3.1.3 Diamond anvil cell .....	22
1.3.2 Analytical techniques .....	24
1.3.2.1 Raman spectroscopy.....	24
1.3.2.2 X-ray diffraction.....	25
1.3.3 Electron microscopy techniques.....	26
1.3.3.1 Scanning electron microscopy and electron microprobe analysis.....	26
1.3.3.2 Transmission electron microscopy.....	27
2 SYNOPSIS (scope of the articles) .....	29
2.1 Synthesis of single crystals of $\alpha$ -boron .....	29
2.2 Investigation of single crystals of $\alpha$ -boron.....	30
2.3 Synthesis of single crystals of $\beta$ - and $\gamma$ -boron.....	34
2.4 The phase PT diagram construction and the ground state determination .....	37
2.5 Synthesis of metastable boron phases: $\delta$ - and $\epsilon$ -boron.....	40
2.5.1 Tetragonal metastable boron phase ( $\delta$ -boron).....	40
2.5.2 Newly synthesized rhombohedral metastable boron phase ( $\epsilon$ -boron).....	42
3 LIST OF MANUSCRIPTS AND STATEMENT OF AUTHORS CONTRIBUTION .....	47
4 MANUSCRIPTS .....	49
4.1 High pressure synthesis of single crystals of $\alpha$ -boron .....	49
4.1.1 Abstract .....	49
4.1.2 Introduction .....	49
4.1.3 Experimental .....	50
4.1.3.1 Sample preparation.....	50
4.1.3.2 Synthesis technique .....	51
4.1.3.3 Analytical techniques .....	52
4.1.4 Results and discussion.....	53
4.1.5 Conclusion.....	58
4.2 Raman spectroscopy investigation of $\alpha$ -boron at elevated pressures and temperatures .....	61
4.2.1 Abstract .....	61
4.2.2 Introduction .....	61
4.2.3 Experimental .....	62
4.2.4 Results and discussion.....	64
4.2.5 Conclusions .....	69

4.3	Experimental pressure-temperature phase diagram of boron: resolving the long-standing enigma.....	72
4.3.1	Abstract .....	72
4.3.2	Introduction .....	72
4.3.3	Results .....	75
4.3.3.1	Boron phases .....	75
4.3.3.2	Boron phase diagram.....	81
4.3.4	Discussion .....	83
4.4	High pressure synthesis and investigation of single crystals of metastable boron phases.....	92
4.4.1	Abstract .....	92
4.4.2	Introduction .....	92
4.4.3	Experimental details .....	93
4.4.4	Results and discussion.....	96
4.4.5	Conclusion.....	104
	FULL LIST OF PUBLICATIONS (WITH PAPERS NOT INCLUDED INTO THE THESIS) .....	107
5	BIBLIOGRAPHY .....	109
6	ACKNOWLEDGMENTS.....	116

## SUMMARY

Boron, discovered as an element in 1808 and produced in pure form in 1909, still remains one of the most complicated light elements full of surprises. Even the number of pure boron polymorphs is a subject of intensive discussions. It is proven the existence of  $\alpha$ -,  $\beta$ - and  $\gamma$ -boron phases. Structural details of the most common boron phase ( $\beta$ -B) are still not fully revealed. For decades boron remained the last stable element in the periodic table, whose ground state was not determined. It has been a subject of a longstanding controversy, whether  $\alpha$ -B or  $\beta$ -B is the thermodynamically stable phase at ambient pressure and temperature.

The existence of the  $\alpha$ -tetragonal boron phase T-50 has been an open question since its first discovery. It was not clear if T-50 could be synthesized as a pure boron phase or its structure must be stabilized by the presence of carbon or nitrogen. Theorists claimed that T-50 could not exist at all because of its unstable electronic configuration.

The tasks of the present work were (a) to develop a methodology of a reproducible synthesis of known boron phases (first of all  $\alpha$ -boron), (b) to investigate if there are any still unknown boron phase(s) stable or metastable at pressures up to 20 GPa and temperatures up to 2200 K, (c) to study high-pressure and high-temperature behaviour of boron phases, and (d) to establish the experimental *PT* phase diagram of boron.

We have developed a method of synthesis of single crystals of  $\alpha$ -boron. They were crystallized from a boron-platinum melt at high pressures (6-11 GPa) and high temperatures (1450-1875 K). An average size of the as-grown isometric crystals was 60  $\mu\text{m}$  to 80  $\mu\text{m}$  in maximum dimension. An accurate refinement of the crystal structure of  $\alpha$ -B using single-crystal X-ray diffraction data was possible due to the excellent quality of the single crystals. The crystal structure is in good agreement with the literature data. Detailed investigation of single crystals of  $\alpha$ -boron using Raman spectroscopy was performed under elevated pressures and temperatures. The behaviour of the Raman modes under pressure was studied both theoretically and experimentally. We confirmed  $\alpha$ -boron to be stable at least up to 36 GPa and 600 K and derived its mode Grüneisen parameters. We established the pressure-temperature dependence of the  $A_{1g}$  mode of  $\alpha$ -B.

Single crystals of  $\beta$ -boron were grown at temperatures above 1550 K and pressures up to 11 GPa using the similar methodology like that worked out for synthesis of  $\alpha$ -boron. An average size of  $\beta$ -boron crystals was 60  $\mu\text{m}$ . Their quality was sufficient for the structure refinement based on single crystal X-ray diffraction data. Their size allowed measurements of the microhardness.

In a series of experiments above 8 GPa we synthesized single crystals of tetragonal  $\delta$ -boron (also known in literature as  $\alpha$ -tetragonal boron or T-50) and refined the crystal structure of this phase based on synchrotron X-ray diffraction data. The purity of  $\delta$ -boron was confirmed by means of the microprobe analysis and the electron energy loss spectroscopy (EELS).

A new, so far unknown boron phase,  $\varepsilon$ -boron, was synthesized at pressures of 8-10 GPa and temperatures between 2000-2250 K. The microprobe analysis and EELS revealed that the samples were not contaminated. The crystal structure of the new phase was determined by means of single crystal X-ray diffraction.  $\varepsilon$ -boron crystallizes in a  $R\bar{3}m$  space group with the unit cell parameters  $a = 5.5940(7)$  Å and  $c = 12.0756(16)$  Å (in hexagonal setting). The unit cell contains 15 boron atoms. The structure can be presented by the network of  $B_{12}$  icosahedra with a group of three boron atoms in the inter-icosahedra space. This phase is isostructural to boron carbide  $B_{13}C_2$  (if carbon atoms are substituted by boron ones). The X-ray density of  $\varepsilon$ -boron is  $2.41$  g/cm<sup>3</sup>. Measured hardness is  $\sim 60$  GPa which places  $\varepsilon$ -boron in the family of superhard materials.

We have demonstrated that  $\delta$ -boron and  $\varepsilon$ -boron are metastable polymorphs because (a) they were found only together with other stable boron phases ( $\alpha$ -,  $\beta$ -, or  $\gamma$ -B), and (b) upon heating at high pressure, both  $\delta$ -B and  $\varepsilon$ -B transform to  $\beta$ - or  $\gamma$ -B, if the PT conditions correspond to the fields of stability of the latter.

Summarising, in the course of the present work the high-pressure high-temperature synthesis of the five boron polymorphs was established as a reproducible, verifiable and well-documented process. Following the synthesis prescription one can grow single crystals of  $\alpha$ -B,  $\beta$ -B,  $\gamma$ -B,  $\delta$ -B, and  $\varepsilon$ -B phases. Based on results of numerous HPHT experiments, the phase boundaries between the stable boron phases ( $\alpha$ -B,  $\beta$ -B,  $\gamma$ -B) were found. Thus, our serial exploration of the pressure-temperature field using the large volume press synthesis technique resulted in establishing the phase diagram of boron (showing also the PT fields of the appearance of its two metastable phases,  $\delta$ -B and  $\varepsilon$ -B) in the pressure interval of 3 GPa to 18 GPa at temperatures between 1073 K and 2423 K. Based on our experimental data and linear extrapolation of the  $\alpha/\beta$  phase boundary down to ambient pressure we could resolve a longstanding controversy on the ground state of boron in favour of the  $\alpha$ -B phase.

# ZUSAMMENFASSUNG

Das im Jahre 1808 entdeckte und seit 1909 in reiner Form produzierte Element Bor gilt weiterhin als eines der komplexesten der leichten Elemente und bietet auch heute noch Erstaunliches. Allein schon darüber, wie viele reine Bor-Polymorphe existieren, wird eine intensive Diskussion geführt. Bisher ließen sich  $\alpha$ -,  $\beta$ - und  $\gamma$ -Bor-Phasen nachweisen. Strukturelle Details über die am häufigsten auftretende  $\beta$ -Bor-Phase sind jedoch immer noch nicht vollständig geklärt. Über Jahrzehnte war Bor das letzte der stabilen Elemente des Periodensystems, dessen Grundzustand noch unbestimmt war. Über lange Zeit wurde kontrovers diskutiert, ob  $\alpha$ -B oder  $\beta$ -B die thermodynamisch stabile Phase bei normalen Umgebungsbedingungen (Druck und Temperatur) ist.

Die Existenz von  $\alpha$ -tetragonalem Bor T-50 ist immer noch zweifelhaft geblieben. Es konnte nicht dargelegt werden, ob T-50 als reine Bor-Phase synthetisiert werden kann oder ob seine Struktur durch die Zugabe von Kohlenstoff oder Stickstoff stabilisiert werden muss. Theoretiker führen an, dass T-50 aufgrund seiner instabilen Elektronenkonfiguration nicht existent sein kann.

Die Aufgabenstellung der hier präsentierten Arbeit umfasste, (a) eine Methodik für reproduzierbare Synthesen der bekannten Bor-Phasen (insbesondere  $\alpha$ -Bor) zu entwickeln, (b) zu untersuchen, ob weitere bisher unbekannte Bor-Phasen existieren, die bei Drücken bis 20 GPa und Temperaturen bis 2200 K stabil bzw. metastabil sind, (c) das Hochdruck-/Hochtemperaturverhalten von Bor-Phasen zu erforschen und (d) ein  $PT$ -Phasendiagramm für Bor auf experimenteller Basis zu erstellen.

Es wurde im Verlauf dieser Arbeit eine Synthesemethode für  $\alpha$ -Bor-Einkristalle entwickelt. Die Einkristalle wurden bei hohen Drücken (6-11 GPa) and hohen Temperaturen (1450-1875 K) aus einer Bor-Platin-Schmelze auskristallisiert. Die durchschnittliche Größe der Kristalle (wie gewachsen) lag zwischen 60 und 80  $\mu\text{m}$  in ihrer größten Ausdehnung. Eine präzise Verfeinerung der  $\alpha$ -Bor-Kristallstruktur mit Hilfe von Röntgenbeugungsanalysen war aufgrund der hervorragenden Qualität der Einkristalle möglich. Die Kristallstruktur stimmt gut mit Literaturdaten überein. Einkristalle von  $\alpha$ -Bor wurden mit Hilfe der Raman-Spektroskopie bei erhöhten Drücken und Temperaturen genauer untersucht. Das Verhalten von Raman-Moden unter Druck wurde sowohl mit theoretischen als auch experimentellen Ansätzen erforscht. Die hier präsentierte Arbeit bestätigt die Stabilität von  $\alpha$ -Bor bis mindestens 36 GPa und 600 K und leitet daraus den Grüneisen-Parameter ab. Sie stellt die Druck-Temperatur-Beziehung der  $A_{1g}$ -Mode von  $\alpha$ -B vor.

Einkristalle von  $\beta$ -Bor wurden bei Temperaturen oberhalb von 1550 K und bei Drücken bis 11 GPa mit der gleichen Methodik wie bei der Synthese von  $\alpha$ -Bor gezüchtet. Die  $\beta$ -Bor-Kristalle waren durchschnittlich 60  $\mu\text{m}$  groß, ihre Qualität erwies sich für Feinbestimmungen auf der Basis von Einkristall-Beugungsdaten als ausreichend. Die Kristallgröße erlaubte Bestimmungen der Mikrohärtigkeit.

In einer Reihe von Experimenten oberhalb von 8 GPa wurden Einkristalle tetragonales  $\delta$ -Bors (in der Literatur auch als  $\alpha$ -tetragonales Bor oder T-50 beschrieben) synthetisiert. Die Kristallstruktur dieser Phase wurde mit Beugungsdaten aus Synchrotron-Anwendungen verfeinert. Den Reinheitsgrad des  $\delta$ -Bors belegen Mikrosondenmessungen und Ergebnisse der Elektronen-Energieverlust-Spektroskopie (EELS).

Eine neue, bisher unbekannte Bor-Phase ( $\epsilon$ -Bor), wurde bei Drücken zwischen 8-10 GPa und Temperaturen zwischen 2000-2250 K erzeugt. Mikrosondenanalysen und EELS ergaben, dass die Proben nicht kontaminiert waren. Die Kristallstruktur der neuen Phase wurde mit Röntgenbeugungsanalysen an Einkristallen bestimmt. Die  $\epsilon$ -Bor-Phase kristallisiert in der Raumgruppe  $R\bar{3}m$  mit folgenden Parametern für die Einheitszelle:  $a = 5.5940(7)$  Å und  $c = 12.0756(16)$  Å (in hexagonaler Anordnung). Die Einheitszelle weist 15 Bor-Atome auf. Die Struktur kann durch ein ikosaedrisches (zwanzigflächiges) Netzwerk aus 12 Bor-Atomen ( $B_{12}$ ) mit einer Gruppe aus 3 Bor-Atomen im inter-ikosaedrischen Raum dargestellt werden. Die Phasenstruktur ist isometrisch zu Borkarbid  $B_{13}C_2$  (wenn Kohlenstoff-Atome durch Bor-Atome substituiert werden). Die mittels Röntgenbeugungsmethoden bestimmte Dichte von  $\epsilon$ -Bor beträgt  $2.41 \text{ g/cm}^3$ , die gemessene Härte liegt bei  $\sim 60$  GPa, wodurch  $\epsilon$ -Bor der Gruppe der superharten Materie zuzuordnen ist.

Es konnte gezeigt werden, dass  $\delta$ -Bor und  $\epsilon$ -Bor metastabile Polymorphe sind, da sie (a) stets nur zusammen mit anderen stabilen Bor-Phasen ( $\alpha$ -,  $\beta$ -, oder  $\gamma$ -B) vorkommen und (b) sowohl  $\delta$ -B als auch  $\epsilon$ -B beim Aufheizen unter hohem Druck sich zu  $\beta$ - oder  $\gamma$ -B umwandeln, wenn die PT-Bedingungen den Stabilitätsfeldern dieser Bor-Phasen entsprechen.

Zusammenfassend lässt sich festhalten, dass mit der hier präsentierten Studie die Hochdruck-/Hochtemperatur-Synthese von fünf Bor-Polymorphen als reproduzierbarer, verifizierbarer und gut dokumentierbarer Prozess eindeutig belegt ist. Mit den vorgelegten Syntheseanleitungen können Einkristalle von  $\alpha$ -B,  $\beta$ -B,  $\gamma$ -B,  $\delta$ -B und  $\epsilon$ -B gezüchtet werden. Aufgrund der Ergebnisse aus zahlreichen HP/HT-Experimenten wurden die Phasengrenzen zwischen den stabilen Bor-Phasen  $\alpha$ -B,  $\beta$ -B und  $\gamma$ -B festgelegt. Die Reihenuntersuchungen im Druck/Temperatur-Feld durch Materialsynthesen mit Hilfe von großvolumigen Hochdruck-Pressen führten zur Festlegung des Phasendiagramms von Bor im Druckintervall zwischen 3

und 18 GPa bei Temperaturen zwischen 1073 und 2423 K. Auch die PT-Felder der zwei metastabilen Phasen  $\delta$ -B und  $\varepsilon$ -B können in diesem Phasendiagramm dargestellt werden. Aufgrund der in dieser Studie gewonnenen experimentellen Daten und der linearen Extrapolation der  $\alpha/\beta$ -Phasengrenze bis hinunter in Bereiche des Umgebungsdrucks kann eine schon lang anhaltende Kontroverse über den Grundzustand von Bor zugunsten der  $\alpha$ -B-Phase beendet werden.

# 1 INTRODUCTION

## 1.1 Motivation and background

Boron does not exist in nature as a pure elemental phase because of its extreme chemical activity but, being utilised in compounds it plays an important role in human activities since antiquity (Garett 1998). Boron compounds are widely used as engineering materials (dielectrics, B-doped semiconductors), superhard materials (cBN, boron carbide), reinforcing chemical additives, for example, for obtaining special glass or corrosion- or heat-resistant alloys (Perkins 2011), and superconducting materials (ex.,  $\text{MgB}_2$ ) (Braccini *et al.* 2007). Surprisingly, despite centuries of application and decades of intensive studies of boron compounds, elemental boron still remains in focus of wide scientific interest due to its enigmatic properties and largely unknown phase diagram (Albert & Hillebrecht 2009; Zarechnaya *et al.* 2009; Masago & Shirai 2006; van Setten *et al.* 2007), pressure induced metallization and superconductivity (Eremets *et al.* 2001), formation of unusual chemical bonds (Mondal *et al.* 2011), and potential technological applications, exceptional chemical stability combined with very high hardness and interesting semiconducting and optical properties (Zarechnaya *et al.* 2009; Zhou *et al.* 2010).

Boron is the fifth element in the periodic table with only three valence electrons. In spite of its apparent simplicity, boron has complex chemistry and remains likely one of the stable element so far, whose enigmas are not completely uncovered after 200 years since its discovery. For example, until very recently the electron density distribution based on experimental data was unknown for all boron modifications. So that the chemical bonding is still not entirely clarified for boron polymorphs.

A great contribution in comprehension of boron chemistry was made by William Lipscomb (Lipscomb 1981a; Lipscomb 1981b). He studied chemical bonding and structure of boranes  $\text{B}_x\text{H}_{x+4}/\text{B}_x\text{H}_{x+6}/\text{B}_x\text{H}_{x+8}$  trying to explain why so many of them exist (Lipscomb 1966). As a result he introduced for example, two-electron three-center (2e3c) bonding concept (figure 1.1.1) (Lipscomb 1973). For his “studies on the structure of boranes illuminating problems of chemical bonding”, William Lipscomb was awarded Nobel Prize in chemistry in 1976.

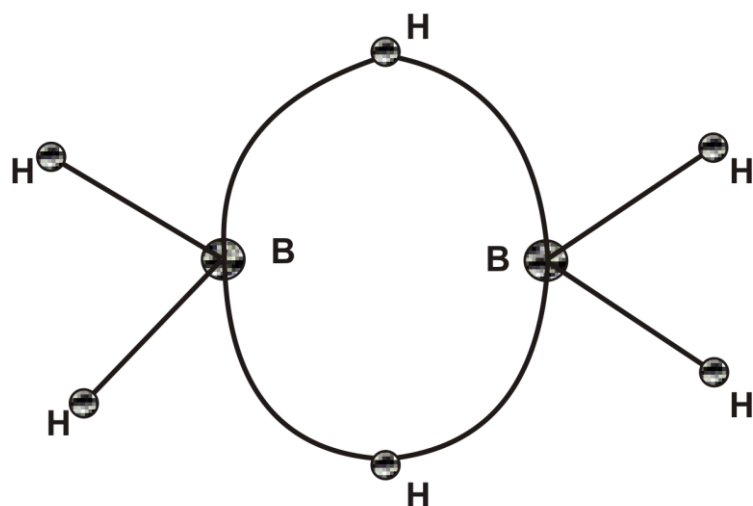


**Figure 1.1.1** A pair of 2e3c bonds in the  $B_2H_6$  molecule.

But scientists challenged boron as well. Although both carbon and nitrogen can form compounds with stable homoatomic triple bonds, they have not been known for boron until recently. It was predicted that structures with triple B-B bonds are possible (Mitoraj & Michalak 2011; Holzmann *et al.* 2011) and Braunschweig *et al.* challenged such a synthesis starting with a precursor that already had one boron-boron bond in place (Braunschweig *et al.* 2012). They succeeded to synthesize compounds with double B-B and triple B-B bonds. The chromophore properties and robustness of these compounds, according to Braunschweig *et al.* (2012), offer exciting possibilities for the further study of the reactivity and optical properties of B-B double and triple bonds, in line with the recent interest in boron-based functional materials (Braunschweig *et al.* 2012).

Due to establishing the method of synthesis of high quality single crystals of  $\gamma$ -boron (Zarechnaya *et al.* 2009), synchrotron X-ray diffraction data was acquired. Quality of the data made possible to perform the first topological analysis of the experimentally obtained electron density for the high pressure (HP)  $\gamma$ -boron polymorph and to reveal 1e2c and 2e3c bonds in this phase (Mondal *et al.* 2011).

There are two polymorphs of pure crystalline boron synthesized at ambient pressure:  $\alpha$ -rhombohedral boron and  $\beta$ -rhombohedral boron, and their existence is proven beyond doubt (Albert & Hillebrecht 2009). The tetragonal structures described in literature have been considered to be insufficiently supported by evidence for elemental modifications (Albert & Hillebrecht 2009).

Below these phases of elemental boron are described and problems with their synthesis and characterisation are illuminated.

## 1.2 Elemental boron modifications

### 1.2.1 $\alpha$ -boron

Pure boron was obtained in a crystalline form for the first time in 1909 (Weintraub 1909). The first detailed report of synthesis of  $\alpha$ -boron single crystals was described only in 1958 (McCarty *et al.* 1958). It was observed that the product of the pyrolytic decomposition of  $\text{BI}_3$  on a surface heated at 1073-1273 K contained a crystalline modification of boron (McCarty *et al.* 1958) with a simple rhombohedral structure ( $\alpha$ -boron). Tantalum, tungsten and boron nitride have all been used successfully as substrates decomposition of the boron iodide or boron hydride resulting in synthesis of single crystals of  $\alpha$ -boron. Above  $\sim 1770$  K those crystals transformed to the structurally more complex  $\beta$ -rhombohedral form (McCarty *et al.* 1958). In 1959 single crystals of  $\alpha$ -boron were made by crystallizing amorphous boron in a platinum melt (Horn 1959). After a few reports in the 1950s and 1960s (McCarty *et al.* 1958; Horn 1959; Amberger & Dietze 1960; Wald 1970, see also Albert & Hillebrecht 2009 for review) there was a long time of the absence of any references to synthesis of  $\alpha$ -boron single crystals.

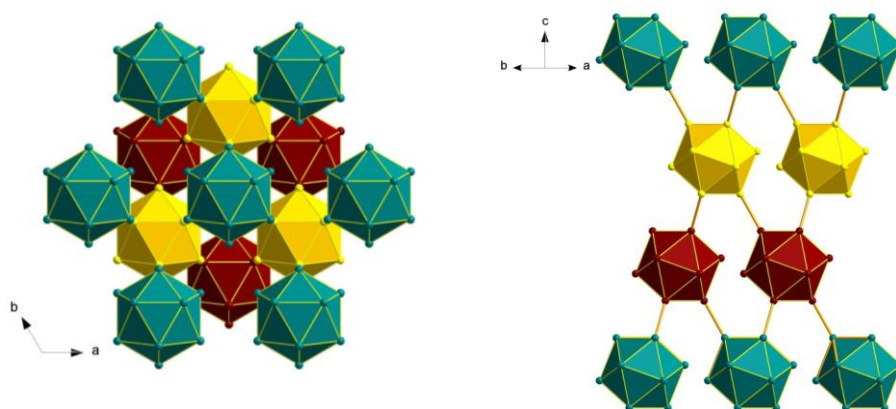


**Figure 1.2.1** The framework of  $\text{B}_{12}$  icosahedra in  $\alpha$ -boron.

$\alpha$ -boron has the simplest structure (Will & Kiefer 2001; Decker & Kasper 1959; Morosin *et al.* 1986; Switendick & Morosin 1990; Parakhonskiy *et al.* 2011) among three established stable boron phases: it consists of  $\text{B}_{12}$  icosahedra located in corners of a rhombohedral unit cell (figure 1.2.1). The structure was solved in 1959 (Decker & Kasper 1959).  $\alpha$ -boron crystallizes in a rhombohedral structure ( $R\bar{3}m$  space group) with unit cell parameters  $a = 4.9179(5)$  Å,  $c = 12.5805(16)$  Å in a hexagonal setting (Parakhonskiy *et al.* 2011).

$\alpha$ -boron demonstrates a truly spectacular combination of properties – it is a direct band gap semiconductor (with the reported band gap of 2.0 eV (Horn 1959), 2.4 eV (Terauchi *et al.* 1997), or 2.15(2) eV as derived by us from EELS data), has a very high hardness (we measured the Vickers hardness of 38(2) GPa on polycrystalline aggregates), thermally and chemically highly resistive, and quite light (the density of  $\alpha$ -B is 2.46 g/cm<sup>3</sup> vs 4.89 g/cm<sup>3</sup> of CdS or 6.11 g/cm<sup>3</sup> of GaN having comparable band gaps). Such properties may make  $\alpha$ -B material of choice in many industrial semiconductors applications, and, especially, as a working element of solar cells with high efficiency of sun light conversion into electrical power.

Inter- and intricosahedra vibration modes assignment based on Raman spectroscopy was made at pressures up to 35 GPa (Richter & Ploog 1975; Vast *et al.* 1997). X-ray diffraction and Raman spectroscopy analysis was performed later on single crystals at pressures up to 100 GPa (Polian *et al.* 2008).  $\alpha$ -boron is claimed to be stable in this pressure range (Polian *et al.* 2008).

Raman spectra from the samples of  $\alpha$ -boron investigated by Werheit *et al.* (Werheit *et al.* 2010), revealed new very weak Raman bands at 494, 552, 750, 1094 and 1238 cm<sup>-1</sup> in respect to previous theoretical (Shirai & Katayama-Yoshida 1998) and experimental (Vast *et al.* 2007) data. The authors interpreted them as surface modes excited by the Ar ion laser of 488 nm. No information was provided regarding purity of the crystals of  $\alpha$ -B studied in Werheit *et al.* 2010 and their synthesis technique. Discrepancy between previous theoretical and experimental data (Vast *et al.* 1997; Polian *et al.* 2008; Shirai & Katayama-Yoshida 1998; Werheit *et al.* 2010) and recent observations required clarification.

It is already more than 50 years passed since  $\alpha$ -boron was obtained in a crystalline form for the first time, but several problems still remain. A methodology of reproducible synthesis is needed to be developed. Pressure-temperature stability range is needed to be verified. The Raman spectroscopy data required clarification.

### 1.2.2 $\beta$ -boron

$\beta$ -boron is the most common phase and most complicated from the structural point of view.  $\beta$ -boron powder is commercially available. The  $\beta$ -B crystallizes from melt at ambient pressure and can be also produced by different chemical methods including vapour deposition (Cueilleron & Viala 1979; Greenwood 1973).

The structure of  $\beta$ -boron was solved for the first time by Sands & Hoard (1957) and later refined (Hoard *et al.* 1970; Callmer 1977).  $\beta$ -boron crystallizes in a rhombohedral

structure ( $R\bar{3}m$  space group) with the unit cell parameters  $a = 10.932(1) \text{ \AA}$ ,  $c = 23.818(3) \text{ \AA}$  in a hexagonal setting (Slack *et al.* 1988). Measured experimental density was  $2.35 \text{ g/cm}^3$ .  $\beta$ -boron consists of  $B_{12}$  icosahedra and  $B_{27}$ - $B$ - $B_{27}$  clusters.  $B_{27}$  cluster consists of 3  $B_{12}$  icosahedra sharing their faces. They are connected with the similar  $B_{27}$  cluster through the B atom, and form the  $B_{27}$ - $B$ - $B_{27}$  unit.  $B_{12}$  icosahedra form a 3-dimensional framework with  $B_{27}$ - $B$ - $B_{27}$  clusters inside the voids (figure 1.2.2.1). Presence of voids and partially occupied positions makes  $\beta$ -boron the most complex structure among all boron polymorphs (Slack *et al.* 1988).

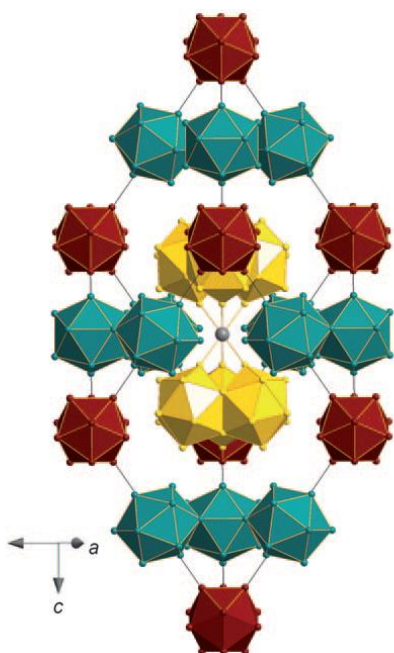


**Figure 1.2.2.1** Crystal structure of rhombohedral  $\beta$ -boron (picture is taken from Albert & Hillebrecht 2009).

Availability of  $\beta$ -boron crystals makes this phase well-studied. Optical (Spitzer & Kaiser 1958), electrical (Greiner & Gutowski 1957) and mechanical (Tsagareishvili & Khvedelidze 1980) properties of  $\beta$ -boron were measured. It was theoretically predicted (Mailhiot *et al.* 1990) and experimentally found that  $\beta$ -boron changes its state from a wide band gap semiconductor to metal and even a superconductor at 160 GPa (Eremets *et al.* 2001).

But due to its complexity, the structure of  $\beta$ -boron is not entirely understood. The electron density distribution has not been determined. The Raman spectroscopy investigation of  $\beta$ -boron single crystals under high pressure has not been done so far.

### 1.2.3 The controversy on the ground state of boron and a relative stability of the two modifications ( $\alpha$ -B and $\beta$ -B) at ambient conditions

Relative stability of  $\alpha$ -B and  $\beta$ -B at ambient conditions still remains a puzzle. Boron is the last stable element in a periodic table, which ground state is needed to be clarified. Due to the ground state energies of the two modifications are very similar, theoreticians do not have consensus on that problem. Using density-functional (DFT) calculations Shirai *et al.* (Masago and Shirai 2006; Shirai *et al.* 2007) studied ground-state and thermodynamic properties (including the effect of atomic disorder and phonons) of  $\alpha$ - and  $\beta$ -boron and found that at zero temperature  $\alpha$ -B is more stable than  $\beta$ -B. That agrees with the conclusion of Shang *et al.* (2007), who considered defect free  $\alpha$ - and  $\beta$ -B using first-principle quasi-harmonic phonon calculations. By considering the phonon contribution as the major source of the temperature dependence of the free energy, Masago *et al.* (Masago & Shirai 2006) obtained 970 K as the transition temperature of  $\alpha$ -to- $\beta$  boron. This is at odds with conclusions of van Setten *et al.* (2007), who introduced the quantum mechanical zero-point vibrational energy as a mechanism to stabilize  $\beta$ -B at absolute zero temperature and found  $\beta$ -B to be the ground state of elemental boron in their DFT calculations. Moreover, theoretical calculations indicate that it is possible to find an arrangement of partially occupied sites in  $\beta$ -boron that also increase its stability with respect to the  $\alpha$ -phase (Ogitsu *et al.* 2009; Widom and Mihalkovič 2008; van Setten *et al.* 2007). Ogitsu *et al.* (2009), using lattice Monte Carlo techniques combined with *ab initio* calculations, found that boron could be a frustrated system and a series of  $\beta$ -boron structures, nearly degenerate in energy, may be stabilized by a macroscopic amount of intrinsic defects. According to Ogitsu *et al.* (2009) defects are responsible not only for entropic effects but also for a reduction in internal energy making  $\beta$ -B more stable than  $\alpha$ -B at zero temperature.

This long-standing controversy has not been resolved experimentally so far as well. On heating at ambient pressure to temperatures above  $\sim 1500$  K  $\alpha$ -B slowly transforms to  $\beta$ -B, which means that a stable high-temperature form of boron is the  $\beta$ -phase. The fact that  $\beta$ -B could not be transformed to  $\alpha$ -B at ambient pressure may indicate that  $\alpha$ -B is metastable (Shalamberidze *et al.* 2000). In this respect, although  $\alpha$ -B is completely ordered, its relative structural simplicity does not make it self-evident that  $\alpha$ -B is more stable compared to  $\beta$ -B at ambient conditions. Slow kinetics of transformations (i.e. large kinetic barriers) and/or high melting temperature of boron make difficult accurate measurements by unambiguous techniques, such as calorimetry (Ogitsu *et al.* 2009).

This controversy could be resolved by determining of phase boundary between  $\alpha$ -B and  $\beta$ -B phases and hence the stable phase at ambient pressure and zero temperature.

#### 1.2.4 $\gamma$ -boron

The existence of a HP boron phase was reported for the first time in 1965 (Wentorf 1965), when a new phase was obtained as a powder at 10 GPa and 1770 K. The structure could not be solved from the powder diffraction that time. Even the unit cell parameters could not be determined. But later polycrystalline HP phase with the same diffraction pattern was synthesized by Zarechnaya *et al.* (Zarechnaya *et al.* 2008). Due to advances of diffraction techniques and software the structure was solved from a powder diffraction data (Zarechnaya *et al.* 2008). The existence of this phase was also theoretically predicted by Oganov *et al.* (Oganov *et al.* 2009). The HP phase of boron was called  $\gamma$ -boron. Its structure was confirmed (Zarechnaya *et al.* 2009) and then refined from the single crystal synchrotron X-ray diffraction data. Oganov *et al.* (2009) pointed on an partial ionic character of the bonds in this phase. However, the accurate structure analysis including analysis of the electron density revealed the polar covalent character of bonds in  $\gamma$ -boron (Zarechnaya *et al.* 2009, Mondal *et al.* 2011).

$\gamma$ -boron crystallizes in an orthorhombic structure ( $Pnmm$  space group) with the unit cell parameters  $a = 5.0563 \text{ \AA}$ ,  $b = 5.6126 \text{ \AA}$  and  $c = 6.9710 \text{ \AA}$ . The structure is similar to that of  $\alpha$ -boron, with  $B_2$  dumbbells, filling the octahedral voids formed by centers of six  $B_{12}$  icosahedra (figure 1.2.4.1).

For the last few years  $\gamma$ -boron has become an object of intensive studies. It is extremely hard (Vickers microhardness is 58 GPa) (Solozhenko *et al.* 2009; Zarechnaya *et al.* 2009), optically transparent with an optical absorption edge of 2.1 eV. It is a poor electrical conductor with a resistivity on the order of  $10^6 \text{ \Omega-cm}$  at ambient conditions. Resistivity decreases with increasing temperature, indicating semiconductor behavior of  $\gamma$ -boron (Zarechnaya *et al.* 2009).

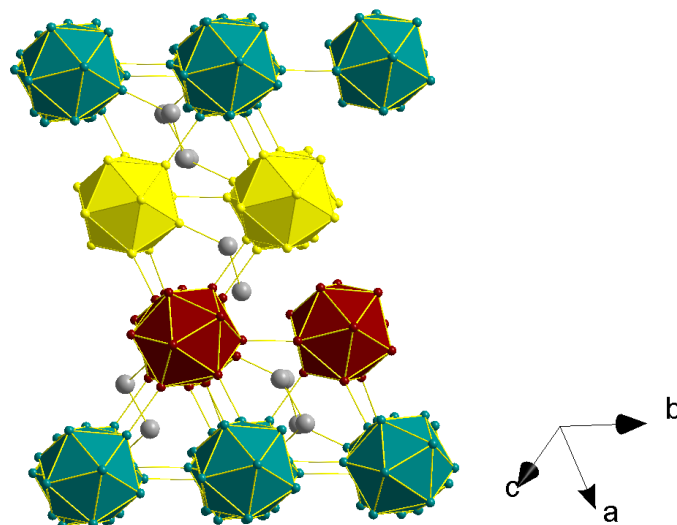


**Figure 1.2.4.1** Structure of  $\gamma$ -boron:  $B_{12}$  icosahedra are connected by  $B_2$  dumbbells.

The X-ray density of  $\gamma$ -boron is  $2.54(1) \text{ g/cm}^3$ . High density, compared with  $\alpha$ - and  $\beta$ -boron, and strong covalent bonding, suggest the lesser compressibility of  $\gamma$ -boron. High pressure investigations of  $\gamma$ -boron single crystals evidence its stability to at least 30 GPa and 2000 K (Zarechnaya *et al.* 2010). Above  $\sim 40$  GPa splitting of several Raman peaks occurs. Explicit analysis of boron atoms vibrations upon pressures was made by Zarechnaya *et al.* up to 100 GPa (Zarechnaya *et al.* 2010).

### 1.2.5 Tetragonal boron, T-50 and T-192 phases

There is still a wide gap in knowledge about reported in literature but still not well established boron phases: tetragonal  $B_{50}$  (T-50) and  $B_{192}$  (T-192) (also known as I- and II-tetragonal phases). The fact of existence of T-50 boron phase is still a topic of debates between theorists and experimentalists. The T-50 was first mentioned in literature in a 1943 by Laubengayer (Laubengayer & Hurd 1943). It was synthesized by a reduction of a  $BBr_3$  vapour on a Ta filament in a crystalline form (Laubengayer & Hurd 1943). The structure was solved from X-ray diffraction data collected from those crystals (Hoard *et al.* 1958; Hoard & Geller 1951). T-50 was shown to crystallize in a tetragonal structure ( $P4_2/nmm$  space group) with the unit cell parameters  $a = 8.75 \text{ \AA}$ ,  $c = 5.06 \text{ \AA}$  (Hoard *et al.* 1958). The structure consists of  $B_{12}$  icosahedra connected together into 3-dimensional network, with additional boron atoms located in the following positions:  $2b (0, 0, \frac{1}{2})$  (figure 1.2.5.1).

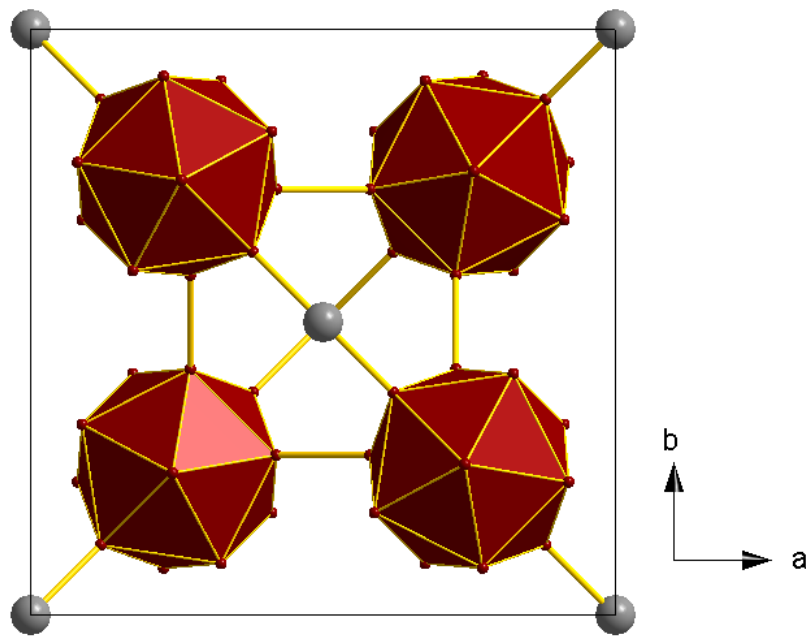


**Figure 1.2.5.1** Unit cell of T-50, viewed along  $c$  axis.

However later, in 1954 Longuet-Higgins and Roberts pointed out that the proposed  $B_{50}$  structure would not have a stable electronic configuration and therefore could not exist (Longuet-Higgins & Roberts 1954). In 1974 Hoard's *et al.* (1958) results on T-50 were refuted by Will and Ploog (Will & Ploog 1974), because they (a) failed to reproduce of Laubengayer's experiment, (b) theoretically proved an instability of  $B_{50}$  due to its electronic configuration, and (c) found that X-ray diffraction measurement revealed the N and C impurities in the samples surpassingly T-50 phase (Will & Ploog 1974). Then a series of works showed that  $B_{50}$  is stabilized by small amounts of foreign atoms such as carbon, nitrogen or transition elements forming, for example,  $B_{48}B_2C_2$ ,  $B_{48}B_2Ti_2$  or other compounds (Becher 1960; Becher & Neidhard 1968; Bullett 1982). In 1992 theoretical work by Lee *et al.* supported these results, showing that the total energies of  $B_{50}C_2$  and  $B_{50}N_2$  are lower than those of a mixture of pure  $B_{50}$  and carbon or nitrogen (Lee *et al.* 1992). Synthesized nanoribbons of  $\alpha$ -tetragonal boron also contained small amounts of oxygen and carbon (Xu *et al.* 2004).

Only in 2007 possibility of the existence of the pure  $\alpha$ -tetragonal boron polymorph in a nanocrystalline form was theoretically demonstrated (Hayami & Otani 2007). In 2009 nanowires of pure  $\alpha$ -tetragonal crystalline boron with a 25 nm diameter was finally synthesized (Liu *et al.* 2009). Recently T-50 powder was obtained at HPHT conditions in a mixture with other boron phases. No X-ray diffraction data was presented (Qin *et al.* 2012).

Qin *et al.* suggested that T-50 is an intermediate phase in the phase transition between  $\gamma$ -B or  $\beta$ -B to T-192, however it was not experimentally supported (Qin *et al.* 2012)

There is very limited information regarding T-192 phase in literature. The only reported synthesis of T-192 was in 1960 (Talley *et al.* 1960). Specimens were prepared by the reduction of  $\text{BBr}_3$  by  $\text{H}_2$  on incandescent tungsten and rhenium filaments. Deposition was performed at ambient pressure and temperature of 1813 K. Measured density of T-192 was  $2.364(5) \text{ g/cm}^3$  at a room temperature. Powder diffraction data revealed that the unit cell is tetragonal with  $a = 10.12 \text{ \AA}$  and  $c = 14.14 \text{ \AA}$  and contains 192 atoms, grouped in 16  $\text{B}_{12}$  icosahedra (Talley *et al.* 1960). Later, the structure was refined from single crystal data (Vlasse *et al.* 1979). Then every attempt to produce T-192 crystals was failed.

It was proposed that phase transition of  $\beta$ -boron to the tetragonal T-192 structure occurs at pressures higher than 10 GPa and temperatures higher than 1500 K (Ma *et al.* 2003). The suggestion was based on alteration of powder diffraction pattern of  $\beta$ -boron after heating, but the purity of tetragonal phase was not confirmed by any means.

Therefore there are still much unknown regarding tetragonal boron phases T-50 and T-192. Do they really exist? What are their relations to the other boron phases? Where are their places on the phase diagram? Are they stable or metastable?

### 1.2.6 The phase PT diagram of boron

Phase diagrams are established for the majority of elements and compounds, but reliable phase diagram is still absent for elemental boron. The phase boundary separating the  $\beta$ -B and  $\gamma$ -B phases was experimentally found by Zarechnaya *et al.* (Zarechnaya *et al.* 2009). The two other phase boundaries have not been reported based on experimental data until recently. The phase diagram drawn by Oganov (2011) (figure 1.2.6.1a) is schematic and based only on a few experimental points related to the HPHT synthesis conditions of  $\beta$ -B. The author (Oganov 2011) sketched the  $\alpha$ -/ $\beta$ -B phase boundary in accordance with the theoretical data of van Setten *et al.* (2007).

The experimental phase diagram, published by Qin *et al.* (2012) resulted from studies of solid-solid phase transitions in boron under pressure, thus the phase boundaries drawn in the phase diagram of Qin *et al.* (figure 1.2.6.1b) do not correspond to equilibrium ones. Applied temperature might not be enough to overcome the energy barrier for a phase transition. That means the equilibrium phase boundaries may be shifted to lower pressures and temperatures.

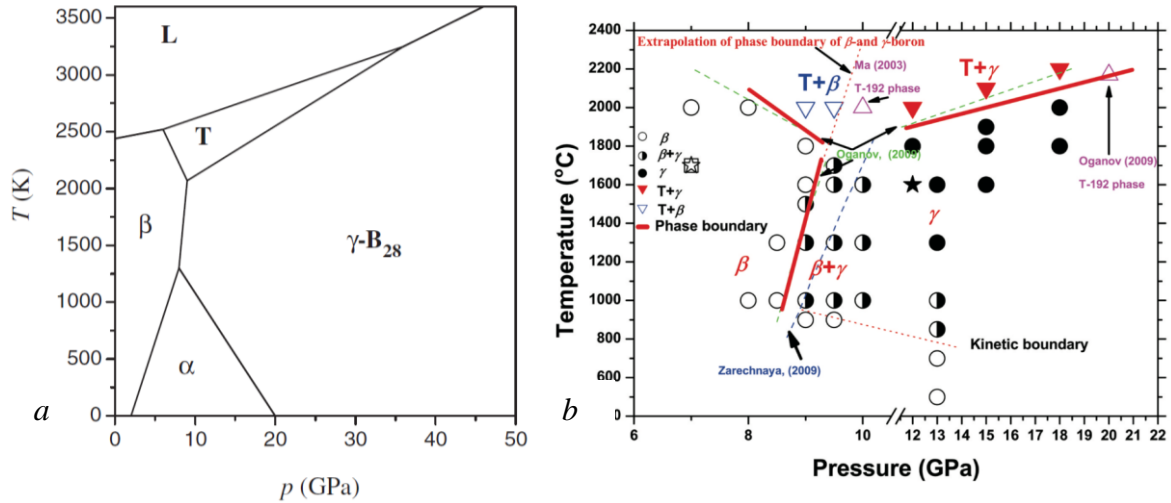


**Figure 1.2.6.1** a) Theoretically predicted phase diagram (Oganov 2011). b) Experimental phase diagram built by Qin *et al.* (2012).

Summarizing, the goals of the present work were to develop a methodology synthesis of  $\alpha$ -boron, to investigate relations between known boron phases and to construct the experimental boron phase diagram.

## 1.3 Experimental techniques

Below I summarize experimental and analytical techniques used in the present research. For high-pressure synthesis multi-anvil large volume presses and piston cylinder apparatus were used. For *in situ* studies of boron phases diamond anvil cells were used. The Raman spectroscopy, X-ray diffraction, Scanning Electron Microscopy (SEM) and Transmission Electron Microscopy (TEM) were used for a chemical and structure analysis of prepared samples.

### 1.3.1 High pressure techniques

#### 1.3.1.1 Multi-anvil apparatus

Multi anvil apparatus is a device for pressure generation. Attained pressures and temperatures could be 28 GPa and 3000 K respectively (Frost *et al.* 2004). The pressure range can be extended to over 90 GPa using inner-anvils of sintered diamond (Ito 2012). We used two 6-8 Kawai type multi-anvill systems (Kawai & Endo 1970; Kawai *et al.* 1973; Ohtani *et al.* 1987; Walker *et al.* 1990) installed at Bavarian Geoinstitute (BGI, Bayreuth University): 1000 ton Hymag and 1200 ton Sumitomo presses. Pressure was generated by a hydraulic press and transmitted by six tool-steel outer anvils and eight tungsten carbide cubic inner-anvils to focus an applied load on a Cr<sub>2</sub>O<sub>3</sub>-doped MgO octahedral high-pressure chamber, which is used as a pressure transmitting medium. By varying the corner truncation size of the inner-anvils, various sample-pressure ranges can be attained. Capsule with the sample is enclosed inside the pressure chamber as presented on figure 1.3.1.1.1. The volume of the sample and the pressure that could be reached with specific assemblies is presented in a table 1.3.1.1.1. Comparative octahedra sizes are presented on a figure 1.3.1.1.2. Perofilite gaskets are used as a support of an octahedral pressure chamber.

**Table 1.3.1.1.1** Sample sizes for different octahedron edge length (OEL)/cube truncated edge length (TEL).

OEL/TEL, mm	Size (length/ diameter/ wall width), mm	Volume of the capsule, mm <sup>3</sup>	Largest pressure, can be attained
25/17	4x4x0.15	2.4	6 GPa
25/15	4x4x0.15	2.4	8 GPa
18/11	3.5x2x0.25	1.75	11 GPa
14/8	2.8x1.6x0.15	0.672	15 GPa
10/5	2x1.6x0.15	0.48	20 GPa

A sample under investigation is put inside the cylindrical  $\text{LaCrO}_3$  or C heater, which is isolated from the sample by  $\text{MgO}$  or  $\text{Al}_2\text{O}_3$  layer. It prevents contamination and resistance changing due to chemical reaction between heater and sample. The heater is also separated from the octahedron by a  $\text{ZrO}_2$  tube. To provide electrical conductivity through the heaters, tube was closed by Mo or C electrodes (figure 1.3.1.1.1).

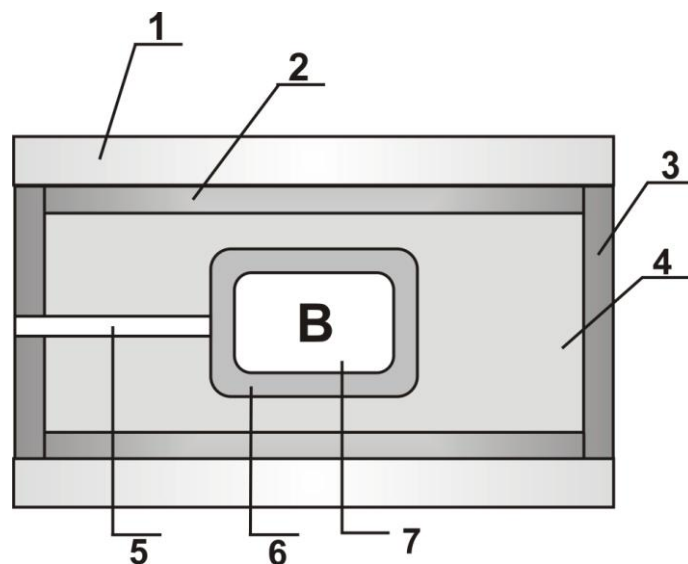


**Figure 1.3.1.1.1** A cross-section of the pressure chamber (not scaled), which is enclosed into the  $\text{MgO}$  octahedron (not shown). The capsule size is 4/4/0.3 mm (length/ outer diameter/ thickness of a metallic tube used for the capsule) in the 25/15 assembly and 3.5/2/0.5 mm in the 18/11 assembly. (1)  $\text{ZrO}_2$  tube; (2) heater; (3) Mo disc (4)  $\text{MgO}$ ; (5) cylindrical hole for a thermocouple; (6) capsule; (7) sample.

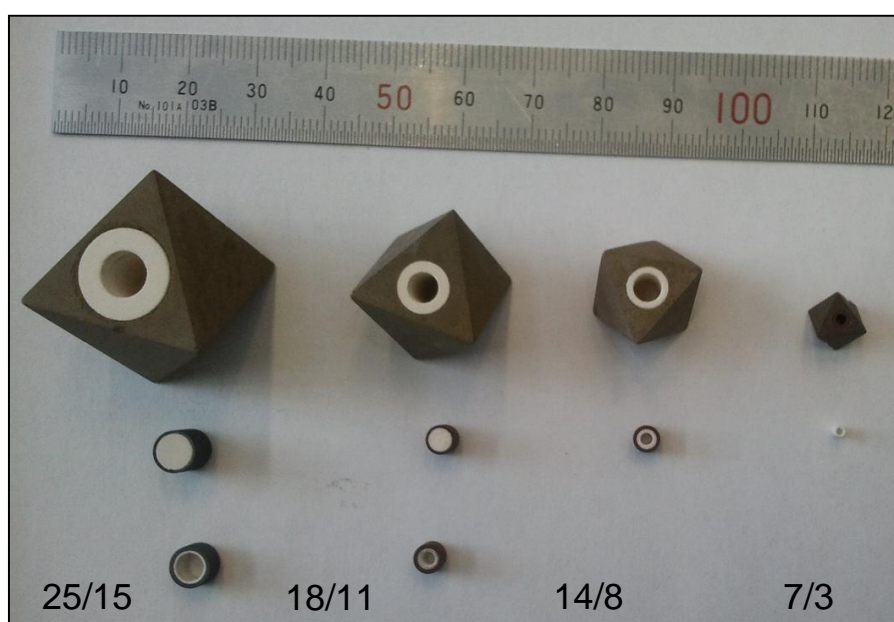


**Figure 1.3.1.1.2** Comparative sizes of octahedra. The ratios OEL/TEL (in mm) are given at the bottom.

### 1.3.1.2 Piston cylinder apparatus

Piston cylinder apparatus is a device which could attain pressures up to 4.5 GPa. These hydraulic presses drive a piston through a cylinder against a top plate to provide a load. Sample could be safely heated upon compression up to 3000 K with graphite furnace (by passing current through it). To minimize thermal stress in the pressure vessel, cold water circulates through the stack top plate, pressure vessel and bridge during heating. Pressure vessel contains a WC core supported by concentric rings of hardened steel. Pressure chamber is compressed in the core of the vessel by a piston, driven by a WC push piece. The force is provided by the main hydraulic ram acting against stack top plate and sample assembly, which is pushed by the end load ram from the other side. Size of the sample is a 10x5x0.25 (mm), hence a volume is 12.5 mm<sup>3</sup>.

In a present work Voggenreiter 220 ton piston cylinder apparatus were used to conduct experiments below 3 GPa and 3000 K.

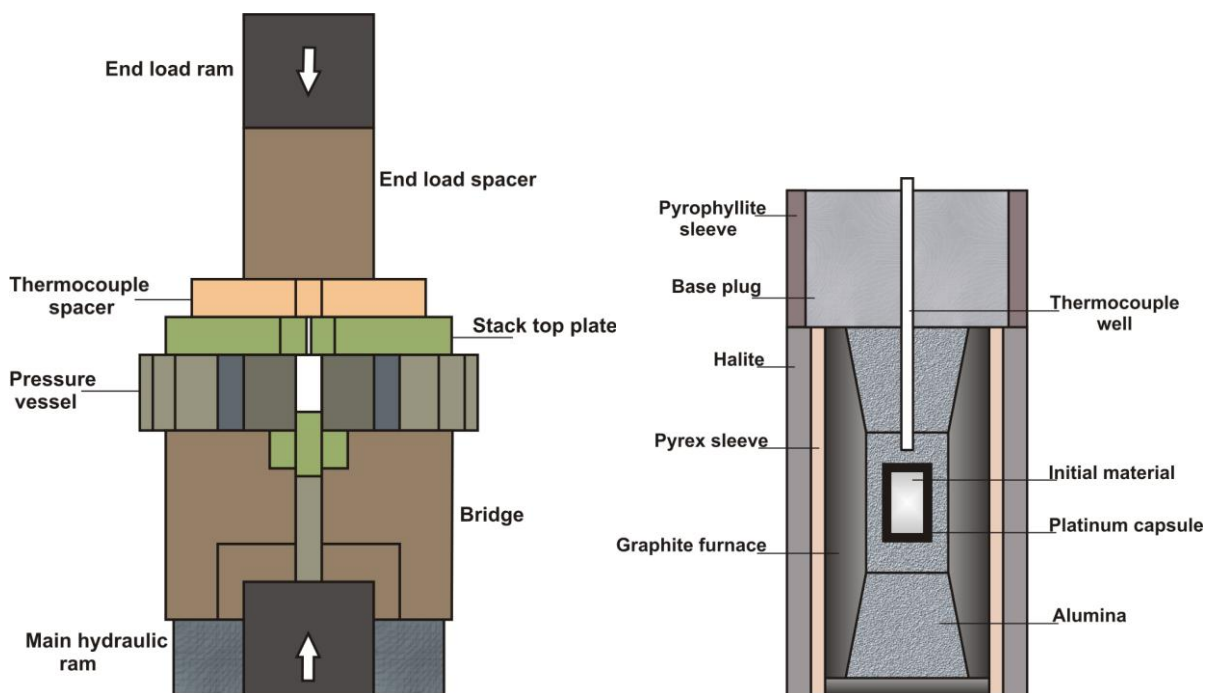
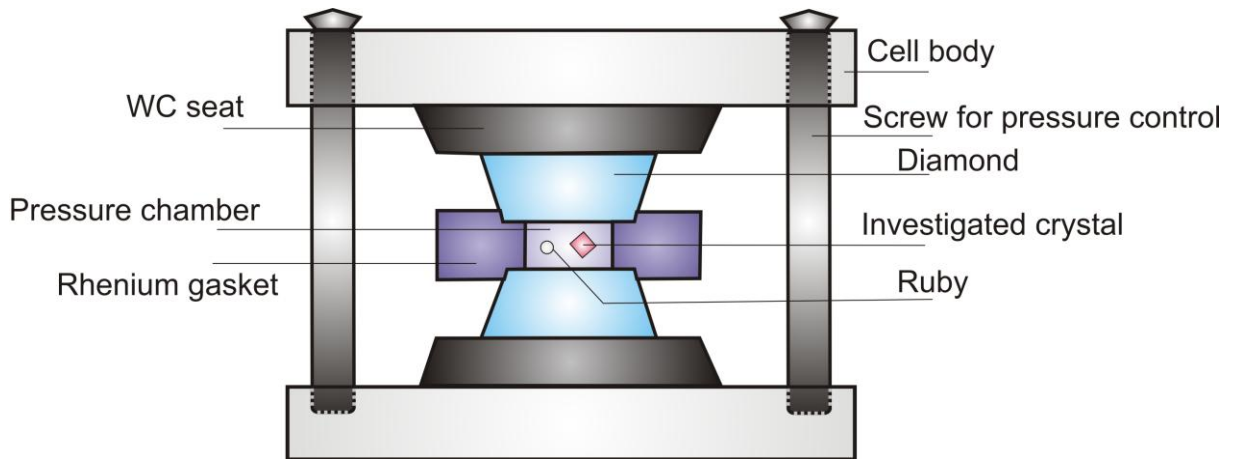


Figure 1.3.1.2.1 Piston cylinder apparatus and the sample assembly.

### 1.3.1.3 Diamond anvil cell

Diamond anvil cell is a universal device for obtaining extremely high pressure (up to 300 GPa) in a small volume, which makes it ideally appropriate to single crystal high pressure measurements. Pressure chamber is formed inside the rhenium gasket, which is squeezed between the two diamond culets to 30-50 micron thickness. Then the hole of

appropriate diameter is drilled in the indentation centre. Material under investigation is placed in such a cylindrical void along with a ruby ball, which serves as a pressure gauge. The pressure chamber is then filled with neon which brings the conditions close to hydrostatic. Initial pressure could be as low as a few hundred bars (figure 1.3.1.3.1).



**Figure 1.3.1.3.1** Diamond anvil cell scheme.

There are two major methods of heating in diamond anvil cells — laser and electrical one (Dubrovinsky *et al.* 2009; Dubrovinskaia & Dubrovinsky 2003) (figure 1.3.1.3.2).

Laser heating technique covers a wide temperature field: between 1300 and 5000 K. The sample preparation for laser-heating experiments is relatively easy and there is no practical risk to the diamonds due to heating (Dubrovinsky *et al.* 2009).

The other one is an external heating device that heats the whole diamond anvil cell. In this method thermal isolation of cell is required, e.g. aluminium foil. It covers temperature range 300-900 K with precision of 2 K. Temperature is directly measured by means of S-type Pt-Pt<sub>0.9</sub>Rh<sub>0.1</sub> thermocouple.

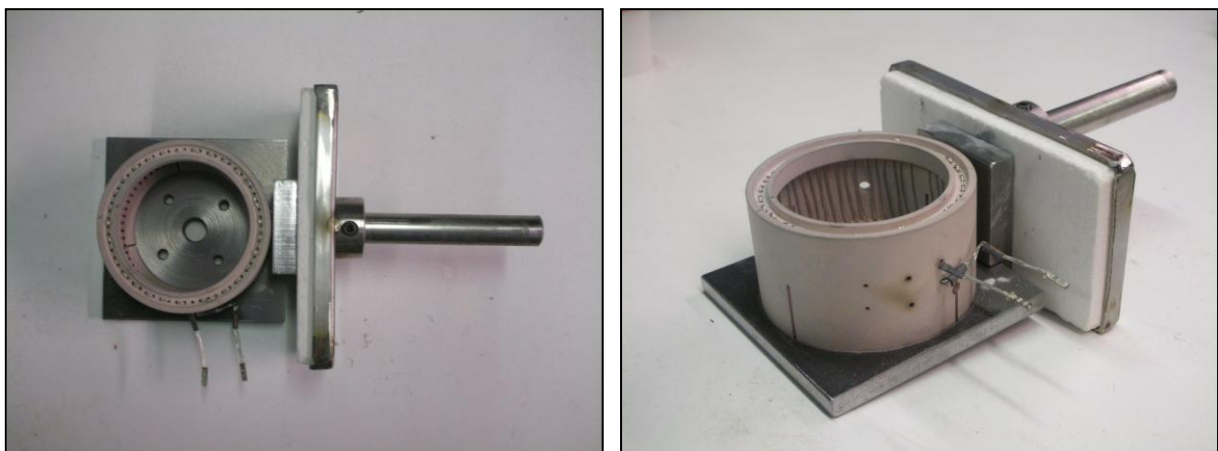


**Figure 1.3.1.3.2** Portable external heater for a diamond anvil cell.

## 1.3.2 Analytical techniques

### 1.3.2.1 Raman spectroscopy

Raman spectroscopy is the powerful non-destructive tool for analysing phonon spectra of crystalline solids. Material is exposed to the laser irradiation in a near ultraviolet – near infrared range. Raman effect occurs due the interaction between laser light and phonons. Photon excites molecule from the ground state to a virtual energy state. Then several possibilities could occur. Molecule relaxes and emits photon of the same energy  $\nu$ , which is called Rayleigh scattering. The molecule relaxes to a different state and emits a photon of a slightly different energy  $\nu_1$ , which gives a rise to a Raman scattering. This difference in energies  $h(\nu \pm \nu_1)$  provides information about frequency of the oscillation modes (figure 1.3.2.1.1). Combinations of the measured frequencies are unique and could be considered as a material fingerprint.

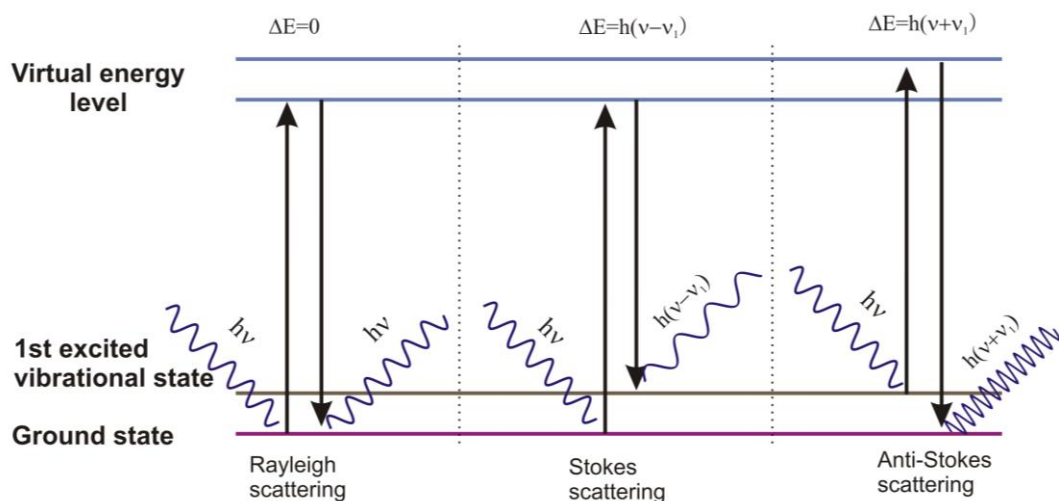


**Figure 1.3.2.1.1** Scattering process scheme.

Raman spectra represent the change of frequencies of the emitted and exciting light versus intensity. The electromagnetic wave induces electric field

$$E = E_0 \cos(2\pi\nu t),$$

where  $\nu$  is frequency of induced electric field.

$$P = \alpha \cdot E,$$

where  $\alpha$  is a polarizability, and  $P$  – dipolar momentum.

If we consider  $q$  as a shift of a nuclei, and  $\nu_1$  is an oscillation frequency of the molecule, then

$$q = q_0 \cos(2\pi\nu_1 t).$$

And if oscillations are small  $\alpha \cong \alpha_0 + \left(\frac{\partial\alpha}{\partial q}\right)_0 q$ .

Combining:

$$P = \left(\alpha_0 + \left(\frac{\partial\alpha}{\partial q}\right)_0 q\right) E_0 \cos(2\pi\nu t) = \left(\alpha_0 + \left(\frac{\partial\alpha}{\partial q}\right)_0 q_0 \cos(2\pi\nu_1 t)\right) E_0 \cos(2\pi\nu t) =$$

$$\alpha_0 E_0 \cos(2\pi\nu t) + \frac{1}{2} \left(\frac{\partial\alpha}{\partial q}\right)_0 q_0 E_0 (\cos(2\pi(\nu + \nu_1)t) + \cos(2\pi(\nu - \nu_1)t)),$$

where the first term describes Rayleigh scattering on the frequency  $\nu$ , and the second term describes Raman scattering on the Stokes ( $\nu - \nu_1$ ) and anti-Stokes ( $\nu + \nu_1$ ) frequencies. It is clearly seen that Raman scattering is absent for materials whose polarizability is not changed with oscillations ( $\left(\frac{\partial\alpha}{\partial q}\right)_0 = 0$ ).

In the present work Raman spectra were collected using Dilor XY and LabRAM spectrometers equipped with the He-Cd (325 nm), Ar (514 nm) and He-Ne (632.8 nm) laser sources.

### 1.3.2.2 X-ray diffraction

The X-ray diffraction is one of the most popular non-destructive analytical techniques, which allows determining the phase composition and crystal structure of material. X-rays are electromagnetic waves with wavelengths from 0.01 nm to 10 nm. There are two most common ways to produce X-rays: X-ray tubes and synchrotrons. In an X-ray tube, X-rays are generated by bombarding a target of a suitable material with a focused electron beam. In synchrotrons, high-energy electrons are deflected by electromagnetic fields, yielding X-ray emission.

X-ray diffraction technique is based on the scattering of X-rays by electrons, which is also known as Thomson scattering. It occurs because the electron oscillates in the electric field of the incoming X-ray beam and an oscillating electric charge radiates electromagnetic waves. Thus, X-rays are radiated from the electron at the same frequency as the primary beam.

As a consequence of the regular arrangement of the atoms in solid matter, coherent scattering of the X-rays at the atoms results in a constructive interference from the reflections of the atomic planes at certain well-defined angles. The positions of the reflections are calculated using optical path difference  $2s$  with  $s = d \sin \theta$ . Maxima are produced for integer

multiples of  $\lambda$ . It results in Bragg's law, which gives the geometrical conditions under which a diffracted beam can be observed:

$$n\lambda = 2d \sin \theta ,$$

where  $d$  is the interplanar spacing,  $\theta$  is the Bragg angle,  $n$  is the order of interference,  $\lambda$  is the wavelength.

Every  $d$  has corresponding indexes in the reciprocal space  $h, k, l$ . Measuring array of intensities with corresponding  $hkl$  makes possible to determine the structure parameters, the unit cell and solve the structure.

In the present work X-ray diffraction techniques were used for the phase identification and the structure solution. Boron is a light element, which makes it to be a weak X-rays scatterer. Therefore acquiring data of acceptable quality requires a long exposure time on the order of 12 hours. Another solution could be to increase beam intensity, which is possible using synchrotron radiation.

The synchrotron radiation is produced by acceleration of electrons in a very large circle by external electromagnetic field. The energy of accelerated electrons could reach 8 GeV. Electrons emit very intense electromagnetic radiation with a continuous spectrum from the far infrared to the  $\gamma$ -ray region, called synchrotron radiation. Synchrotron radiation has extremely low beam divergence, strong polarization, and it is emitted in very short pulses, typically less than a nano-second. Using such radiation it is possible to study very small samples in a very short time.

Selection of single crystals, and preliminary structural analysis was carried out on a high-brilliance diffractometer installed at Bayreisches Geoinstitut. Diffractometer consists of RIGAKU FR-D high brilliance source, OSMIC Inc. Confocal Max-Flux optics, and SMART APEX 4K CCD detector. The diffraction patterns were processed using Fit2D software (Hammersley 1998).

### **1.3.3 Electron microscopy techniques**

#### **1.3.3.1 Scanning electron microscopy and electron microprobe analysis**

The scanning electron microscopy (SEM) can image the surface of bulk samples with a great depth of view and a well-defined, three-dimensional appearance. In contrast to TEM, where transmitted electrons are detected, in SEM mainly backscattered and secondary electrons, which are emitted from the surface due to excitation by the primary electron beam are detected. Moreover, the electron beam with a focal spot size of 1-5 nm is rastered across

the sample to generate the image pixel-wise. The scanning electron microscope has many advantages compared to optical microscopes. The SEM has a large depth of field, which allows more of a specimen to be in focus at one time. The SEM also has much higher resolution, thus closely spaced specimens can be magnified at much higher levels. Because the SEM uses electromagnets rather than lenses, the researcher has much more control in the degree of magnification. All of these advantages, as well as the strikingly clear images, make the scanning electron microscope one of the most useful instruments in research today.

The morphology of the synthesized samples of single crystals were studied by means of the scanning electron microscopy (SEM) (LEO-1530). The chemical composition of the sample was studied by X-ray microprobe analysis.

The quantitative chemical analysis of synthesized products was performed using JEOL JXA-8200 instrument under conditions of 20 keV for acceleration voltage and of 20 nA for acceleration current in wavelength dispersive mode (WDX). The size of the focused electron beam was about several microns. All samples were carbon coated with a thickness less than 10 nm. Counting time for each element was 20 s at the peak position and 10 s at each background position.

### **1.3.3.2 Transmission electron microscopy**

The transmission electron microscopy (TEM) is a microscopy technique, which uses a high energy beam of electrons transmitted through a very thin specimen, to image and analyse the material with the atomic scale resolution. The image is magnified and focused onto a fluorescent screen or some other imaging device, for example CCD camera. TEM has a significantly higher resolution than other microscopes due to the very small de Broglie electrons wavelength, but resolution is limited by electromagnetic lenses aberrations.

It also could be used to define chemical composition of the investigated sample, using Electron Energy Loss Spectroscopy (EELS) technique. The sample exposed to the electron beam, with known energies, and some of them are inelasticity scattered which results in an energy loss. Electron energy difference is strongly dependent on the chemistry of the bombarded material. Difference between initial electron energies and resulting electron energies are measured by an electron spectrometer.

Electron transparent foils were prepared by focused ion beam (FIB) techniques. FIB allows preparation of site-specific TEM foils with typical dimensions of 15–20  $\mu\text{m}$  wide, approximately 10  $\mu\text{m}$  high and 0.15  $\mu\text{m}$  thick (Wirth 2004).

The TEM investigations were performed with a TECNAI F20 XTWIN transmission electron microscope operating at 200 kV with a field emission gun electron source. The TEM is equipped with a Gatan Tridiem™ filter, an EDAX Genesis™ X-ray analyzer with ultra thin window and a Fishione high angle annular dark field detector (HAADF). The Tridiem filter was used for the acquisition of energy-filtered images applying a 20 eV window to the zero loss peak. EEL spectra were acquired with a dispersion of 0.1 eV/channel and an entrance aperture of 2 mm. The resolution of the filter was 0.9 eV at full width of half maximum of the zero loss peak. Acquisition time was 1 second. Spectra of the different K-edges (B, C, N, O) were acquired in diffraction mode with a camera length of 770 mm. Spectra processing (background subtraction, removal of plural scattering, quantification) was performed using the DigitalMicrograph software package. EDX spectra were usually acquired in the scanning transmission mode (STEM) using the TIA™ software package of the TEM. Significant mass loss during analysis was avoided by scanning the beam in a pre-selected window (20 x 20 nm or larger). Spot size was approx. 1 nm, and acquisition time 60 s at an average count rate of 60 – 80 counts/s. This resulted in a counting error of about 4 -5% at a 3 $\sigma$  level.

## 2 SYNOPSIS (scope of the articles)

In this section I summarize experiments and main results, which have been presented in four papers in peer-reviewed journals (published or submitted for publication). These papers comprise the present thesis.

### 2.1 Synthesis of single crystals of $\alpha$ -boron

Synthesis of  $\alpha$ -boron single crystals has been a long-standing problem obstructing deeper investigations of this boron polymorph. Last documented synthesis of  $\alpha$ -boron single crystals was done in 1960s and not reproduced since then (Albert & Hillebrecht 2009).

In our work in a series of experiments we have reproducibly obtained single crystals of pure  $\alpha$ -boron using  $\beta$ -boron as a starting material. The synthesis was realised at high pressures, while all previous methods of  $\alpha$ -boron synthesis were based on techniques realised at ambient pressure (see section 1.3 for the HP synthesis details). The experiments were conducted at pressures of 6 to 11 GPa and at temperatures of 1450 to 1875 K (table 2.1.1).

**Table 2.1.1** Summary of experiments on synthesis of single crystals of the rhombohedral  $\alpha$ -boron phase. All synthesis products contain additionally platinum boride. Typical uncertainty in temperature is  $\pm 50$  K, and 0.5 GPa in pressure.

Experiment	Starting material	Experimental conditions				HP assembly	Synthesis products
		capsule material	temperature, K	pressure, GPa	heating time, min		
H3161	85 at.% $\beta$ -B + 15 at.% Pt	Au	1473	10.5	5	18/11	$\alpha$ -B, $\gamma$ -B
H3170	85 at.% $\beta$ -B + 15 at.% Pt	Au	1473	7.2	5	18/11	$\alpha$ -B, $\beta$ -B
S4894	$\beta$ -B	Pt	1873	7	5	25/15	$\alpha$ -B, $\beta$ -B
H3255	$\beta$ -B	Pt	1573	8.5	3	18/11	$\alpha$ -B, $\beta$ -B
H3271	$\beta$ -B	Pt	1673	6	5	18/11	$\alpha$ -B, recrystallized $\beta$ -B

H3273	$\beta$ -B	Pt	1573	6	5	18/11	$\alpha$ -B, $\beta$ -B
H3286	$\beta$ -B	Pt	1873	8	5	18/11	$\alpha$ -B, $\gamma$ -B

$\alpha$ -boron is known as a material of red or maroon colour (Albert & Hillebrecht 2009). Tiny crystals of this characteristic colour extracted from the capsule were first identified as  $\alpha$ -boron using the Raman spectroscopy. This phase identification was confirmed by X-ray diffraction. The colour of the crystals varied from light red to deep red and yellowish depending on the size of the crystals and experimental conditions (figure 2.1.1). The size of the crystals depends on the heating time.

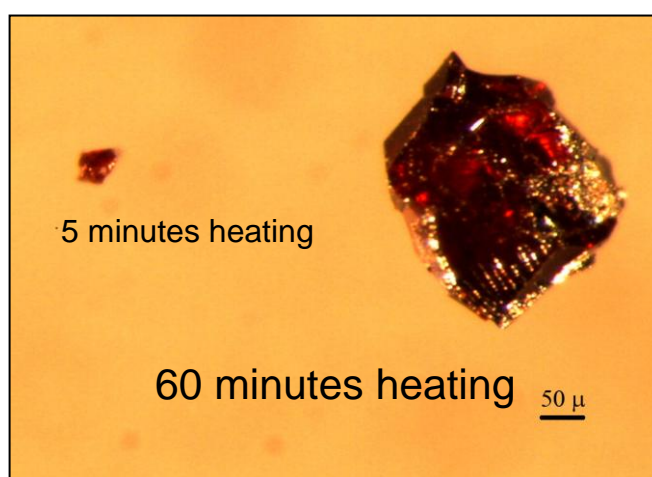


**Figure 2.1.1** Comparison of  $\alpha$ -boron single crystals, synthesized upon different heating time.

## 2.2 Investigation of single crystals of $\alpha$ -boron

The refinement of the crystal structure of  $\alpha$ -boron was carried out using the data collected at room temperature from a crystal with dimensions of  $0.08 \times 0.04 \times 0.03 \text{ mm}^3$ . Initial coordinates of the two crystallographically independent boron atoms were taken from the literature. The final refinement with 15 parameters, including an isotropic extinction parameter, results in a good fit to the diffraction data ( $R_f=0.0275$ ,  $wR_f = 0.0453$  ( $I>3\sigma$ )). The refined crystal structure is in agreement with that reported in the literature (table 2.2.1). High quality synchrotron single crystal X-ray diffraction data was used for analyzing the electron density distribution.

**Table 2.2.1** The data on the crystal structure and the unit cell parameters of  $\alpha$ -B obtained in the present study in comparison with the literature data.

	This Study	(Decker & Kasper 1959)	(Will & Kiefer 2001)	(Switendick <i>et al.</i> 1991)	(Morosin <i>et al.</i> 1986)
$a$ , Å	4.9065(4)	4.9179	4.9179	4.9075(9)	4.927(3)
$c$ , Å	12.5658(5)	12.5805	12.5805	12.559(3)	12.564(7)
$V$ , Å <sup>3</sup>	261.98(3)	263.5	263.50	261.94	264.13
B1, $x$	0.11880(6)	0.11886	0.11886(1)	0.11892(3)	0.1187(2)
B1, $z$	0.89125(4)	0.89133	0.89133(1)	0.89122(2)	0.8912(1)
B2, $x$	0.19678(7)	0.19686	0.19686(1)	0.19688(3)	0.1965(2)
B2, $z$	0.0242484)	0.02432	0.02432(1)	0.02428(2)	0.0243(1)

To clarify the discrepancy between theoretical and experimental Raman spectroscopy data (Vast *et al.* 1997; Polian *et al.* 2008; Shirai & Katayama-Yoshida 1998; Werheit *et al.* 2010), detailed Raman spectroscopy investigation on the  $\alpha$ -boron crystals was undertaken. The piston-cylinder-type diamond anvil cells made at Bayerisches Geoinstitut and diamonds with the culet diameters of 200 microns were used in high pressure experiments (see section 1.3.1). Previously synthesized  $\alpha$ -boron (Parakhonskiy *et al.* 2011a; Parakhonskiy *et al.* 2011b) crystals were selected and placed into the pressure chamber (figure 2.2.1). Sizes of the used crystals were 90x45, 80x40 and 25x40 microns. Neon was used as a pressure transmitting medium. Small ruby ball was placed along with the  $\alpha$ -boron crystal to serve as a pressure marker (Syassen 2008). The DACs were heated using the external resistivity heating system (Dubrovinskaia & Dubrovinsky 2003).

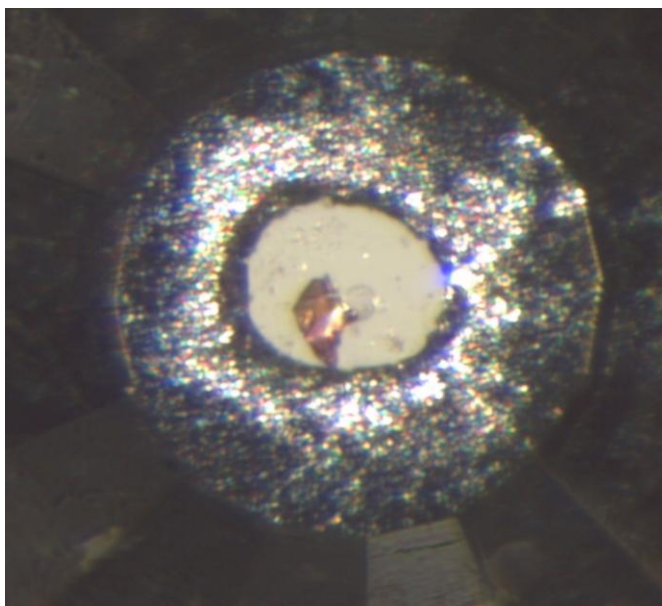


**Figure 2.2.1** Image of the sample chamber of a diamond anvil cell: the  $\alpha$ -boron crystal (orange) placed into a 120-micron hole drilled in the rhenium gasket. A transparent circle in the middle is a ruby ball. Neon is a pressure transmitting medium.

Experimental Raman spectroscopy results obtained at ambient conditions are presented in table 2.2.2 in comparison with the literature data. Experimentally measured frequencies of the Raman modes of  $\alpha$ -boron at ambient conditions agree well with those previously reported in (Werheit *et al.* 2012; Richter & Ploog 1976; Vast *et al.* 1997; Shirai *et al.* 2006). Complementarily, we performed first-principles calculations using the density-functional theory (DFT) and the density-functional perturbation theory (DFPT). The wavenumbers of the Raman bands calculated in the present study (see table 2.2.2, figure 2.2.2) are systematically about  $40 \text{ cm}^{-1}$  higher than the corresponding experimental values. The only exception is the first  $E_g$  peak experimentally observed at  $519 \text{ cm}^{-1}$ . The most likely explanation is an overestimation of the B-B bonding, specific to local density approximation. In a molecular solid, usually the lowest-frequency modes are lattice modes, characterized by large units of the structure vibrating as rigid parts, and thus are less affected by overestimations of the intramolecular bond strengths. Furthermore the behaviour of the mode at  $519 \text{ cm}^{-1}$  ( $525 \text{ cm}^{-1}$  theoretical) is noteworthy as it exhibits a clear softening under pressure. This suggests that the compression mechanism in the structure of  $\alpha$ -boron is dominated by rotations of the  $B_{12}$  cages.

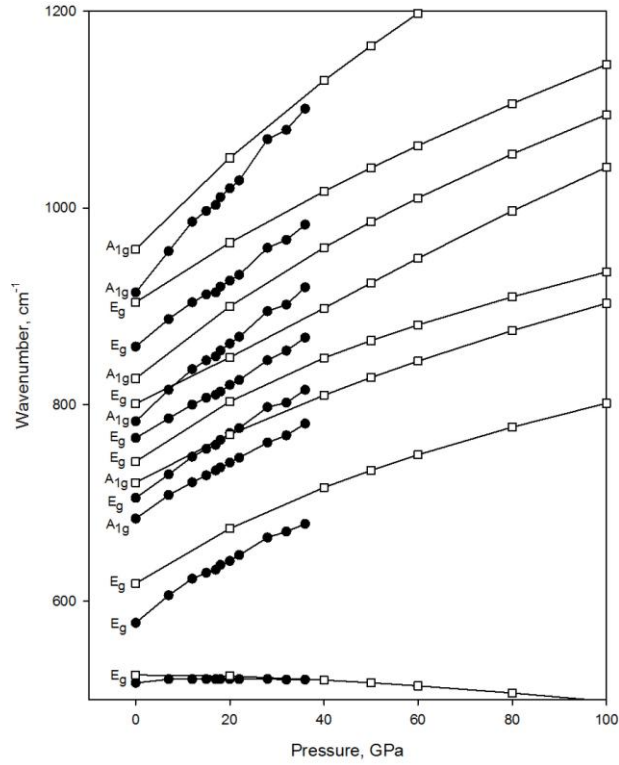


**Figure 2.2.2** The pressure dependence of the wavenumbers of the Raman modes of  $\alpha$ -boron. Black circles are experimentally obtained values, white squares – theoretically calculated ones.

**Table 2.2.2** Phonon frequencies of  $\alpha$ -boron observed in the present study compared with our theoretical calculations and the literature data (experimental uncertainties are  $2 \text{ cm}^{-1}$ ).

	$\omega, \text{cm}^{-1}$ , exp. this work	$\omega, \text{cm}^{-1}$ , theor. this work	$\omega, \text{cm}^{-1}$ , (Richter and Ploog 1975)	$\omega, \text{cm}^{-1}$ , (Vast et al. 1997)	$\omega, \text{cm}^{-1}$ , (Vast et al. 1997)	$\omega, \text{cm}^{-1}$ , (Shirai and Katayama-Yoshida 1998)	$\omega, \text{cm}^{-1}$ , (Werheit et al. 2010)
weak surface mode							494
$E_g$	519	525	524	525	529	497	527
weak surface mode							552
$E_g$	581	618	587	586	608	572	589
$A_{1g}$	686	720	693	692	708	710	694
$E_g$	703	742	710	708	729	743	713
weak surface mode							750
$E_g$	768	801	776	774	790	818	778
$A_{1g}$	784	826	796	793	815	759	795
$E_g$	862	903	872	870	890	884	873
$A_{1g}$	917	958	931	925	947	965	934
weak surface mode							1094
$E_g$	1118	1146	1125	1122	1138	1169	1125
$A_{1g}$	1153		1157				1160
$A_{1g}$	1185	1201	1185	1186	1192	1191	1187
$A_{1g}$	1190		1198				1201
weak surface mode							1238

Based on our experimental data, we were able to write an empirical equation which allows determining pressure (in GPa) if temperature and the wavenumber of the  $A_{1g}$  mode of  $\alpha$ -B is known:

$$P = 0.293\omega + 0.03T - 239,$$

where  $P$  – pressure in GPa,  $\omega$  – the peak position in  $\text{cm}^{-1}$  and  $T$  is the temperature in K with estimated uncertainties 0.5 GPa, 3  $\text{cm}^{-1}$  and 5 K respectively.

Grüneisen parameters were measured and compared with literature data (table 2.2.3).  $\alpha$ -boron confirmed to be stable up to 36 GPa.

**Table 2.2.3** Mode Grüneisen parameters of  $\alpha$ -B Raman active vibrations.

mode	$E_g$	$E_g$	$A_{1g}$	$E_g$	$E_g$	$A_{1g}$	$E_g$	$A_{1g}$	$E_g$
$\omega, \text{cm}^{-1}$	519	581	686	703	768	784	862	917	1118
This work, $\gamma_i$	0.325	1.541	1.037	1.287	0.939	1.321	1.114	1.493	1.233
$\gamma_{\text{exp}}$ , [12]	0.130	1.260	0.973	1.139	0.756	1.186	0.904	1.306	1.040
$\gamma_{\text{theor}}$ , [12]	0.077	1.215	0.889	1.077	0.656	1.155	0.834	1.229	1.083

The active Raman modes of  $\alpha$ -boron at pressures up to 36 GPa were theoretically calculated up to 100 GPa and experimentally measured. Experimentally measured frequencies at ambient conditions agree well with those previously reported in Richter & Ploog 1976; Vast *et al.* 1997; Shirai *et al.* 2006. We performed a detailed investigation of the particular ranges, where additional weak surface modes were found by Werheit (Werheit *et al.* 2012). Raman spectra in those regions were measured for about an hour on both Ar and He-Ne laser systems. Although we used He-Cd laser with the excitation light wavelength of 325 nm, which is smaller than used in Werheit *et al.* (2012), neither of these surface modes was detected in our study. This observation may suggest that the observed "surface modes" could be either artefacts or the result of possible contamination of the boron samples studied in Werheit *et al.* 2012), taking into account that characterisation of their purity was not provided in the paper.

### **2.3 Synthesis of single crystals of $\beta$ - and $\gamma$ -boron**

In order to experimentally constrain relations between  $\alpha$ -,  $\beta$ -, and  $\gamma$ -boron phases we performed more than 30 experiments in a multi-anvil apparatus, extending high pressure

synthesis methodology described previously, for other  $P$ - $T$  ranges (table 2.3.1). Every trial aimed at establishing the phases that can be crystallised from melt or by solid-solid phase transformation of the precursor. Recovered samples were analysed by scanning electron microscopy and electron microprobe for chemical purity, X-ray diffraction and Raman spectroscopy for phase composition, and some samples were studied by TEM for characterising their structure (see experimental techniques).

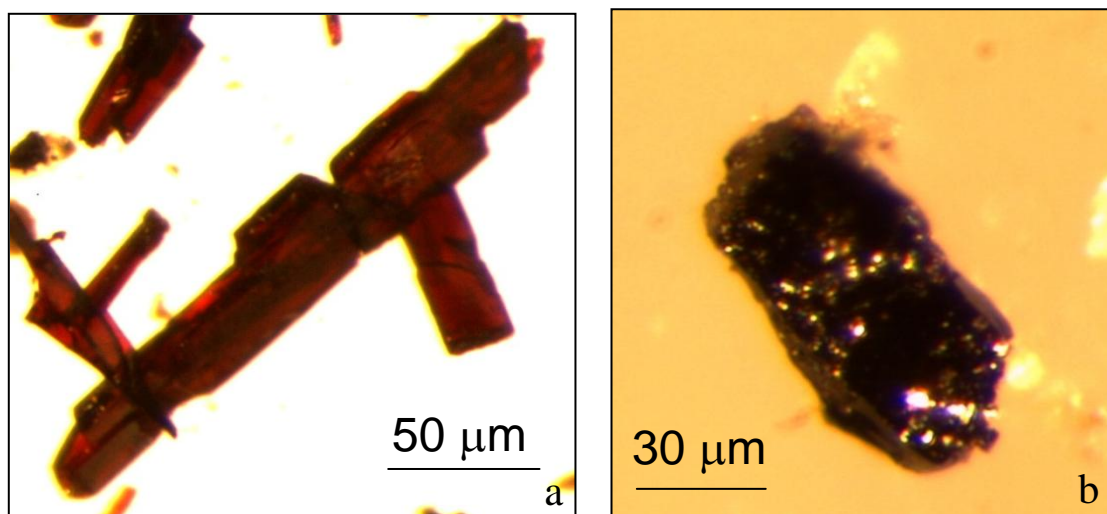


**Figure 2.3.1** Single crystals of  $\gamma$ -boron (a) and  $\beta$ -boron (b).

**Table 2.3.1** Summary of high-pressure high-temperature experiments on boron.

Experiment*	Starting material	Experimental conditions**				Synthesis results***
		capsule material	temperature, K	pressure, GPa	heating duration, min	
H3161 MA	85 at.% $\beta$ -B + 15 at.% Pt	Au	1473	10.5	5	$\alpha$ -B, $\gamma$ -B
H3170 MA	85 at.% $\beta$ -B + 15 at.% Pt	Au	1473	7.2	5	$\alpha$ -B, initial $\beta$ -B
S4894 MA	$\beta$ -B	Pt	1873	7	5	$\alpha$ -B, initial $\beta$ -B
H3255 MA	$\beta$ -B	Pt	1573	8.5	3	$\alpha$ -B, initial $\beta$ -B
H3271 MA	$\beta$ -B	Pt	1673	6	5	$\alpha$ -B, recrystallized $\beta$ -B
H3273 MA	$\beta$ -B	Pt	1473	6	5	$\alpha$ -B, initial $\beta$ -B
H3286 MA	$\beta$ -B	Pt	1873	8	5	$\alpha$ -B, $\gamma$ -B

S4805 MA	85 at.% $\beta$ -B + 15 at.% Pt	Au	1773	9.5	5	$\gamma$ -B, initial $\beta$ -B
H3154 MA	85 at.% $\beta$ -B + 15 at.% Pt	Au	1773	10.5	5	$\gamma$ -B, initial $\beta$ -B
H3191 MA	$\beta$ -B	Pt	2193	12	1	$\gamma$ -B, initial $\beta$ -B
H3244 MA	$\beta$ -B	Pt	1873	14	2	$\gamma$ -B, initial $\beta$ -B
H3260 MA	$\beta$ -B	Pt	1073	9.7	10	initial $\beta$ -B
H3270 MA	$\beta$ -B	Pt	1723	5	5	initial $\beta$ -B, recrystallized $\beta$ -B
S5068 MA	$\beta$ -B	Pt	1423	4	5	initial $\beta$ -B, $\alpha$ -B, recrystallized $\beta$ -B
S5156 MA	$\beta$ -B	Pt	1473	6	60	$\alpha$ -B
H3292 MA	$\beta$ -B	Pt	1573	7	5	$\alpha$ -B, initial $\beta$ -B
S4979 MA	$\beta$ -B	Au	1373	7	5	$\alpha$ -B, initial $\beta$ -B
H3313 MA	$\beta$ -B	Au	1823	7	5	$\alpha$ -B, initial $\beta$ -B, recrystallized $\beta$ -B
S4995 MA	$\beta$ -B	Au	1623	7	5	$\alpha$ -B, initial $\beta$ -B
H3315 MA	$\beta$ -B	Pt	1523	5	5	$\alpha$ -B, recrystallized $\beta$ -B
S5016 MA	$\beta$ -B	Pt	2023	7.5	5	recrystallized $\beta$ -B
S5017 MA	$\beta$ -B	Pt	2123	9.0	5	$\gamma$ -B, recrystallized $\beta$ -B
S5046 MA	$\beta$ -B	Pt	2023	8	5	$\gamma$ -B, recrystallized $\beta$ -B
S5053 MA	$\beta$ -B	Pt	2023	8.5	5	$\gamma$ -B, initial $\beta$ -B
S5060 MA	$\beta$ -B	Pt	2123	8	5	recrystallized $\beta$ -B
S5061 MA	$\beta$ -B	Pt	1723	8	5	$\alpha$ -B, $\gamma$ -B
S5064 MA	$\beta$ -B	Pt	1923	7.5	5	$\alpha$ -B, $\gamma$ -B, recrystallized $\beta$ -B
A404 PC	$\beta$ -B	Pt	1773	3	5	recrystallized $\beta$ -B
A405 PC	$\beta$ -B	Pt	2423	3	5	recrystallized $\beta$ -B
DAC1	$\alpha$ -B	Re	1550	11.5	7	$\gamma$ -B
DAC2	$\alpha$ -B	Re	1600	4.7	7	$\beta$ -B

\* MA – multi-anvil runs, PC – piston cylinder, and DAC – diamond anvil cell experiments

\*\* Typical uncertainty in temperature is  $\pm 50$  K, and 0.5 GPa in pressure.

\*\*\* Platinum borides were found in all experiments at temperatures above eutectic if platinum as capsules material or component of starting mixture was used. In some experiments synthesis products contain initial non-transformed  $\beta$ -boron powder.

## **2.4 The phase *PT* diagram construction and the ground state determination**

Proven chemical and phase purity of boron crystals obtained at different pressure-temperature conditions creates a basis for construction of the experimental phase diagram. Different runs resulted in crystallization of one, two or even all three boron phases simultaneously (table 2.3.1), that allows defining stability fields of the  $\alpha$ -B,  $\beta$ -B and  $\gamma$ -B phases (figure 2.4.1). The phase boundary separating the  $\beta$ -B and  $\gamma$ -B phase stability fields agrees well with the phase relations experimentally found in a previous work (Zarechnaya *et al.* 2009). The other two phase boundaries ( $\alpha$ -/ $\beta$ -B, and  $\alpha$ -/ $\gamma$ -B) have not been reported so far based on experimental data. We argue that the  $\alpha$ -B has the thermodynamic stability field, because its crystallization is controlled only by pressure and temperature conditions of the experiments independently on the type of metallic solvent (Au or Pt, table 2.3.1). Observation of simultaneous crystallization of chemically pure  $\alpha$ - and  $\beta$ -B (at 5 GPa and 1520 K, for example) or  $\alpha$ - and  $\gamma$ -B (at 8 GPa and 1570 GPa, for example) demonstrates the existence of monovariant boundaries in the pressure-temperature phase diagram. The invariant (triple) point in the phase diagram could be determined by intersections of  $\alpha$ -/ $\beta$ -B,  $\alpha$ -/ $\gamma$ -B, and  $\beta$ -/ $\gamma$ -B boundaries. The all three lines cross at 7.6(5) GPa and 1880(50) K (figure 2.4.1). Indeed, at 7.5 GPa and 1920 K we observed simultaneous crystallisation of all  $\alpha$ -,  $\beta$ -, and  $\gamma$ -boron phases (table 2.3.1, figure 2.4.1).

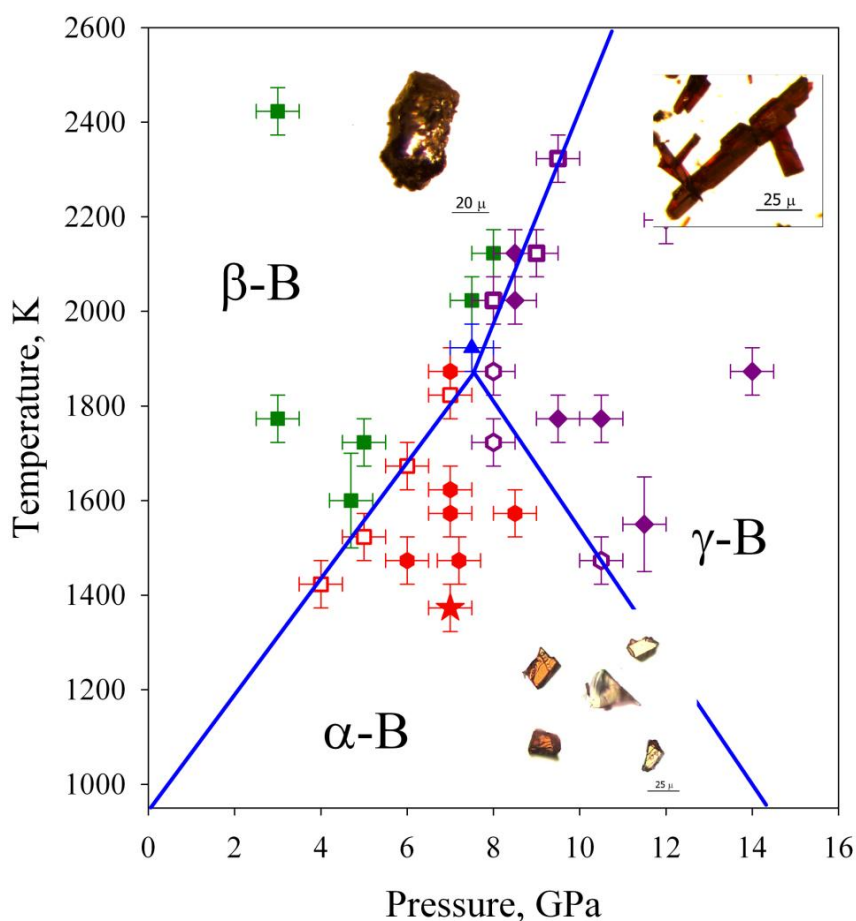


**Figure 2.4.1** Pressure-temperature phase diagram of boron. PT conditions at which crystallisation of various boron phases occurred are marked by different signs: green squares –  $\beta$ -boron; purple diamonds –  $\gamma$ -boron; red hexagons –  $\alpha$ -boron; open red squares –  $\alpha$ - and  $\beta$ -boron; open purple squares –  $\beta$ - and  $\gamma$ -boron; open purple hexagons –  $\alpha$ - and  $\gamma$ -boron; blue triangle –  $\alpha$ -,  $\beta$ -, and  $\gamma$ -boron; the red star marks the conditions of the multi-anvil experiment which led to the solid-solid  $\beta$ -to- $\alpha$ -B phase transition; continues blue lines show apparent phase boundaries. The inserts present images of synthesized crystals of  $\alpha$ -,  $\beta$ -, and  $\gamma$ -boron.

In 1960s and 1970s arguments were raised (Greenwood 1973; Polian *et al.* 2010; Zarechnaya *et al.* 2008; Horn 1959) that crystallization of small crystals of  $\alpha$ -B from different metallic solvents (Pt, Au, Ag, Cu, Cu-Ni, etc.) at temperature around 1100–1200 K may indicate stability of the  $\alpha$ -B polymorph at temperatures below these values. However, inability to grow larger crystals of  $\alpha$ -B, its crystallization simultaneously with the  $\beta$ -B form, and failure to transform  $\beta$ -B into the  $\alpha$ -B phase or to synthesize  $\alpha$ -B from an amorphous boron precursor supports arguments that  $\alpha$ -B may be just a metastable, or even monotropic, form of boron. In our experiments at appropriate pressure-temperature conditions (figure 2.4.1)  $\alpha$ -B crystals grow at the expense of  $\beta$ -B and in some runs (table 2.3.1) all starting  $\beta$ -boron transforms into the  $\alpha$ -phase. Moreover, we observed direct transformation of  $\beta$ -B into

$\alpha$ -B. All mentioned observations prove that  $\alpha$ -boron is a thermodynamically stable phase. Extrapolation of the  $\alpha$ -/ $\beta$ -B boundary to ambient pressure (figure 2.4.1) also suggests that  $\alpha$ -boron is the thermodynamically stable low-temperature boron phase below  $\sim 970$  K. The linear extrapolation is totally justified by considering a potential phase diagram of the unary boron system. Indeed, knowing one point on the coexistence line in the fundamental property diagram one can determine the direction of the line by applying the Gibbs-Duhem relation to both phases using the fact that  $dT$ ,  $dP$  and  $d\mu_A$  must be the same in both phases if they still coexist:

$$d\mu_A = -S_\alpha dT + V_\alpha dP$$

$$d\mu_A = -S_\beta dT + V_\beta dP,$$

where  $\mu_A$  is the chemical potential of boron,  $S_\alpha$ ,  $S_\beta$  – molar entropies and  $V_\alpha$ ,  $V_\beta$  – molar volumes of  $\alpha$ - and  $\beta$ -B, correspondingly.

This system of equations above defines the direction of the  $\alpha + \beta$  coexistence line in the fundamental property diagram. The direction of the projected line in the  $PT$  phase diagram, i.e. the  $\alpha + \beta$  phase field, is obtained by eliminating  $d\mu_A$  from the Gibbs-Duhem relations:

$$dP = \frac{S_\alpha - S_\beta}{V_\alpha - V_\beta} dT.$$

Except for very low temperatures the equilibrium line is almost a straight line because the differences in  $S$  and  $V$  stay rather constant for solid phases.

Previously reported difficulties and even failure to synthesize  $\alpha$ -B at ambient pressure could be explained based on the phase diagram we have experimentally constructed (figure 2.4.1):  $\alpha$ -B is stable below about 1000 K and strictly speaking, should not crystallize from metallic fluxes with the eutectic point at temperature above  $\sim 1100$  K. However, according to the Ostwald step rule at conditions not far from equilibrium not the most stable but the least stable polymorph that crystallizes first (Niemycki & Zawadzki 1962), so that  $\alpha$ -B may appear if a boron-rich metallic flux solidified at relatively low temperature (Greenwood 1973). Transformation of  $\beta$ -B or amorphous boron into the  $\alpha$ -phase requires very significant rearrangement and/or rupture of  $B_{12}$  icosahedra. It is impossible to activate such a rearrangement at relatively low temperatures (below 1000 K) in the field of stability of  $\alpha$ -B. With a pressure increase the temperature stability field of  $\alpha$ -boron increases and, as we demonstrated in a DAC experiment, it becomes possible to realize the direct  $\beta$ -to- $\alpha$ -B transition.

Theoretical works (van Setten *et al.* 2007; Widom & Mihalkovič 2008; Ogitsu *et al.* 2009) suggesting that  $\beta$ -B is the ground state of boron are not supported by our experimental observations. The phase diagram drawn by Oganov *et al.* (2009) is schematic and based on only a few experimental points related to the HPHT synthesis conditions of  $\beta$ -B. The authors (Oganov *et al.* 2009) sketched the  $\alpha$ -/ $\beta$ -B phase boundary in accordance with the theoretical data of van Setten *et al.* (van Setten *et al.* 2007) and consequently suggested that  $\beta$ -B is stable down to 0 K at ambient pressure at odds with our experimental data. Combining *ab initio* pseudopotential calculations and some experimental data (Grüneisen parameters, particularly), Masaga *et al.* (2006) and Shirai *et al.* (2007) estimated the phase boundary between  $\alpha$ - and  $\beta$ -phases and apparently found that  $\alpha$ -B is more stable below about 1000 K, in good agreement with our experimental results. However, these authors calculated total energy of  $\beta$ -B using an ideal, defects free structural model which contradicts available experimental crystallographic data. Such a simplification of the structure of  $\beta$ -B in calculations could result in “underestimating”  $\beta$ -boron stability compared to other calculations (van Setten *et al.* 2007); i.e. the agreement with the experimental results could be reached just by chance, because indeed, according to the works of van Setten *et al.* (2007), Widom & Mihalkovič (2008), and Ogitsu *et al.* (2009), structural defects in  $\beta$ -B play a key role in stabilization of the phase. Thus, our results call for further detailed theoretical investigations related to stability of boron polymorphs.

A phase diagram, as a projection of the fundamental property diagram, allows materials scientist indirect use of thermodynamics (Hillert 2007). It can be utilized to understand materials behaviour and propose optimal ways of their synthesis. The phase diagram of boron (figure 2.4.1) shows that  $\alpha$ -B is not only thermodynamically stable phase in a large pressure-temperature range, but it also can be reproducibly synthesized (Parakhonskiy *et al.* 2011) at conditions readily accessible by modern industry for large-scale production (like synthetic diamonds, for example).

## **2.5 Synthesis of metastable boron phases: $\delta$ - and $\varepsilon$ -boron**

### **2.5.1 Tetragonal metastable boron phase ( $\delta$ -boron)**

At pressures above 9 GPa along with the  $\gamma$ -B crystals, some needle-shaped crystals were obtained. They were grey-reddish in colour and semitransparent (figure 2.5.1.1). The size of the crystals varied from  $30 \times 2 \mu\text{m}$  to  $150 \times 5 \mu\text{m}$ . Each time the new phase was obtained

in the presence of “plate-shaped”  $\gamma$ -boron crystals (figure 2.3.1a) and never found as a single phase that points towards its metastability.

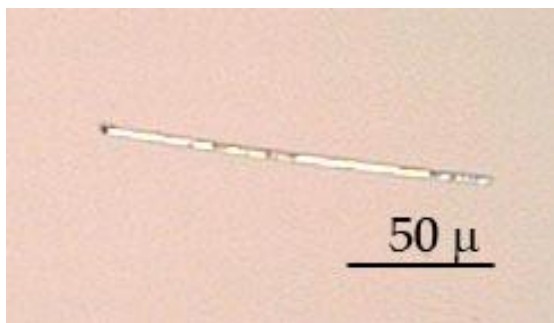


**Figure 2.5.1.1** Single crystal of T-50 (designated as  $\delta$ -B later in this work).

Single crystal X-ray diffraction data was collected at the Swiss-Norwegian Beam Line at the European Synchrotron Radiation Facility. The phase was identified as a tetragonal boron phase with the structure of T-50 (Hoard *et al.* 1958) reported in literature (figure 1.2.5.1). Interatomic B-B distances in  $B_{12}$  icosahedra are 1.715(10)–1.801(12), which well correspond to those in other boron icosahedral structures, like  $\alpha$ -boron ( $B_{12}$ ) (1.7486(4)–1.8042(4)) and  $\gamma$ -boron ( $B_{28}$ ) (1.766(3)–1.880(3)) (Zarechnaya *et al.* 2009). The chemical purity of the T-50 phase was proven by EELS. Thus, it can be designated as  $\delta$ -B in a row of the known stable  $\alpha$ -,  $\beta$ - and  $\gamma$ - polymorphs.

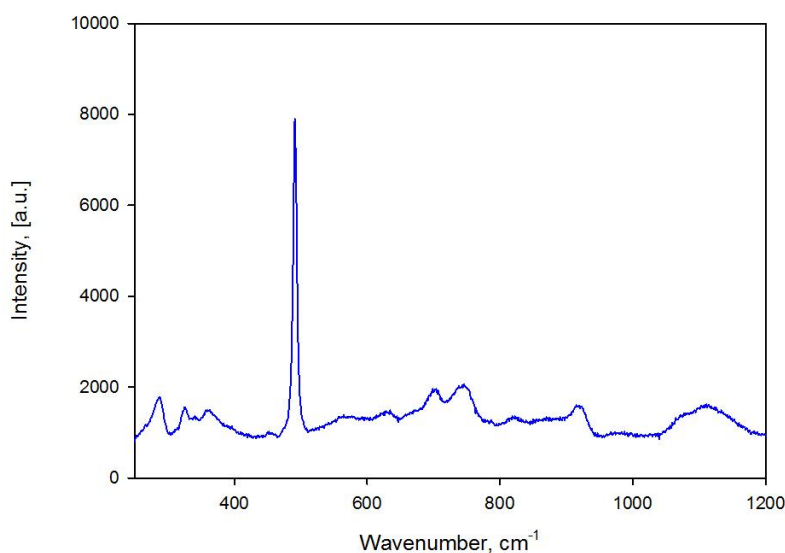


**Figure 2.5.1.2** Raman spectrum of single crystal of  $\delta$ -boron.

Raman spectrum of the synthesized crystals has one intense Raman peak at 491  $cm^{-1}$  (figure 2.5.1.2), which may serve as a fingerprint of the  $\delta$ -boron. Other peaks at 287, 325, 361, 561, 631, 703, 745, 821, 918, 1078 and 1112 ( $cm^{-1}$ ) are much less intense. Peaks at 361

$\text{cm}^{-1}$ ,  $491 \text{ cm}^{-1}$ ,  $703 \text{ cm}^{-1}$ ,  $745 \text{ cm}^{-1}$ ,  $1112 \text{ cm}^{-1}$  are presented in the spectrum of tetragonal boron, measured by Xu *et al.* from nanoribbons (Xu *et al.* 2004). The Raman spectrum reported by Qin *et al.* (2012) measured from a T-50 powder is very fuzzy and looks differently. Since the peak positions were not presented in the work of Qin *et al.*, it is not possible to compare them more precisely.

Summarising, we have confirmed reality of the tetragonal boron phase (as metastable one) whose existence was disputed for more than a half of a century. For the first time this phase was reproducibly synthesised in form of single crystals.

## 2.5.2 Newly synthesized rhombohedral metastable boron phase ( $\epsilon$ -boron)

In course of our experiments at  $P$ - $T$  conditions of 8-9 GPa and 1900-2100 K, except known boron phases, some other yellow-reddish-orange, transparent, plate-shaped crystals were obtained (figure 2.5.2.1). Sizes of these crystals vary from 20 to 150 microns. The Raman spectrum of these crystals is characterized by following peak positions:  $336 \text{ cm}^{-1}$ ,  $484 \text{ cm}^{-1}$ ,  $537 \text{ cm}^{-1}$ ,  $732 \text{ cm}^{-1}$ ,  $807 \text{ cm}^{-1}$  and  $1086 \text{ cm}^{-1}$ . It does not look similar to spectra of any other boron phases (Parakhonskiy *et al.* 2011), but akin to that of  $\text{B}_{13}\text{C}_2$ , with a small shift of about  $5 \text{ cm}^{-1}$  (fig. 2.5.2.2). EELS measurements on this phase revealed however the absence of carbon. Taking into account that the crystals were obtained only in the presence of other boron phases, this phase is likely metastable, similarly to  $\delta$ -B, and was called  $\epsilon$ -boron.

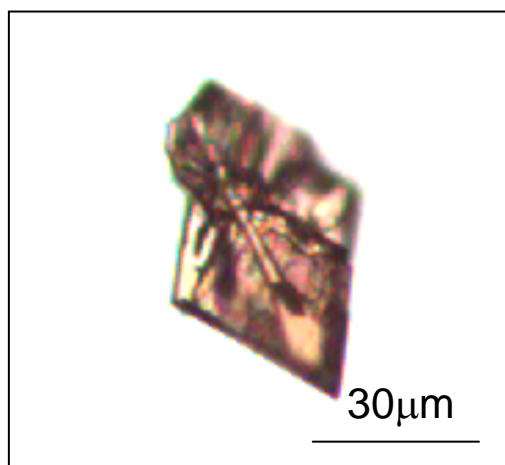


**Figure 2.5.2.1** Single crystal of the new boron phase (later designated as  $\epsilon$ -B).

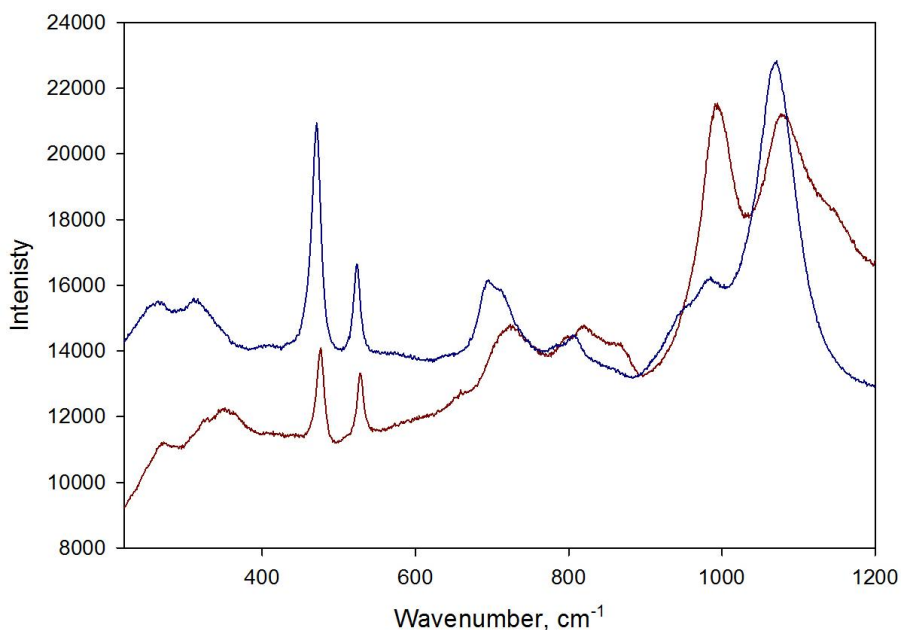


**Figure 2.5.2.2** Raman spectra of  $B_{15}$  (red) and  $B_{13}C_2$  (blue).

Single crystal X-ray diffraction revealed that this phase is isostructural to  $B_{13}C_2$  (Clark & Hoard 1943), but the carbon atom is substituted by boron in the B-C-B chain. The unit cell parameters:  $a = 5.5940(7) \text{ \AA}$ ,  $c = 12.0756(16) \text{ \AA}$ ; the space group is  $R\bar{3}m$ . The structure is similar to that of  $\alpha$ -boron described above, but compared to  $\alpha$ -B, it contains a chain of three boron atoms in the intericosahedral space (figure 2.5.2.3).

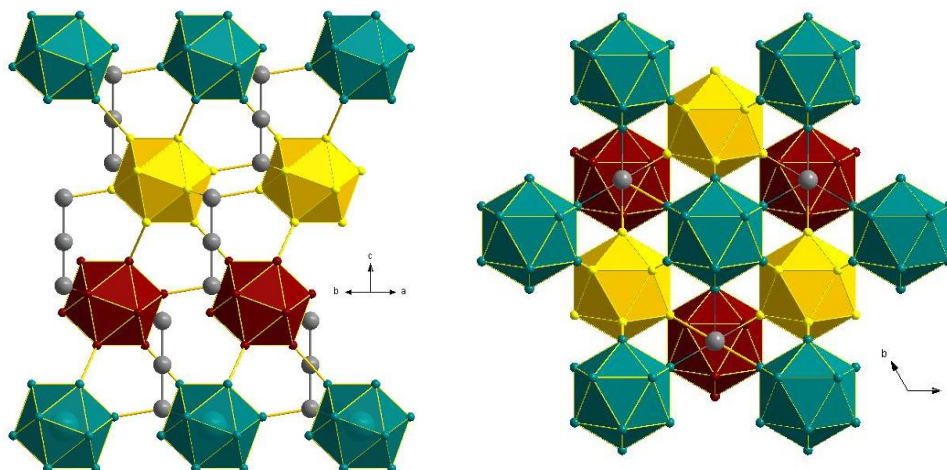


**Figure 2.5.2.3** Crystal structure of  $\epsilon$ -boron.

To study phase transformations in  $\epsilon$ -B in the field of stability of  $\gamma$ -B, an  $\epsilon$ -boron crystal along with a  $\beta$ -B crystal was loaded into a diamond anvil cell and then compressed to 11 GPa. Neon was used as a pressure transmitting medium and a ruby ball as a pressure gauge. After pressurising, both crystals were heated by laser to 2300 K. At these  $P$ - $T$

conditions pure boron must transform to the  $\gamma$ -B phase according to the phase diagram (figure 2.4.1). After heating the Raman spectra were measured again. As seen in figure 2.5.2.4, both  $\beta$ - and  $\varepsilon$ -B fully transformed to  $\gamma$ -B that may serve as an additional evidence of the pure boron composition of the  $\varepsilon$ -boron phase.

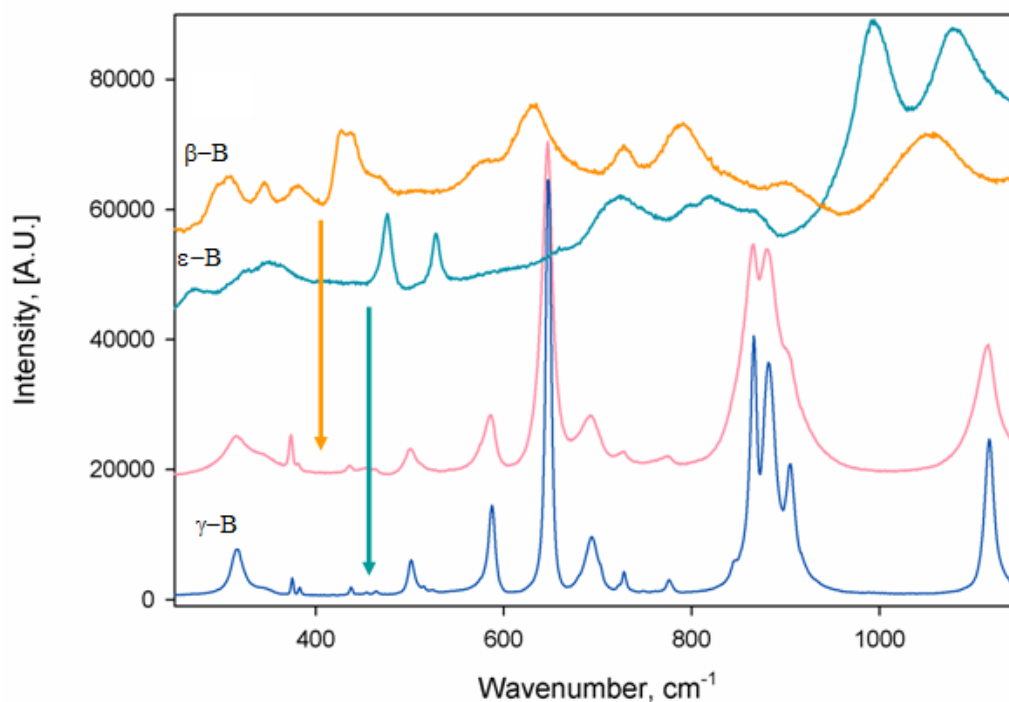


**Figure 2.5.2.4** Raman spectra of  $\varepsilon$ - and  $\beta$ -boron crystals taken in a DAC before (upper two curves) and after (lower two curves) laser heating to 2300 K at 11 GPa.

**Table 2.5.2.1** Summary of high-pressure high-temperature experiments on boron, conducted in a multi-anvil press in addition to the previous (**Table 2.3.1**). Heating duration in every experiment was 5 minutes. (Typical uncertainty in temperature is  $\pm 40$  K and 0.5 GPa in pressure. In a synthesis product initial non-transformed  $\beta$ -boron powder and platinum boride are not mentioned).

Experiment	Starting material	Experimental conditions			Synthesis results
		capsule material	temperature, K	pressure, GPa	
S4805	85 at.% $\beta$ -B + 15 at.% Pt	Au	1773	9.5	$\gamma$ -B, $\delta$ -B
H3154	85 at.% $\beta$ -B + 15 at.% Pt	Au	1773	10.5	$\gamma$ -B, $\delta$ -B
S5064	$\beta$ -B	Pt	1923	7.5	$\alpha$ -B, $\gamma$ -B, $\beta$ -B, $\delta$ -B

S5110	$\beta$ -B	Pt	1373	14.5	$\delta$ -B, $\gamma$ -B
S5150	$\beta$ -B	Pt	1673	13	$\delta$ -B, $\gamma$ -B
S5166	$\beta$ -B	Pt	1673	14	$\delta$ -B, $\gamma$ -B
S5231	$\beta$ -B	Pt	1573	16	$\delta$ -B, $\gamma$ -B
S5225	$\beta$ -B	Pt	1873	16	$\gamma$ -B
S5194	$\beta$ -B	Pt	1573	18	$\gamma$ -B
S5206	$\beta$ -B	Pt	1923	18	$\gamma$ -B
S5187	$\beta$ -B	Pt	2073	18	$\gamma$ -B
S5063	$\beta$ -B	Pt	1873	8.5	$\gamma$ -B, $\epsilon$ -B
S5053	$\beta$ -B	Pt	2023	8.5	$\gamma$ -B, $\epsilon$ -B
S5027	$\beta$ -B	Pt	1873	9	$\gamma$ -B, $\epsilon$ -B
S5062	$\beta$ -B	Pt	1973	9	$\gamma$ -B, $\epsilon$ -B
S5084	$\beta$ -B	Pt	2073	9	$\gamma$ -B, $\beta$ -B, $\epsilon$ -B
S5080	$\beta$ -B	Pt	2123	9	$\gamma$ -B, $\beta$ -B
S5090	$\beta$ -B	Pt	2023	10	$\gamma$ -B
S5095	$\beta$ -B	Pt	1873	10	$\gamma$ -B, $\delta$ -B
S5103	$\beta$ -B	Pt	1773	10	$\gamma$ -B, $\delta$ -B
S5148	$\beta$ -B	Pt	1423	13	$\gamma$ -B, $\delta$ -B
S5123	$\beta$ -B	Pt	1323	13	$\gamma$ -B, $\delta$ -B
S5169	$\beta$ -B	Pt	1473	14	$\gamma$ -B, $\delta$ -B
S5073	$\beta$ -B	Pt	2323	9.5	$\gamma$ -B, $\beta$ -B

Table 2.5.2.1 summarizes HPHT experiments conducted with the purpose of synthesis of metastable boron phases. Based on these results, a new version of the boron phase diagram, which included metastable phases, was drawn (figure 2.5.2.5).

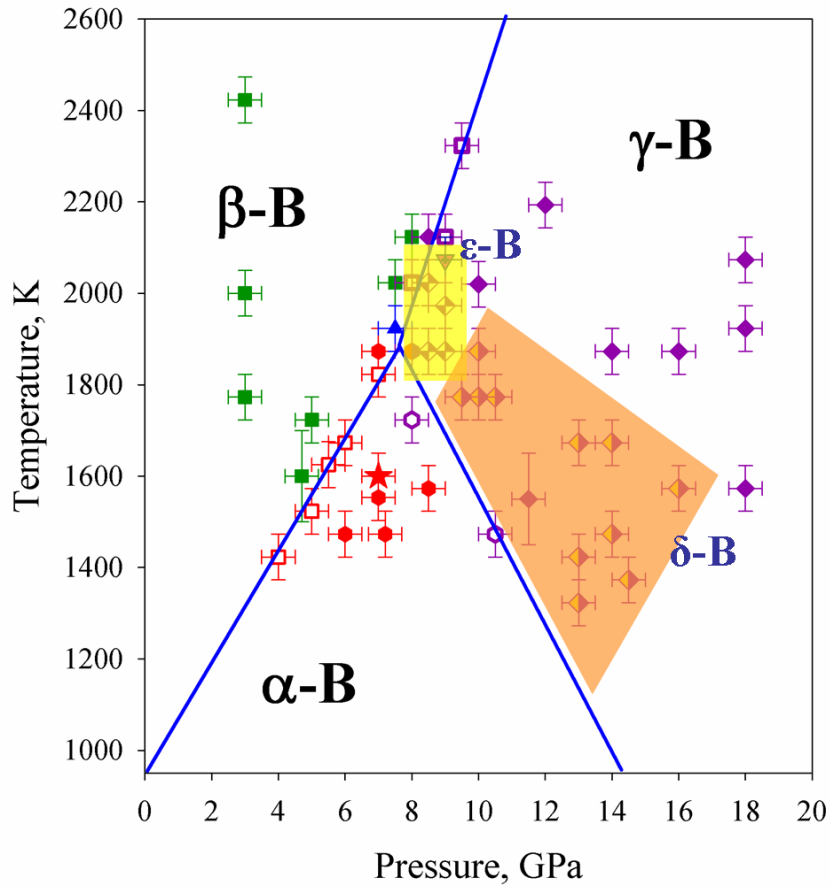


**Figure 2.5.2.5** The pressure-temperature phase diagram of boron. P-T conditions at which crystallisation of various boron phases occurred are marked by different signs: green squares –  $\beta$ -boron; purple diamonds –  $\gamma$ -boron; red hexagons –  $\alpha$ -boron; open red squares -  $\alpha$ - and  $\beta$ -boron; open purple squares -  $\beta$ - and  $\gamma$ -boron; open purple hexagons -  $\alpha$ - and  $\gamma$ -boron; blue triangle –  $\alpha$ -,  $\beta$ -, and  $\gamma$ -boron; red triangle –  $\epsilon$ -,  $\beta$ -, and  $\gamma$ -boron; the red star marks the conditions of the multi-anvil experiment which led to the solid-solid  $\beta$ -to- $\alpha$ -B phase transition; continues blue lines show apparent phase boundaries. Hour-glass rhombuses in the yellow area and semi-filled rhombuses in the orange area mark PT conditions of experiments when correspondingly single crystals of  $\epsilon$ -B and  $\delta$ -B were synthesized.

Measured microhardness of  $\epsilon$ -boron is  $H_V \approx 55$  GPa. An experiment in a diamond anvil cell showed the kinetic stability of  $\epsilon$ -boron at room temperature up to 62 GPa. These important properties of the newly synthesised material may be useful for prospective applications.

### 3 LIST OF MANUSCRIPTS AND STATEMENT OF AUTHORS CONTRIBUTION

[1]. G. Parakhonskiy, N. Dubrovinskaia, L. Dubrovinsky, S. Mondal, and S. van Smaalen, High pressure synthesis of single crystals of  $\alpha$  boron. *Journal of Crystal Growth* **321**, 162-166 (2011).

Single crystals of  $\alpha$ -boron were synthesized by Gleb Parakhonskiy (G.P.). Raman spectroscopy was performed by G.P. X-Ray diffraction experiments were conducted by G.P. and Swastik Mondal (S.M.). Structure was solved and refined by S.M. and Sander van Smaalen. Leonid Dubrovinsky (L.D.) and Natalia Dubrovinskaia (N.D.) supervised the work. G.P, L.D and N.D. wrote the manuscript.

[2]. G. Parakhonskiy, N. Dubrovinskaia, E. Bykova, R. Wirth, and L. Dubrovinsky, Experimental pressure-temperature phase diagram of boron: resolving the long-standing enigma. *Scientific Reports* **1**, 1-7 (2011) DOI: 10.1038/srep00096.

G.P. made the high-pressure synthesis, and phase identification by X-ray diffraction and Raman spectroscopy. Elena Bykova (E.B.) performed the structure refinement based on single crystal X-ray data. Richard Wirth (R.W.) performed the TEM and EELS analysis. G.P., L.D., and N.D. interpreted the results and wrote the paper. L.D. and N.D. supervised the work.

[3]. G. Parakhonskiy, V. Vtech, N. Dubrovinskaia, R. Caracas and L. Dubrovinsky, Raman spectroscopy investigation of  $\alpha$ -boron at elevated pressures and temperatures. *J. Sol. State Com.*, **154**, 34-39 (2013).

G.P and Vojtech Vtech (V.V.) conducted high pressure spectroscopy experiments. G.P., V.V, N.D and L.D performed the data analysis. Razvan Caracas (R.C.) performed *ab initio* calculations of Raman spectra. G.P., N.D. and L.D interpreted the results. G.P, L.D, and N.D. wrote the manuscript.

[4]. G. Parakhonskiy, N. Dubrovinskaia, E. Bykova, R. Wirth, and L. Dubrovinsky. "High pressure synthesis and investigation of single crystals of metastable boron phases." *Submitted to J. High Press. Res.*

Single crystals were synthesized by G.P. The Raman spectroscopy and the phase analysis was performed by G.P. The structure solution and refinement were made by E.B. Data analysis was performed by G.P., N.D. and L.D. The TEM measurements were made by R.W. Work was supervised by N.D. and L.D. G.P. wrote the manuscript.

## 4 MANUSCRIPTS

### 4.1 High pressure synthesis of single crystals of $\alpha$ -boron

Gleb Parakhonskiy,<sup>a</sup> Natalia Dubrovinskaia,<sup>b,c</sup> Leonid Dubrovinsky,<sup>a</sup> Swastik Mondal,<sup>c</sup> and Sander van Smaalen<sup>c</sup>

<sup>a</sup> *Bayerisches Geoinstitut, Universität Bayreuth, D-95440 Bayreuth, Germany*

<sup>b</sup> *Mineralphysik und Strukturforchung, Mineralogisches Institut, Universität Heidelberg, D-69120 Heidelberg, Germany*

<sup>c</sup> *Lehrstuhl für Kristallographie, Physikalisches Institut, Universität Bayreuth, D-95440 Bayreuth, Germany*

*Published in Journal of Crystal Growth, 321(1), 162-166 (2011)*

#### 4.1.1 Abstract

A method of synthesis of single crystals of alpha-boron ( $\alpha$ -B) is presented.  $\alpha$ -Boron has been crystallized from a boron-platinum melt at high pressures (6-11 GPa) and high temperatures (1200-1600 °C). The method is based on the high-pressure large volume (multi-anvil) press technique. An average size of the as-grown isometric crystals is 60  $\mu\text{m}$  to 80  $\mu\text{m}$  in maximum dimension. A refinement of an accurate crystal structure of  $\alpha$ -B against single-crystal X-ray diffraction data demonstrates the excellent quality of the single crystals. The crystal structure is in good agreement with the literature.

#### 4.1.2 Introduction

Boron-rich compounds are very attractive materials for research because of their unique physical properties suitable for many applications. They are widely used in thermally stable glasses and ceramics. Boron-containing reagents are used for synthesis of organic compounds, including intermediates to pharmaceuticals. The variety of applications of boron compounds all over the world is uncountable [1].

There are two polymorphs of pure crystalline boron obtained at normal pressure:  $\alpha$ -rhombohedral boron and  $\beta$ -rhombohedral boron ( $\beta$ -B); recently a new high pressure high temperature boron phase, orthorhombic  $\gamma$ -B<sub>28</sub>, was synthesized [2]. The most easily available

modification of boron is the  $\beta$ -B phase that can be purchased or relatively easy obtained in a chemical laboratory.

For the first time amorphous boron was obtained in 1808 via reduction of boron oxide  $B_2O_3$  or boric acid  $B(OH)_3$  with potassium [2]. Later it was found that amorphous boron could be obtained not only by means of chemical reactions, but also in the process of electrolysis [2]. It took time until 1958, when a way of synthesis of pure boron in a crystalline form [3] was found. It was observed that the product of the pyrolytic decomposition of  $BI_3$  on a surface heated at 800-1000 °C contained a crystalline modification of boron [3] with a simple rhombohedral structure ( $\alpha$ -boron). Tantalum, tungsten and boron nitride have all been used successfully as substrates on which decomposition of the boron iodide or boron hydride occurred resulting in synthesis of single crystals of  $\alpha$ -boron. Above 1500 °C those crystals transformed to the structurally more complex  $\beta$ -rhombohedral form [3]. In 1959 single crystals of  $\alpha$ -boron were made by crystallizing amorphous boron in a platinum melt [4]. After a few reports in the 1950s and 1960s [3-5], see also [2] for review) there was a long time of the absence of any references to synthesis of single crystals of  $\alpha$ -boron. There is a very recent report on studying microcrystalline samples of  $\alpha$ -B consisting of single crystals “prepared by recrystallization from solution of isothermal saturation of molten palladium-boron alloys, using a vapour source of boron” [6-7]. Unfortunately, it is not clear from the publication, when the crystals were synthesised, and the paper [7] does not contain a detailed description of the procedure, which could allow reproducing the synthesis.

In the present work in a series of experiments we have reproducibly obtained single crystals of pure  $\alpha$ -boron using  $\beta$ -boron as a starting material. Our synthesis was realised at high pressures, while all previous methods of  $\alpha$ -boron synthesis were based on techniques realised at ambient pressure. Obtained single crystals were investigated by means of the Raman spectroscopy and X-ray diffraction.

### **4.1.3 Experimental**

#### **4.1.3.1 Sample preparation**

Highly crystalline  $\beta$ -boron (purity of 99.995 at.%, grain size of  $<1000 \mu m$ ), purchased from *Chempur Inc.*, was used as a source of boron. Either pure  $\beta$ -B was loaded into a Pt capsule, or a mixture of  $\beta$ -B and Pt powders (in proportion of 85:15 wt. %, Table 4.1.3.1) was loaded into a gold capsule. The capsules were made from Pt or Au tubes.

**Table 4.1.3.1** Summary of experiments on synthesis of single crystals of the rhombohedra  $\alpha$ -boron phase. All synthesis products contain additionally platinum boride.

Experiment	Starting material	Experimental conditions				HP assembly	Synthesis products
		capsule material	temperature, °C	pressure, GPa	heating time, min		
H3161	85 at.% $\beta$ -B + 15 at.% Pt	Au	1200	10.5	5	18/11	$\alpha$ -B, B <sub>28</sub>
H3170	85 at.% $\beta$ -B + 15 at.% Pt	Au	1200	7.2	5	18/11	$\alpha$ -B, $\beta$ -B
S4894	$\beta$ -B	Pt	1600	7	5	25/15	$\alpha$ -B, $\beta$ -B
H3255	$\beta$ -B	Pt	1300	8.5	3	18/11	$\alpha$ -B, $\beta$ -B
H3271	$\beta$ -B	Pt	1400	6	5	18/11	$\alpha$ -B, B <sub>28</sub> , recrystallized $\beta$ -B
H3273	$\beta$ -B	Pt	1200	6	5	18/11	$\alpha$ -B, $\beta$ -B
H3286	$\beta$ -B	Pt	1300	8	5	18/11	$\alpha$ -B, B <sub>28</sub>

#### 4.1.3.2 Synthesis technique

Synthesis was realised at various pressure-temperature conditions using 1000-ton (Hymag) and 1200-ton (Sumitomo) multi-anvil hydraulic presses. The synthesis technique is similar to that described in details in our previous publications [8-10] The Kawai-type multi-anvil system employs six tool-steel outer anvils and eight tungsten carbide cubic inner anvils to focus an applied load on an octahedral high-pressure chamber formed as a result of corner truncations on the inner-anvils. By varying the corner truncation size of the inner-anvils, various pressures can be attained. An octahedron made of magnesium oxide that matches the pressure chamber was used as a pressure transmitting medium. A cross-section of the octahedron is shown in Figure 4.1.3.2.1. In our experiments 18/11 (the edge-length of an octahedron /anvil truncation edge-length, in millimeters) assemblies for pressures of 7-11 GPa and 25/15 assemblies for pressures of 5-8 GPa were used. Although a clear advantage of large

assemblies is the increase of the amount of synthesized material, reaching very high temperatures in large assemblies is more difficult. In our experiments temperature was increased stepwise with a speed of about 80 K/min. Duration of heating was 5 or 3 minutes. Then the sample was quenched.

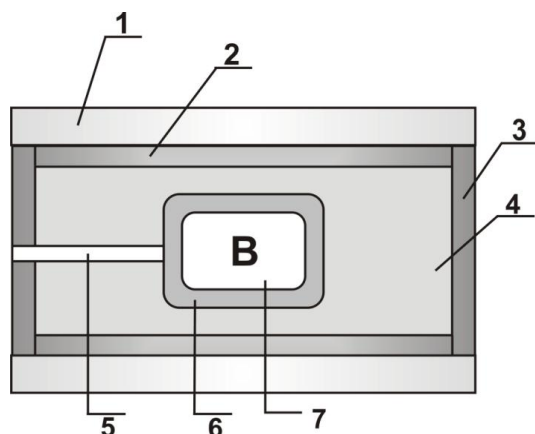


**Figure 4.1.3.2.1** A cross-section of the pressure chamber (not scaled), which is enclosed into the MgO octahedron (not shown). The capsule size is 4/4/0.3 mm (length/ outer diameter/ thickness of a metallic tube used for the capsule) in the 25/15 assembly and 3.5/2/0.5 mm in the 18/11 assembly. (1) ZrO<sub>2</sub> tube; (2) heater; (3) Mo disc (4) MgO; (5) cylindrical hole for a thermocouple; (6) capsule; (7) sample.

#### 4.1.3.3 Analytical techniques

For the phase identification, selection of single crystals, and preliminary structural analysis a high-brilliance Rigaku diffractometer (Mo- $K\alpha$  radiation) equipped with Osmic focusing X-ray optics and Bruker Apex CCD detector was used. The diffraction patterns were processed using Fit2D software[11].

The refinement of the crystal structure of  $\alpha$ -boron at room temperature was carried out using the X-ray diffraction data collected on a MAR345 Imaging Plate diffractometer [12]. Refinement of the lattice parameters and data reduction were performed by EVAL15 [13] and SADABS [14].

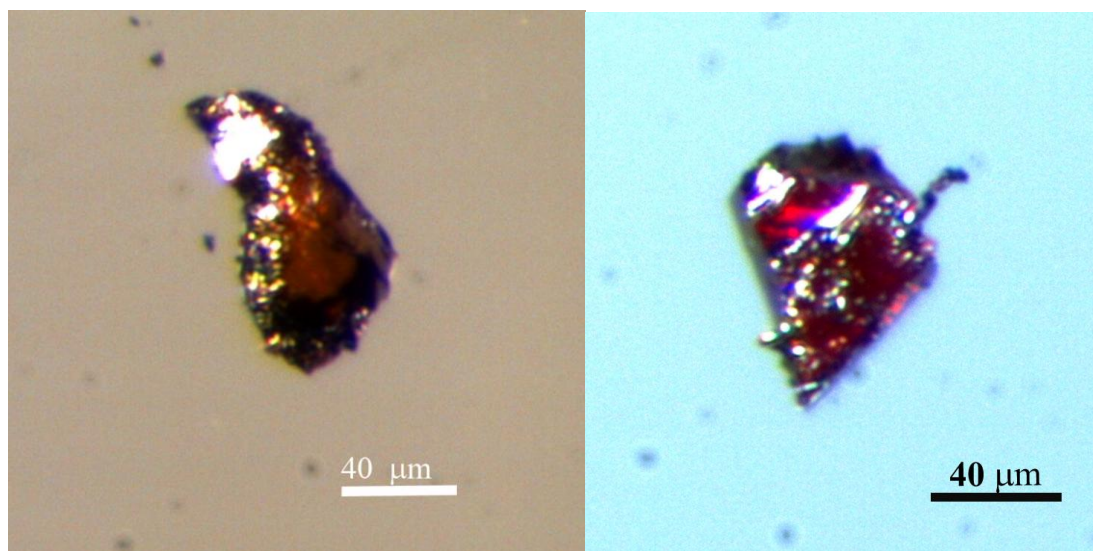
A LabRam spectrometer (with a resolution of 2 cm<sup>-1</sup>), a He-Ne laser (632.8 nm) with a power of 15 mW for excitation, and a 50 $\times$  objective were used for the Raman scattering experiments.

The morphology and chemical composition of the synthesized samples of single crystals were studied by means of the scanning electron microscopy (SEM) (LEO-1530). Chemical purity of the samples was confirmed using WDX microprobe analysis (JEOL JXA-8200; focused beam; 20 keV, 20 nA).

#### 4.1.4 Results and discussion

Experiments on synthesis of single crystals of  $\alpha$ -boron were conducted at pressures of 6 to 11 GPa and at temperatures of 1200 to 1600 °C (Table 4.1.3.1). After extracting from the octahedron, the sample in a gold or platinum capsule was first immersed for several minutes into *aqua regia* to remove the most part of the capsule material. The resulting product was crushed up using tungsten carbide cubes as anvils to get crystals for further investigations.

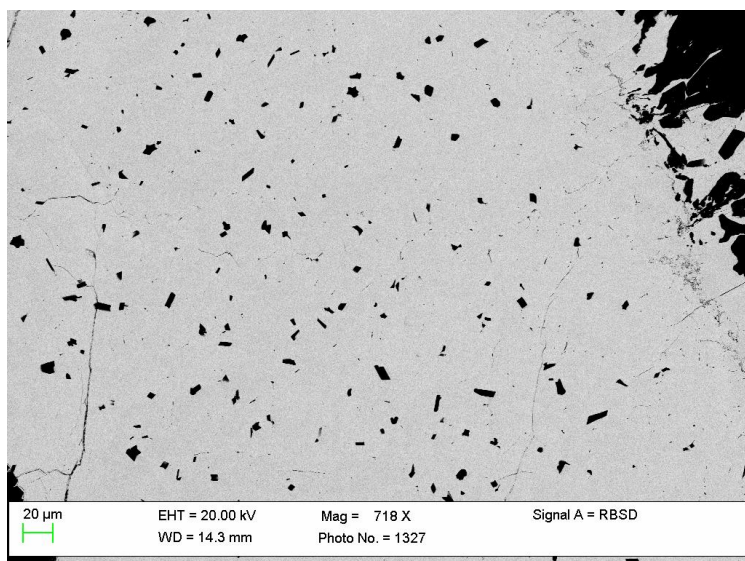
The  $\alpha$ -boron is known as a material of red or maroon colour [2]. Tiny crystals (Figure 4.1.4.1) of this characteristic colour extracted from the capsule were identified as  $\alpha$ -boron using Raman spectroscopy. This phase identification was confirmed by X-ray diffraction. The colour of the crystals varied from light red to deep red and yellowish depending on the size of the crystals and experimental conditions. The quality of crystals was different in different experiments. The crystals of the best quality were obtained in experiments conducted in a platinum capsule with pure  $\beta$ -B as a precursor. Deteriorated quality of the crystals obtained from a mixture of  $\beta$ -B and a Pt powder may be related to possible contaminations of platinum by platinum oxide (usual for “platinum black” used in our experiments). Due to frailness of the crystals, they can be easily fragmented, but the average size of the rather isometric intact crystals is of about 60 to 80  $\mu\text{m}$  (Figure 4.1.4.1).



**Figure 4.1.4.1** As-grown single crystals of  $\alpha$ -boron (experiment S4894) viewed in the optical microscope.

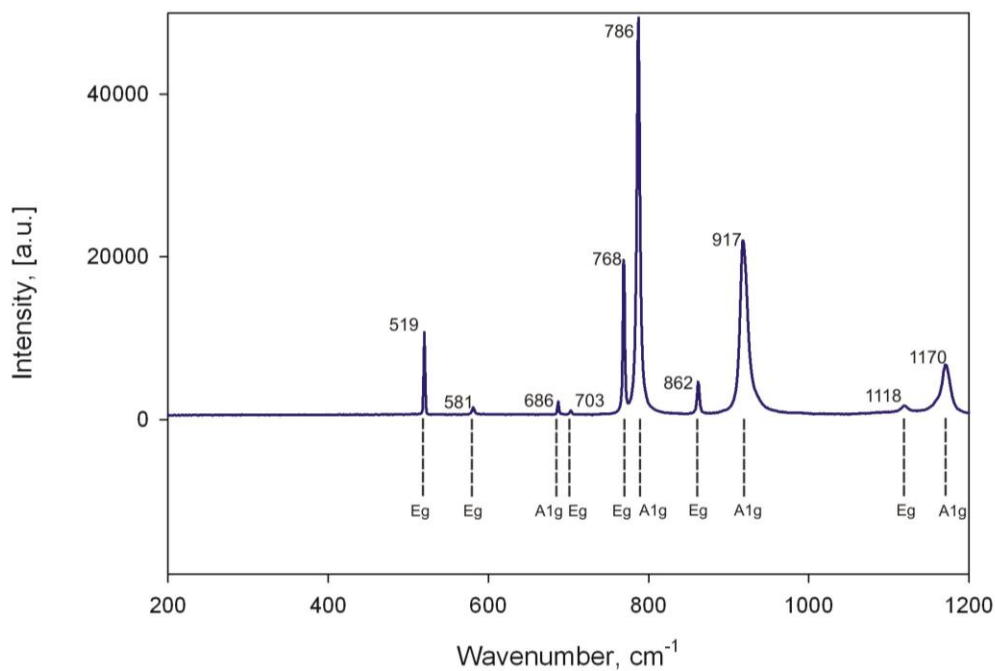
Synthesised  $\alpha$ -boron is a result of recrystallization from a boron-platinum melt at high pressures and high temperatures. The melting point of pure boron is 2300 °C, but the boron-platinum system is known to have a low melting eutectic [5] that results in a considerable

decrease of the melting temperature even at high pressure and a possibility for the synthesis at temperatures as low as 1200 °C. The grown crystals could be observed in the metallic matrix (Figure 4.1.4.2).



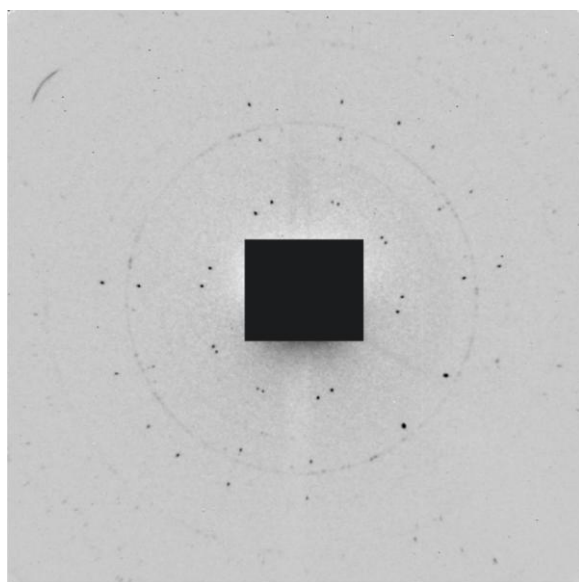
**Figure 4.1.4.2** SEM image of  $\alpha$ -boron crystals grown in the metallic matrix.

An example of a typical Raman spectrum from single crystals of  $\alpha$ -B is shown in Figure 4.1.4.3 that is in agreement with the Raman spectra of  $\alpha$ -B reported in literature [15, 16]. The spectrum is characterised by a number of pronounced Raman peaks at 519, 581, 686, 703, 768, 786, 862 and 917 ( $\text{cm}^{-1}$ ) (Figure 4.1.4.3). The vibrational modes with the wavenumbers of 1118  $\text{cm}^{-1}$  and 1170  $\text{cm}^{-1}$  could be classified as intericosahedral. The modes between 500 and 950  $\text{cm}^{-1}$  are intraicosahedral [14, 15].



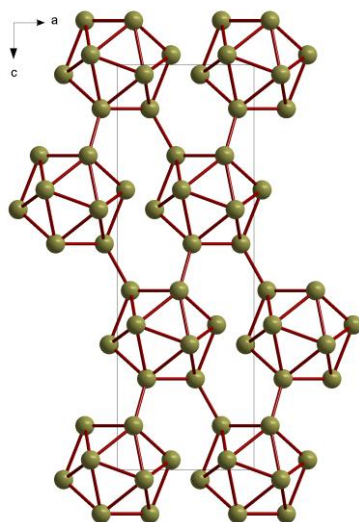
**Figure 4.1.4.3** A typical Raman spectrum obtained from single crystals of  $\alpha$ -boron.

Figure 4.1.4.4 presents a 2D X-ray diffraction pattern obtained in a  $360^\circ$   $\chi$ -rotational scan for the collection time of 300 s using the Rigaku high-brilliance diffractometer. The diffraction of  $\alpha$ -B is presented by individual spots which confirmed that we had a single crystal.



**Figure 4.1.4.4** A 2D X-ray diffraction pattern of an  $\alpha$ -boron single crystal obtained in a  $360^\circ$   $\chi$ -rotational scan for 300 s collection time using the Rigaku high-brilliance diffractometer (Mo- $K\alpha$  radiation). All spots are from the  $\alpha$ -B single crystal and diffraction lines and arcs are from platinum boride.

The structure of  $\alpha$ -boron is simplest of all boron modifications. It consists of  $B_{12}$  icosahedral units simply arranged in a trigonal unit cell (space group R-3m, Z=36 in hexagonal setting) [2, 17]. The refinement of the crystal structure of  $\alpha$ -boron at was carried out using the data collected at room temperature from a crystal with dimensions of  $0.08 \times 0.04 \times 0.03 \text{ mm}^3$ . Initial coordinates of the two crystallographically independent boron atoms were taken from the literature [18]. The crystal structure along with the atom numbering scheme are presented in Figures 4.1.4.5 and 4.1.4.6, which were prepared using the program DIAMOND [19]. An independent spherical atom refinement on F was performed using the computer program JANA2006 [20]. The final refinement with 15 parameters, including an isotropic extinction parameter, results in a good fit to the diffraction data (Table 4.1.4.1). The present crystal structure is in agreement with that reported in the literature [18, 21-23] (Table 4.1.4.2).



**Figure 4.1.4.5** Perspective view of the  $\alpha$ -boron structure showing the packing of the icosahedral building blocks; viewed along the  $b$ -axis of the hexagonal unit cell.

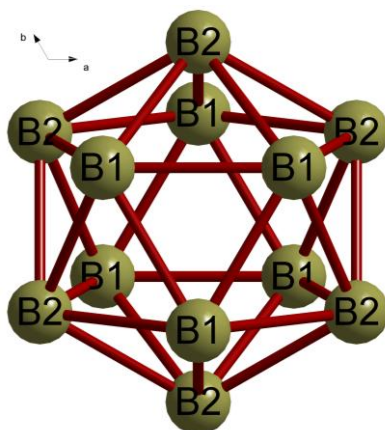


**Figure 4.1.4.6** Perspective view of one boron icosahedron (a building block of the  $\alpha$ -boron structure) along the  $c$ -axis. It is formed by only two crystallographically independent boron atoms present in  $\alpha$ -boron that are labelled as B1 and B2.

**Table 4.1.4.1** Crystallographic parameters for  $\alpha$ -boron obtained in the present study and details of the structure refinement.

Formula	B
Space group	R-3m, Trigonal
Z	36
$a$ (Å)	4.9065(4)
$c$ (Å)	12.5658(5)
Volume (Å <sup>3</sup> )	261.98(3)
$F(000)$	180
Temperature (K)	293
Wavelength (Å)	0.70159
Crystal dimensions (mm <sup>3</sup> )	0.08 × 0.04 × 0.03
$R_{int}$	0.0353
$[\text{Sin}(\theta)/\lambda]_{\text{max}}$ (Å <sup>-1</sup> )	0.9448
Density (g cm <sup>-3</sup> )	2.4659
Absorption coefficient (mm <sup>-1</sup> )	0.091
Observed Criteria	$I > 3\sigma(I)$
No. of observed/unique/total reflections	219/238/3381
<i>ISAM</i> refinement	
$R_F(\text{obs/all})$	0.0275/0.0304
$wR_F(\text{obs/all})$	0.0453/0.0457
$GoF(\text{obs/all})$	3.17/3.28

**Table 4.1.4.2** The data on the crystal structure and the unit cell parameters of  $\alpha$ -B obtained in the present study in comparison with the literature data.

	This Study	Ref. 20	Ref. 17	Ref. 21	Ref. 22
$a$ , Å	4.9065(4)	4.9179	4.9179	4.9075(9)	4.927(3)
$c$ , Å	12.5658(5)	12.5805	12.5805	12.559(3)	12.564(7)
$V$ , Å <sup>3</sup>	261.98(3)	263.5	263.50	261.94	264.13
B1, $x$	0.11880(6)	0.11886	0.11886(1)	0.11892(3)	0.1187(2)

B1, <i>z</i>	0.89125(4)	0.89133	0.89133(1)	0.89122(2)	0.8912(1)
B2, <i>x</i>	0.19678(7)	0.19686	0.19686(1)	0.19688(3)	0.1965(2)
B2, <i>z</i>	0.0242484)	0.02432	0.02432(1)	0.02428(2)	0.0243(1)
$R_{F(\text{obs})}$	0.0275	0.144	0.0196	0.022	0.062

#### 4.1.5 Conclusion

In a series of experiments we have shown a feasibility of obtaining single crystals of  $\alpha$ -boron of a good quality at high pressures and high temperatures. Single crystals of  $\alpha$ -boron were synthesised from  $\beta$ -boron as a starting material. Such a way of synthesis has not been described in literature. Crystal structure was refined from single crystal X-ray diffraction data in good agreement with the literature.

#### Acknowledgments

We thank the German Science Foundation (DFG) for financial support through the DFG priority programs, SPP1236 and SPP1178. GP thanks E. Yu. Zarechnaya for usefull suggestions regarding the HP synthesis technique.

#### References

1. Boron Rich Solids. Eds.:N. Orlovskaya & M. Lugovy, Springer, 2011, 375 p.
2. B. Albert, H. Hillebrecht, Boron: elementary challenge for experimenters and theoreticians, *Angew. Chem. Int. Ed.* 48 (46) (2009) 8640–8668.
3. E.Yu. Zarechnaya, N. Dubrovinskaia, L. Dubrovinsky, Y. Filinchuk, D. Chernyshov, V. Dmitriev, Growth of single crystals of B<sub>28</sub> at high pressures and high temperatures, *J. Cryst. Growth* 312 (2010) 3388–3394.
4. L.V. McCarty, J.S. Kasper, F.H. Horn, B.F. Decker, A.F. Newkirk, A new crystalline modification of boron, *J. Am. Chem. Soc.* 80 (1958) 2592.
5. F. H. Horn, On the crystallization of simple rhombohedral boron from platinum, *J. Electrochem. Soc.* 106 (1959) 905-906.
6. E Amberger, W Dietze, Zur Bildung von  $\alpha$ -rhomboedrischem, rotem Bor, *Z. Anorg. Allg. Chem.* 332 (1964) 131-139.
7. A. Polian, S. Ovsyannikov, M. Gauthier, P. Munsch, J.-C. Chervin, and G. Lemarchand, in *High pressure crystallography: from fundamental phenomena to Technological Applications*, edited by E. Boldyreva and P. Dera, NATO Science for

- Peace and Security Series B: Physics and Biophysics XIV (Springer, Dordrecht, Netherlands, 2010), pp. 241–250.
8. A. Polian, J.C. Chervin, P. Munsch, M. Gauthier,  $\alpha$ -Boron at very high pressure: structural and vibrational properties, *J. Phys.: Conf. Ser.* 121 (2008) 042017.
  9. E.Yu. Zarechnaya, L. Dubrovinsky, N. Dubrovinskaia, N. Miyajima, Y. Filinchuk, D. Chernyshov, V. Dmitriev, Synthesis of an orthorhombic high pressure boron phase, *Sci. Technol. Adv. Mater.* 9 (2008) 044209.
  10. E.Yu. Zarechnaya, L. Dubrovinsky, N. Dubrovinskaia, Y. Filinchuk, D. Chernyshov, V. Dmitriev, N. Miyajima, A. El Goresy, H.F. Braun, S. Van Smaalen, I. Kantor, A. Kantor, V. Prakapenka, M. Hanfland, A.S. Mikhaylushkin, I.A. Abrikosov, S.I. Simak, Superhard semiconducting optically transparent high pressure phase of boron, *Phys. Rev. Lett.* 102 (2009) 185501.
  11. E.Yu. Zarechnaya, N. Dubrovinskaia, L. Dubrovinsky, Y. Filinchuk, D. Chernyshov, V. Dmitriev, Growth of single crystals of B<sub>28</sub> at high pressures and high temperatures, *J. Cryst. Growth*, 312 (2010) 3388–3394.
  12. A.P. Hammersley, *ESRF Internal Report*, ESRF98HA01T, FIT2D V9.129 Reference Manual V3.1 (1998); A. P. Hammersley, S. O. Svensson, M. Hanfland, A. N. Fitch, and D. Häusermann, "Two-Dimensional Detector Software: From Real Detector to Idealised Image or Two-Theta Scan", *High Pressure Research* 14 (1996) 235-248.
  13. Klein, C. *MAR345DTB*. Version 2.2.0. Marresearch GmbH, Norderstedt, Germany, (2003)
  14. A.M.M. Schreurs, X. Xian and L.M. J. Kroon-Batenburg, EVAL15: a diffraction data integration method based on ab initio predicted profiles, *J. Appl. Crystallogr.* 43 (2010) 70-82.
  15. G. Sheldrick, *SADABS*., Version 2008/1. Bruker AXS Inc., Madison, Wisconsin, USA (2008).
  16. N. Vast, S. Baroni, G. Zerah, J. M. Besson, A. Polian, M. Grimsditch and J. C. Chervin, Lattice dynamics of icosahedral  $\alpha$ -boron under pressure, *Phys. Rev. Lett.* 78 (1997) 693–696.
  17. W. Richter and K. Ploog, Raman-active phonons in  $\alpha$ -boron, *Phys. Stat. Sol.* 68 (1975) 201
  18. G. Will, K. Ploog, Crystal structure of I-tetragonal boron, *Nature* 251 (1974) 406–408.
  19. G. Will and B. Kiefer, Electron deformation density in rhombohedral  $\alpha$ -boron, *Z. Anorg. Allg. Chem.* 627 (2001) 2100-2104.

20. Brandenburg, K. *DIAMOND*. Version 3.2. Crystal impact GbR, Bonn, Germany, (2009).
21. V. Petříček, M. Dušek, kb of Physics, Czech Academy of Sciences, Prague, Czech Republic, (2006).
22. B.F. Decker, J.S. Kasper, The crystal structure of simple rhombohedral form boron, *Acta Cryst.* 12 (1959) 503–506.
23. A.C. Switendick, B. Morosin, Electronic charge density and bonding in  $\alpha$ -boron: an experimental-theoretical comparison, American Institute of Physics, Conference Proceedings 231 (1991) 205-211.
24. B. Morosin, A.W. Mullendore, D. Emin, G.A. Slack, Rhombohedral crystal structure of compounds containing boron-rich icosahedra, American Institute of Physics, Conference Proceedings 86 (1986) 70-86.

## **4.2 Raman spectroscopy investigation of $\alpha$ -boron at elevated pressures and temperatures**

G. Parakhonskiy<sup>a,b</sup>, V. Vtech<sup>b</sup>, N. Dubrovinskaia<sup>a</sup>, R. Caracas<sup>c</sup> and L. Dubrovinsky<sup>b</sup>

<sup>a</sup>*Material Physics and Technology at Extreme Conditions, the Laboratory of Crystallography, University of Bayreuth, D-95440 Bayreuth, Germany*

<sup>b</sup>*Bayerisches Geoinstitut, Universität Bayreuth, D-95440 Bayreuth, Germany;*

<sup>c</sup>*Laboratoire de Sciences de la Terre, Centre National de la Recherche Scientifique, Ecole Normale Supérieure de Lyon, 46 allée d'Italie, 69364 Lyon Cedex 07, France*

*Submitted to Solid State Communications*

### **4.2.1 Abstract**

Detailed investigation of single crystals of  $\alpha$ -boron using Raman spectroscopy was performed under elevated pressures and temperatures. The behaviour of the Raman modes under pressure was studied both theoretically and experimentally. The results were compared with the literature data.

### **4.2.2 Introduction**

Raman spectroscopy is recognized as a powerful non-destructive technique for characterization of boron polymorphs and their behaviour under pressure [1–3]. Boron has three polymorphs, currently established as phases ( $\alpha$ -,  $\beta$ -, and  $\gamma$ -B, see Refs. [1, 4]), and each of them possesses its unique Raman spectrum, which can be used as a phase fingerprint [4, 5].  $\alpha$ -boron has the simplest structure [5–9] of the three boron phases: it consists of B<sub>12</sub> icosahedra located at the corners of a rhombohedral unit cell.

The first  $\alpha$ -boron Raman study was performed by Richter and Ploog [10] on crystals made in 1964 [11]. They assigned and described  $\alpha$ -boron modes at ambient conditions and came to the conclusion that the modes exhibiting the highest frequencies (1100 to 1200 cm<sup>-1</sup>) are caused by the strong inter-icosahedral covalent bonds, while the intra-icosahedral modes have frequencies in the intermediate range from 500 to 900 cm<sup>-1</sup> [10]. Librational modes were considered to be due to rotation of the whole icosahedron. Analysis of lattice dynamics of  $\alpha$ -boron under pressure was performed by Vast *et al.* [12]. Mode frequencies were theoretically

calculated and experimentally measured on crystals whose synthesis was reported in Ref. [13]. Based on these data Grüneisen parameters were calculated. It was shown also that the intercluster bonds are of the same strength as the intraccluster ones [12], and that  $\alpha$ -boron is stable up to 30 GPa. Later, stability of  $\alpha$ -boron up to 80 GPa was confirmed experimentally [14] and theoretically predicted up to 270 GPa [15,16]. Ab initio calculations and an assignment of the Raman modes were performed by Shirai and Katayama-Yoshida [17]. The assignment of the Raman bands was clarified recently [18] and the experimentally proven stability range was extended to 100 GPa [13, 17, 18]. The very last assessment of the Raman data on all boron polymorphs was made by Werheit *et al.* [2]. In the Raman spectra from the samples of  $\alpha$ -boron investigated in [2], very weak Raman bands at 494, 552, 750, 1094 and 1238  $\text{cm}^{-1}$  were observed. These bands have not been reported previously. The authors interpreted them as surface modes excited by the Ar ion laser of 488 nm. No information was provided regarding the purity of the crystals of  $\alpha$ -B studied in [2] and their synthesis technique.

The discrepancy between previous theoretical and experimental data [12, 16, 17, 2] required clarification. In the present work we undertook a detailed Raman spectroscopy investigation of  $\alpha$ -boron single crystals at ambient conditions and at pressures up to 36 GPa and temperatures up to 473 K. The crystals studied were synthesized using the high-pressure high-temperature technique [5] and their purity was carefully confirmed [4] to assure the reliability of the obtained experimental results. Experimental data were compared with our theoretical calculations.

### 4.2.3 Experimental

The piston-cylinder-type diamond anvil cells made at Bayerisches Geoinstitut and diamonds with the culet diameters of 200 microns were used in high pressure experiments. Rhenium gaskets were squeezed between the diamonds to make an indentation of a 300-micron thickness. Then a 120-micron round hole was drilled in the center of the indentation. Previously synthesized  $\alpha$ -boron crystals [4, 5] were selected and placed into this hole (Figure 4.2.3.1). Sizes of the used crystals were 90x45, 80x40 and 25x40 microns. Neon was used as a pressure transmitting medium. Ruby served as a pressure marker [19] and ruby balls were placed into the hole. The DACs were heated using the external resistivity heating system [20], which provides a good thermal stability. Temperature was directly measured by means of S-type Pt-Pt<sub>0.9</sub>Rh<sub>0.1</sub> thermocouple.

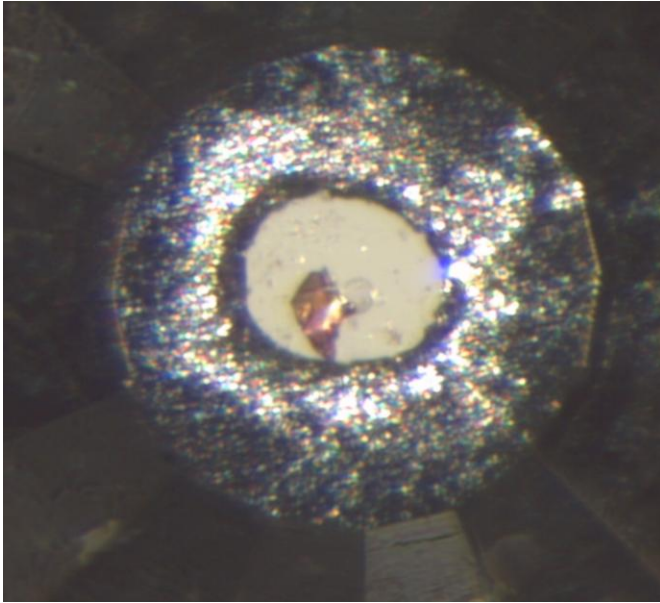


**Figure 4.2.3.1** Image of the sample chamber of a diamond anvil cell: the  $\alpha$ -boron crystal (orange) placed into a 120-micron hole drilled in the rhenium gasket. A transparent circle in the middle is a ruby ball. Neon is a pressure transmitting medium.

The Raman spectra were collected using Dilor XY and LabRam spectrometers equipped with the He-Cd, Ar and He-Ne laser sources, with the excitation wavelength of 325 nm, 514 nm and 632.8 nm, respectively. The laser power in the range of 15 to 1000 mW was used. Raman spectra were collected by means of 50 accumulations for three seconds each on the Raman system with the red laser, five accumulations for 120 seconds each with the UV laser and ten accumulations for 120 seconds each on the Raman system with a green laser. The resulting wavelength resolution was  $3 \text{ cm}^{-1}$ . The position of the Raman peak maximum was determined on the second derivative.

Pressure in the cells was increased up to 36 GPa with a step of about 3 GPa at the temperatures: 293 K, 343 K, 373 K, 423 K and 473 K. Each step the Raman spectrum was measured. Pressure and temperature dependence of the Raman shift was subsequently analyzed. The regression lines and the Clapeyron slope were fitted by the least square method.

Complementarily, we perform first-principles calculations using the density-functional theory (DFT) [21] and the density-functional perturbation theory (DFPT) [22, 23] in the ABINIT implementation [24–27] with planewaves and norm-conserving pseudopotentials [28, 29]. We sample the electron density in the reciprocal space using a regular grid of  $8 \times 8 \times 8$  special k-points [30] and a kinetic energy cut-off of 30 Hartrees (1 Hartree = 27.2116 eV) for the wavefunctions. We use the local density approximation to compute the exchange-correlation energy. We determine the Raman spectra, with both peak position and intensity, in the framework of DFPT. For more details the reader is encouraged

to check the WURM database description [31] or the original paper of the implementation [27].

#### 4.2.4 Results and discussion

Experimental Raman results obtained at ambient conditions are presented in Table 4.2.4.1. It was compared with the literature data. Experimentally measured frequencies of the Raman modes of  $\alpha$ -boron at ambient conditions agree well with those previously reported in [2, 10, 12, 16]. We performed detailed investigation of the particular ranges (Figure 4.2.4.1), where additional weak surface modes were found in [2]. Raman spectra in those regions were measured for about an hour on both Ar and He-Ne laser systems. Although we used He-Cd laser with the excitation light wavelength 325 nm, which is smaller than used in [2], and neither of these surface modes was detected in our study. It can suggest that the observed "surface modes" could be either artefacts or the result of possible contamination of the boron samples studied in [2], taking into account that characterisation of their purity was not provided in the paper.

**Table 4.2.4.1** Phonon frequencies of  $\alpha$  boron observed in the present study compared with our theoretical calculations and the literature data (experimental uncertainties are  $2 \text{ cm}^{-1}$ ).

	$\omega, \text{cm}^{-1}$ , exp. this work	$\omega, \text{cm}^{-1}$ , theor. this work	$\omega, \text{cm}^{-1}$ , (Richter and Ploog 1975)	$\omega, \text{cm}^{-1}$ , (Vast et al. 1997)	$\omega, \text{cm}^{-1}$ , (Vast et al. 1997)	$\omega, \text{cm}^{-1}$ , (Shirai and Katayama-Yoshida 1998)	$\omega, \text{cm}^{-1}$ , (Werheit et al. 2010)
weak surface mode							494
$E_g$	519	525	524	525	529	497	527
weak surface mode							552
$E_g$	581	618	587	586	608	572	589
$A_{1g}$	686	720	693	692	708	710	694
$E_g$	703	742	710	708	729	743	713
weak surface mode							750
$E_g$	768	801	776	774	790	818	778
$A_{1g}$	784	826	796	793	815	759	795
$E_g$	862	903	872	870	890	884	873
$A_{1g}$	917	958	931	925	947	965	934
weak surface mode							1094
$E_g$	1118	1146	1125	1122	1138	1169	1125
$A_{1g}$	1153		1157				1160
$A_{1g}$	1185	1201	1185	1186	1192	1191	1187
$A_{1g}$	1190		1198				1201
weak surface mode							1238

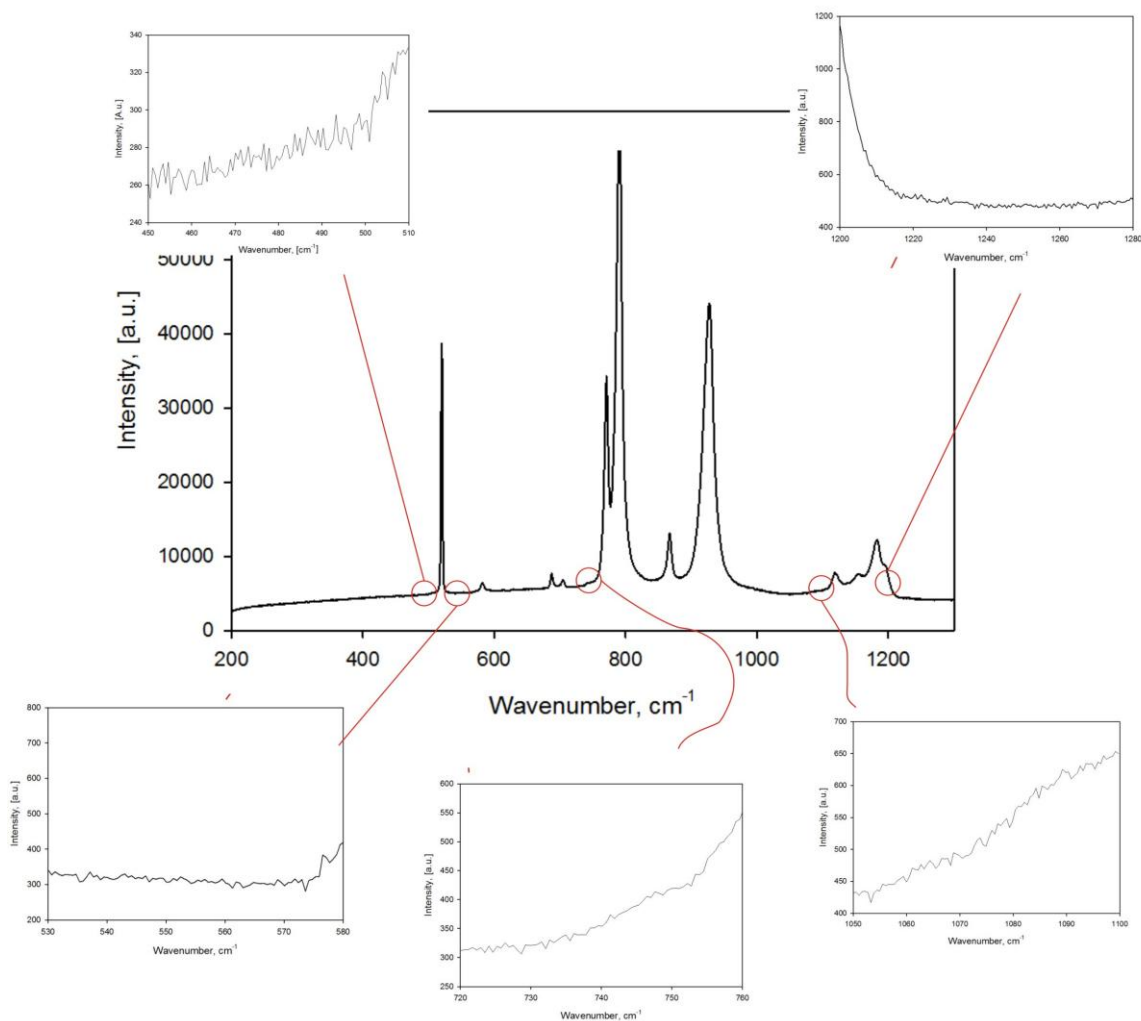


**Figure 4.2.4.1** The Raman spectrum of  $\alpha$  boron obtained at ambient conditions. The insets are enlarged spectral regions, where the additional surface modes were observed in [2].

The wavenumbers of the Raman bands calculated in the present study (see Table 4.2.4.1) are systematically about  $40 \text{ cm}^{-1}$  higher than the corresponding experimental values. The only exception is the first peak,  $E_g$ , experimentally observed at  $519 \text{ cm}^{-1}$ . The most likely explanation is an overestimation of the B-B bonding, specific to LDA [28]. In a molecular solid, usually the lowest-frequency modes are lattice modes, characterized by large units of the structure vibrating as rigid parts, and thus are less affected by overestimations of the intramolecular bond strengths.

Furthermore the behaviour of the mode at  $519 \text{ cm}^{-1}$  ( $525 \text{ cm}^{-1}$  theoretical) is noteworthy as it exhibits a clear softening under pressure. This suggests that the compression mechanism in the structure of  $\alpha$ -boron is dominated by rotations of the  $B_{12}$  cages.



position of the maximum was reported to be shifting to higher wavenumbers followed by moving back to lower values when subjected to pressures exceeding 20 GPa [17]. This behavior was interpreted as an indication of instability that theoretically should occur at pressures of about 210 GPa [15]. Nevertheless, the structure was found to be stable at least up to 100 GPa [17]. We observed that under compression up to 36 GPa the whole Raman profile keeps its form that indicates preserving the icosahedral clusters in the structure of  $\alpha$ -B within the studied pressure range.

**Table 4.2.4.2** Mode Grüneisen parameters of  $\alpha$ -B Raman active vibrations.

mode	$E_g$	$E_g$	$A_{1g}$	$E_g$	$E_g$	$A_{1g}$	$E_g$	$A_{1g}$	$E_g$
This work, $\gamma_i$	0.325	1.541	1.037	1.287	0.939	1.321	1.114	1.493	1.233
$\gamma_{\text{exp}}$ , [12]	0.130	1.260	0.973	1.139	0.756	1.186	0.904	1.306	1.040
$\gamma_{\text{theor}}$ , [12]	0.077	1.215	0.889	1.077	0.656	1.155	0.834	1.229	1.083

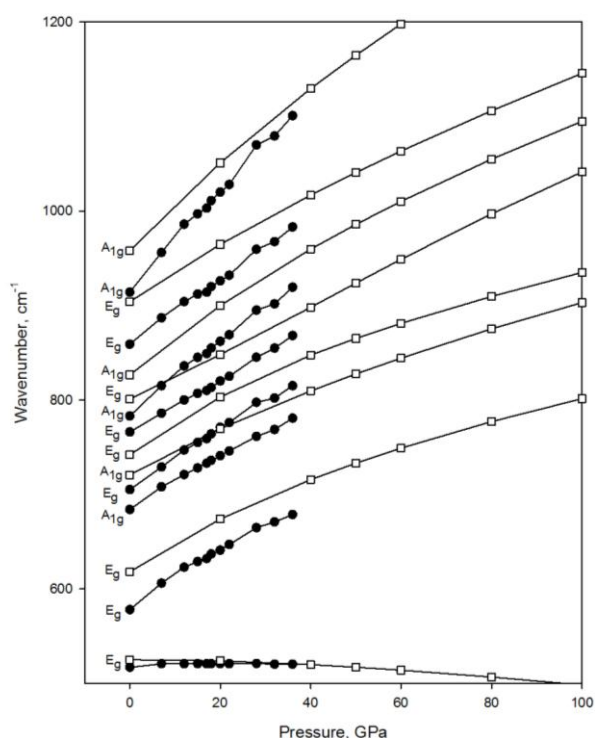


**Figure 4.2.4.3** The pressure dependence of the wavenumbers of the Raman modes of  $\alpha$ -boron. Black circles are experimentally obtained values, white squares – theoretically calculated ones.

The dependence of the Raman  $A_{1g}$  mode of  $\alpha$ -B (at  $784\text{ cm}^{-1}$  at ambient conditions) on pressure and temperature was selected for further analysis due to this line is relatively strong and sharp. The pressure dependence of the  $A_{1g}$  mode of  $\alpha$ -B is presented on the figure 4.2.4.4.a. The fitted value at ambient conditions is  $784\pm 1\text{ cm}^{-1}$  and the pressure dependence is  $3.41\pm 0.05\text{ cm}^{-1}\text{GPa}^{-1}$ . Estimated pressure and peak position uncertainties are 0.5 GPa and  $3\text{ cm}^{-1}$  respectively. During heating the peaks move towards lower wavenumbers. For the  $784\text{ cm}^{-1}$  line the temperature shift was determined relatively to the appropriate value at 298 K.

Based on our experimental data, we are able to write an empirical equation which allows determining pressure (in GPa) if temperature and the wavenumber of the  $A_{1g}$  mode of  $\alpha$ -B are known:

$$P = 0.293\omega + 0.03T - 239 \quad (1)$$

Where  $P$  – pressure in GPa,  $\omega$  - the peak position in  $\text{cm}^{-1}$  and  $T$  is the temperature in K with estimated uncertainties 0.5 GPa,  $3\text{ cm}^{-1}$  and 5 K.

The fitted solid line described by equation (1) (Figure 4.2.4.4.b) has the slope  $0.11\pm 0.02\text{ cm}^{-1}\text{K}^{-1}$ . Temperature shift of each point was calculated by averaging the shifts at different pressures. Estimated uncertainties in temperature and peak positions are 5 K and  $3\text{ cm}^{-1}$  respectively.

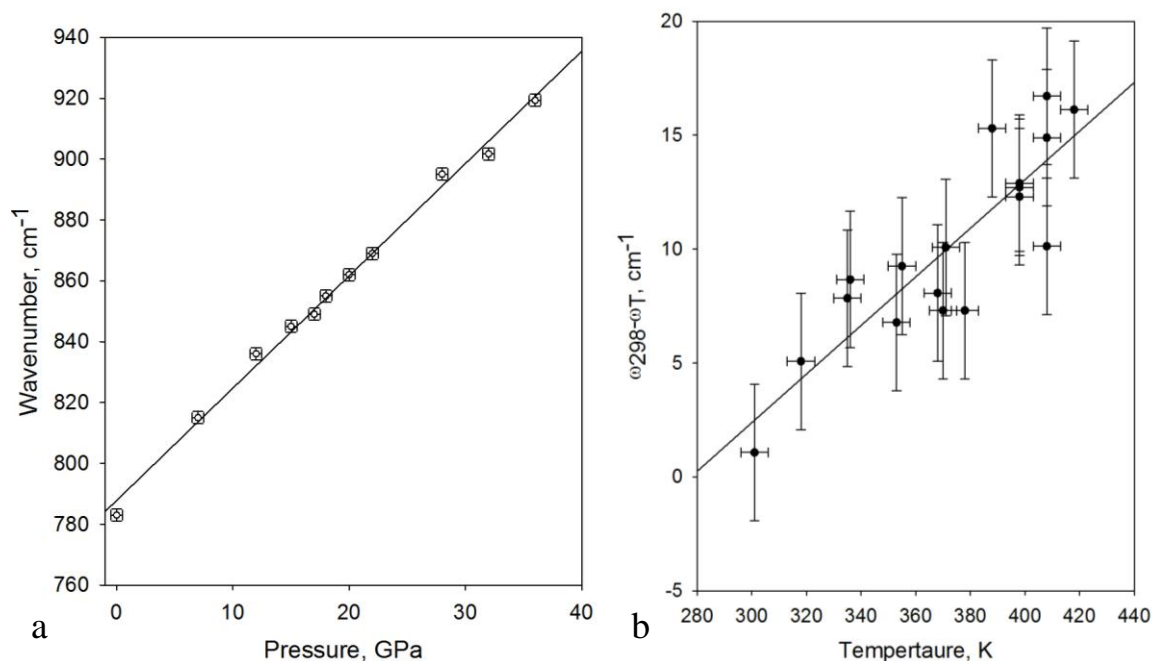


**Figure 4.2.4.4** The pressure (a) and temperature (b) dependence of the position of the  $A_{1g}$  mode ( $784\text{ cm}^{-1}$  line at ambient conditions) of  $\alpha$ -B.

## 4.2.5 Conclusions

The active Raman modes of  $\alpha$ -boron at pressures up to 36 GPa were theoretically calculated and experimentally measured. From the acquired data the Grüneisen parameters were estimated. The temperature dependence of the position of Raman bands in a temperature range of 293 – 473 K was measured as well. Based on that data, an empirical equation describing the dependence of the frequency of the  $A_{1g}$  784  $\text{cm}^{-1}$  Raman mode on pressure and temperature was determined in the pressure-temperature ranges of 0 – 36 GPa and 293 – 473 K.

## Acknowledgments

The work was supported by the German Research Foundation (DFG) through the DFG Priority Program 1236. N.D. thanks DFG for financial support through the Heisenberg Program.

## References

- [1] B. Albert, H. Hillebrecht, Boron: elementary challenge for experimenters and theoreticians, *Angew. Chem. Int. Ed.* 48 (46) (2009) 8640–8668.
- [2] H. Werheit, V. Filipov, U. Kuhlmann, U. Schwarz, M. Armbruster, A. Leithe-Jasper, T. Tanaka, I. Higashi, T. Lundstrom, V.N. Grunin, M.M. Korsukova, Raman effect in icosahedral boron-rich solids, *Sci. Technol. Adv. Mater.* 11 (2010) 023001.
- [3] E. Zarechnaya, N. Dubrovinskaia, L. Dubrovinsky, Polarized Raman spectroscopy of high-pressure orthorhombic boron phase, *High Pressure Res.* 29 (2009) 530–535.
- [4] G. Parakhonskiy, N. Dubrovinskaia, E. Bykova, R. Wirth, L. Dubrovinsky, Experimental pressure-temperature phase diagram of boron: resolving the long-standing enigma, *Sci. Reports.* 1 (2011) 1–7.
- [5] G. Parakhonskiy, N. Dubrovinskaia, L. Dubrovinsky, S. Mondal, S. van Smaalen, High pressure synthesis of single crystals of  $\alpha$ -boron, *J. Cryst. Growth.* 321 (2011) 162–166.
- [6] G. Will, B. Kiefer, Electron deformation density in rhombohedral alpha-boron, *Z. Anorg. Allg. Chem.* 627 (2001) 2100–2104.
- [7] B.F. Decker, J.S. Kasper, The crystal structure of a simple rhombohedral form of boron, *Acta Crystallogr.* 12 (1959) 503–506.
- [8] B. Morosin, A.W. Mullendore, D. Emin, G.A. Slack, Rhombohedral crystal structure of compounds containing boron-rich icosahedra, *AIP Conf. Proc.* 140 (2008) 70–86.

- [9] A.C. Switendick, B. Morosin, Electronic charge density and bonding in  $\alpha$ -boron: an experimental-theoretical comparison, *AIP Conf. Proc.* 231 (1991), 205–211.
- [10] W. Richter, K. Ploog, Raman-active phonons in alpha-boron, *Phys. Status Solidi b.* 68 (1975) 201–205.
- [11] V.E. Amberger, W. Dietze, Zur Bildung von alpha-rhomboedrischem, rotem Bor, *Z. Anorg. Allg. Chem.* 38 (1964) 131–139.
- [12] N. Vast, S. Baroni, G. Zerah, J.M. Besson, A. Polian, M. Grimsditch, J.C. Chervin, Lattice dynamics of icosahedral  $\alpha$ -boron under pressure, *Phys. Rev. Lett.* 78 (1997) 693–696.
- [13] A. Polian, S. Ovsyannikov, M. Gauthier, P. Munsch, J.C. Chervin, G. Lemarchand, in: E. Boldyreva, P. Dera (Eds.), *High pressure crystallography: from fundamental phenomena to technological applications*, NATO Science for Peace and Security Series B: Physics and Biophysics XIV, Springer, Dordrecht, Netherlands, 2010, pp. 241–250.
- [14] M. Kaneshige, S. Hirayama, T. Yabuuchi, T. Matusuoka, K. Shimizu, Y. Mita, H. Hyoudo, K. Kimura, Measurement of electrical resistance and Raman spectrum of boron under high pressure, *J. Phys. Soc. Jpn. Suppl. A.* 76 (2007) 19–20.
- [15] J. Zhao, J. Lu, Pressure-induced metallization in solid boron, *Phys. Rev. B.* 66 (2002) 092101.
- [16] C. Mailhot, J. Grant, A. McMahan, High-pressure metallic phases of boron, *Phys. Rev. B.* 42 (1990) 9033-9039.
- [17] K. Shirai, H. Katayama-Yoshida, The narrow Raman linewidth of a librational mode of alpha-rhombohedral boron and its anharmonic effects, *J. Phys. Soc. Jpn.* 67 (1998) 3801–3808.
- [18] A. Polian, J.C. Chervin, P. Munsch, M. Gauthier,  $\alpha$ -boron at very high pressure structural and vibrational properties, *J. Phys.: Conf. Ser.* 121 (2008) 042017.
- [19] K. Syassen, Ruby under pressure, *High Pressure Res.* 28 (2008) 75–126.
- [20] N. Dubrovinskaia, L. Dubrovinsky, Whole-cell heater for the diamond anvil cell, *Rev. Sci. Instrum.* 74 (2003) 3433-3437.
- [21] W. Kohn, L.J. Sham, Self-consistent equations including exchange and correlation effects, *Phys. Rev.* 140 (1965) A1133–A1138.
- [22] S. Baroni, S. de Gironcoli, A. Dal Corso, Phonons and related crystal properties from density-functional perturbation theory, *Rev. Mod. Phys.* 73 (2001) 515–562.
- [23] G. Xavier, R. Gian-Marco, R. Caracas, First-principle studies of the lattice dynamics of crystals, and related properties, *Z. Kristallogr.* 220 (2005) 458–472.
- [24] X. Gonze, J.M. Beuken, R. Caracas, F. Detraux, M. Fuchs, G.M. Rignanese, L. Sindic, M. Verstraete, G. Zerah, F. Jollet, M. Torrent, A. Roy, M. Mikami, Ph. Ghosez, J.Y.

- Raty, D.C. Allan, First-principles computation of material properties: the ABINIT software project, *Comp. Mater. Sci.* 25 (2002) 478–492.
- [25] X. Gonze, A brief introduction to the ABINIT software package, *Z. Kristallogr.* 220 (2009) 558–562.
- [26] X. Gonze, B. Amadon, P.M. Anglade, J.M. Beuken, F. Bottin, P. Boulanger, *et al.*, ABINIT: First-principles approach to material and nanosystem properties, *Comput. Phys. Commun.* 180 (2009) 2582–2615.
- [27] M. Veithen, X. Gonze, P. Ghosez, Nonlinear optical susceptibilities, Raman efficiencies, and electro-optic tensors from first-principles density functional perturbation theory, *Phys. Rev. B.* 71 (2005) 125107.
- [28] M.C. Payne, T.A. Arias, J.D. Joannopoulos, Iterative minimization techniques for ab initio total-energy calculations: molecular dynamics and conjugate gradients, *Rev. Mod. Phys.* 64 (1992) 1045–1097.
- [29] N. Troullier, J.L. Martinis, Efficient pseudopotentials for plane-wave calculations, *Phys. Rev. B* 43 (1991) 1993–2006.
- [30] H.J. Monkhorst, J.D. Pack, Special points for Brillouin-zone integrations, *Phys. Rev. B.* 13 (1976) 5188–5192.
- [31] R. Caracas, E. Bobocioiu, The WURM project - a freely available web-based repository of computed physical data for minerals, *Am. Mineral.* 96 (2011) 437–443.

### **4.3 Experimental pressure-temperature phase diagram of boron: resolving the long-standing enigma**

Gleb Parakhonskiy<sup>a,b</sup>, Natalia Dubrovinskaia<sup>\*b</sup>, Elena Bykova<sup>a</sup>, Richard Wirth<sup>c</sup>, Leonid Dubrovinsky<sup>a</sup>

<sup>a</sup> *Bayerisches Geoinstitut, Universität Bayreuth, D-95440 Bayreuth, Germany*

<sup>b</sup> *Materialphysik und Technologie, Lehrstuhl für Kristallographie, Physikalisches Institut, Universität Bayreuth, D-95440 Bayreuth, Germany*

<sup>c</sup> *GeoForschungsZentrum Potsdam, Experimental Geochemistry and Mineral Physics, 14473 Potsdam, Germany*

*Published in Scientific Reports, 1, 2011*

#### **4.3.1 Abstract**

Boron, discovered as an element in 1808 and produced in pure form in 1909, has still remained the last elemental material, having stable natural isotopes, with the ground state crystal phase to be unknown. It has been a subject of long-standing controversy, if  $\alpha$ -B or  $\beta$ -B is the thermodynamically stable phase at ambient pressure and temperature. In the present work this enigma has been resolved based on the  $\alpha$ -B-to- $\beta$ -B phase boundary line which we experimentally established in the pressure interval of ca. 3 GPa to 8 GPa and linearly extrapolated down to ambient pressure. In a series of high pressure high temperature experiments we synthesised single crystals of the three boron phases ( $\alpha$ -B,  $\beta$ -B, and  $\gamma$ -B) and established the phase boundaries in the pressure-temperature boron phase diagram that provided evidence of higher thermodynamic stability of  $\alpha$ -B, which possesses the simplest crystal structure among the three stable boron phases. Our work opens a way for reproducible synthesis of  $\alpha$ -boron, an optically transparent direct band gap semiconductor with very high hardness, thermal and chemical stability.

#### **4.3.2 Introduction**

Boron does not exist in nature as a pure elemental phase because of its extreme chemical activity but, being utilised in compounds it plays an important role in human activities since antiquity<sup>1</sup>. Boron compounds are widely used as engineering materials (dielectrics, B-doped semiconductors), superhard materials (cBN, boron carbide), reinforcing chemical additives, for example, for obtaining special glass or corrosion- or heat-resistant alloys<sup>2</sup>, and superconducting materials (ex.,  $\text{MgB}_2$ )<sup>3</sup>. Surprisingly, despite centuries of

application and decades of intensive studies of boron compounds, elemental boron still remains in focus of wide scientific interest due to its enigmatic properties (largely unknown phase diagram<sup>4-7</sup>, pressure induced metallization and superconductivity<sup>8</sup>, formation of unusual chemical bonds<sup>9</sup> and potential technological applications (exceptional chemical stability combined with very high hardness and interesting semiconducting and optical properties<sup>5,10</sup>).

Among elemental boron polymorphs, only  $\alpha$ -rhombohedral ( $\alpha$ -B),  $\beta$ -rhombohedral ( $\beta$ -B), and  $\gamma$ -orthorhombic boron ( $\gamma$ -B) have been currently established as pure phases<sup>4</sup>. They can be synthesised as single crystals at high pressures and high temperatures and preserved at ambient conditions<sup>4, 11-14</sup>. Building blocks of all these polymorphs are quasi-molecular B<sub>12</sub> icosahedra arranged in the structures of different complexity. Among them  $\beta$ -B has the most complex structure, whose details should yet be clarified by further studies. The presence of not fully occupied positions and probably interstitial atoms allow characterising the structure of  $\beta$ -B as a defect one<sup>7,15,16</sup>. The  $\gamma$ -B consists of covalently bonded B<sub>12</sub> icosahedra in a distorted cubic closest packing with B<sub>2</sub> dumbbells placed at the octahedral sites<sup>5,9</sup>.  $\alpha$ -B has the simplest structure with only 12 atoms per a unit cell, where B<sub>12</sub> icosahedra are arranged in a distorted cubic closest packing<sup>17</sup>.

Relative stability of  $\alpha$ -B and  $\beta$ -B at ambient conditions remains a puzzle. The  $\beta$ -B crystallizes from melt at ambient pressure and can be also produced by different chemical methods including vapour deposition<sup>18,19</sup>. The  $\alpha$ -B was crystallized from a variety of metallic solvents in the middle of 1960s<sup>20</sup>, but later the technology of producing the pure crystalline phase was lost<sup>4</sup> and only recently high-pressure synthesis of  $\alpha$ -B single crystals was reported<sup>14</sup>. On heating at ambient pressure at temperatures above ~1500 K  $\alpha$ -B slowly transforms to  $\beta$ -B and it means that a stable high-temperature form of boron is the  $\beta$ -phase. The fact that  $\beta$ -B can not be transformed to  $\alpha$ -B at ambient pressure may indicate that  $\alpha$ -form is metastable<sup>21</sup>. In this respect, although  $\alpha$ -B is completely ordered, its relative structural simplicity does not make it self-evident that  $\alpha$ -B is more stable compared to  $\beta$ -B at ambient conditions. Slow kinetics of transformations (i.e. large kinetic barriers) and/or high melting temperature of boron have possibly prevented accurate measurements by unambiguous techniques, such as calorimetry<sup>22</sup>.

Theoreticians do not have consensus on the problem of relative stability of  $\alpha$ -B and  $\beta$ -B polymorphs. Using density-functional (DFT) calculations Masaga *et al.* and Shirai *et al.*<sup>6,23</sup> studied ground-state and thermodynamic properties (including the effect of atomic disorder and phonons) of  $\alpha$ - and  $\beta$ -B borons and found that at zero temperature  $\alpha$ -B is more stable than  $\beta$ -B. That agrees with the conclusion of Shang *et al.*<sup>24</sup>, who considered defect free  $\alpha$ - and  $\beta$ -B

using first-principle quasi-harmonic phonon calculations. By considering the phonon contribution as the major source of the temperature dependence of the free energy, Masaga *et al.*<sup>6</sup> obtained 970 K as the transition temperature of  $\alpha$ -to- $\beta$  boron. This is at odds with conclusions of van Setten *et al.*<sup>7</sup>, who introduced the quantum mechanical zero-point vibrational energy as a mechanism to stabilize  $\beta$ -B at absolute zero temperature and made  $\beta$ -B in their DFT calculations the ground state of elemental boron. Moreover, investigations indicate that it is possible to find an arrangement of partially occupied states in  $\beta$ -boron that also increase its stability with respect to the  $\alpha$ -phase<sup>7,15,22,25</sup>. Ogitsu *et al.*<sup>22,25</sup>, using lattice model Monte Carlo techniques combined with *ab initio* calculations, found that boron could be a frustrated system and a series of  $\beta$ -boron structures, nearly degenerate in energy, may be stabilized by a macroscopic amount of intrinsic defects. According to Ogitsu *et al.*<sup>22,25</sup>, defects are responsible not only for entropic effects but also for a reduction in internal energy making  $\beta$ -B more stable than  $\alpha$ -B at zero temperature. Thus, if the  $\beta$ -B phase happens to be the ground state, the presence of geometrical frustration will lead to an exotic thermodynamic property in the vicinity of zero temperature that would be very unusual for a pure elemental material.

In the present work we report the results of systematic experimental exploration of the pressure-temperature (PT) phase diagram of boron at pressures of 3 GPa to 14 GPa and temperatures of 1073 to 2423 K aimed at establishing phase boundaries and resolving the long-standing problem regarding relative stability of the  $\alpha$ - and  $\beta$ -B phases.

## 4.3.3 Results

### 4.3.3.1 Boron phases

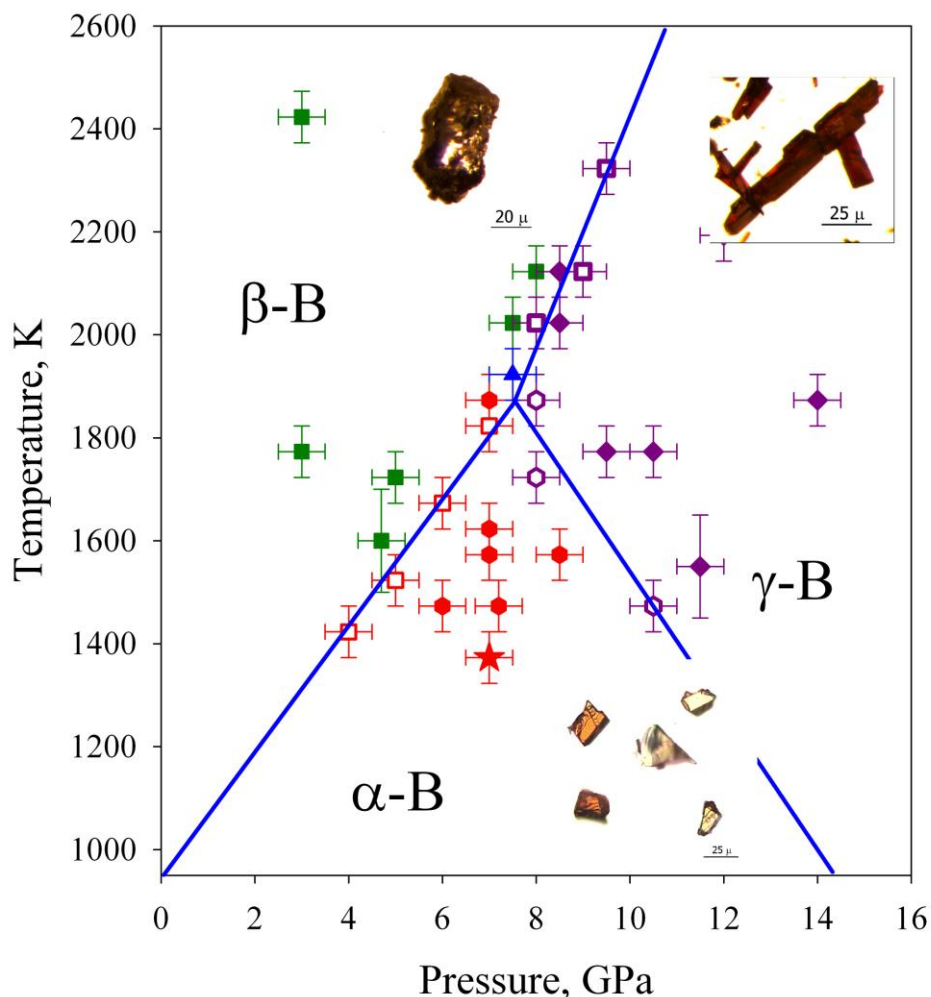


**Figure 4.3.3.1.1 Pressure-temperature phase diagram of boron.** PT conditions at which crystallisation of various boron phases occurred are marked by different signs: green squares –  $\beta$ -boron; purple diamonds –  $\gamma$ -boron; red hexagons –  $\alpha$ -boron; open red squares –  $\alpha$ - and  $\beta$ -boron; open purple squares –  $\beta$ - and  $\gamma$ -boron; open purple hexagons –  $\alpha$ - and  $\gamma$ -boron; blue triangle –  $\alpha$ -,  $\beta$ -, and  $\gamma$ -boron; the red star marks the conditions of the multi-anvil experiment which led to the solid-solid  $\beta$ -to- $\alpha$ -B phase transition; continues blue lines show apparent phase boundaries. The inserts present images of synthesized crystals of  $\alpha$ -,  $\beta$ -, and  $\gamma$ -boron.

In order to experimentally constrain relations between  $\alpha$ -,  $\beta$ -, and  $\gamma$ -boron phases we performed more than 30 experiments in a multi-anvil apparatus (Fig. 4.3.3.1.1, Table 4.3.3.1.1, see also Methods below). In all experiments a boron source (commercially available polycrystalline high purity (99.9995%)  $\beta$ -B, see Methods Summary) was enclosed into a metallic (Au or Pt) capsule with or without addition of a Pt powder and treated at various

high-pressure high-temperature (HPHT) conditions. Every trial aimed at establishing the phases that can be crystallised from melt or by solid-solid phase transformation of the precursor. Recovered samples were analysed by scanning electron microscopy and electron microprobe for chemical purity, X-ray diffraction and Raman spectroscopy for phase composition, and some samples were studied by TEM for characterising their microstructure (Methods Summary).

**Table 4.3.3.1.1** Summary of high-pressure high-temperature experiments on boron.

Experiment*	Starting material	Experimental conditions**			Synthesis results***	
		capsule material	temperature, K	pressure, GPa		heating duration, Min
H3161 MA	85 at.% $\beta$ -B + 15 at.% Pt	Au	1473	10.5	5	$\alpha$ -B, $\gamma$ -B
H3170 MA	85 at.% $\beta$ -B + 15 at.% Pt	Au	1473	7.2	5	$\alpha$ -B
S4894 MA	$\beta$ -B	Pt	1873	7	5	$\alpha$ -B
H3255 MA	$\beta$ -B	Pt	1573	8.5	3	$\alpha$ -B
H3271 MA	$\beta$ -B	Pt	1673	6	5	$\alpha$ -B, recrystallized $\beta$ -B
H3273 MA	$\beta$ -B	Pt	1473	6	5	$\alpha$ -B
H3286 MA	$\beta$ -B	Pt	1873	8	5	$\alpha$ -B, $\gamma$ -B
S4805 MA	85 at.% $\beta$ -B + 15 at.% Pt	Au	1773	9.5	5	$\gamma$ -B
H3154 MA	85 at.% $\beta$ -B + 15 at.% Pt	Au	1773	10.5	5	$\gamma$ -B
H3191 MA	$\beta$ -B	Pt	2193	12	1	$\gamma$ -B
H3244 MA	$\beta$ -B	Pt	1873	14	2	$\gamma$ -B
H3260 MA	$\beta$ -B	Pt	1073	9.7	10	initial $\beta$ -B

H3270 MA	$\beta$ -B	Pt	1723	5	5	recrystallized $\beta$ -B
S5068 MA	$\beta$ -B	Pt	1423	4	5	$\alpha$ -B, recrystallized $\beta$ -B
H3286 MA	$\beta$ -B	Pt	1873	8	5	$\alpha$ -B, $\gamma$ -B
H3292 MA	$\beta$ -B	Pt	1573	7	5	$\alpha$ -B
S4979 MA	$\beta$ -B	Au	1373	7	5	$\alpha$ -B, initial $\beta$ -B
H3313 MA	$\beta$ -B	Au	1823	7	5	$\alpha$ -B, recrystallized $\beta$ -B
S4995 MA	$\beta$ -B	Au	1623	7	5	$\alpha$ -B
H3315 MA	$\beta$ -B	Pt	1523	5	5	$\alpha$ -B, recrystallized $\beta$ -B
S5016 MA	$\beta$ -B	Pt	2023	7.5	5	recrystallized $\beta$ -B
S5017 MA	$\beta$ -B	Pt	2123	9.0	5	$\gamma$ -B, recrystallized $\beta$ -B
S5046 MA	$\beta$ -B	Pt	2023	8	5	$\gamma$ -B, recrystallized $\beta$ -B
S5053 MA	$\beta$ -B	Pt	2023	8.5	5	$\gamma$ -B
S5060 MA	$\beta$ -B	Pt	2123	8	5	recrystallized $\beta$ -B
S5061 MA	$\beta$ -B	Pt	1723	8	5	$\alpha$ -B, $\gamma$ -B
S5064 MA	$\beta$ -B	Pt	1923	7.5	5	$\alpha$ -B, $\gamma$ -B, recrystallized $\beta$ -B
A404 PC	$\beta$ -B	Pt	1773	3	5	recrystallized $\beta$ -B
A405 PC	$\beta$ -B	Pt	2423	3	5	recrystallized $\beta$ -B
DAC1	$\alpha$ -B	Re	1550	11.5	7	$\gamma$ -B
DAC2	$\alpha$ -B	Re	1600	4.7	7	$\beta$ -B

\* MA – multi-anvil runs, PC – piston cylinder, and DAC – diamond anvil cell experiments

\*\* Typical uncertainty in temperature is  $\pm 50$  K, and 0.5 GPa in pressure.

\*\*\* Platinum borides were found in all experiments at temperatures above eutectic if platinum as capsules material or component of starting mixture was used. In some experiments synthesis products contain initial non-transformed  $\beta$ -boron powder.

An image of a cross-section of a typical sample chamber recovered after experiment at 7 GPa and 1573 K is shown in Fig. 4.3.3.1.2 As seen, single crystals of the boron phase are embedded into the matrix of solidified melt of platinum and platinum borides that form in all experiments at temperatures above eutectic.

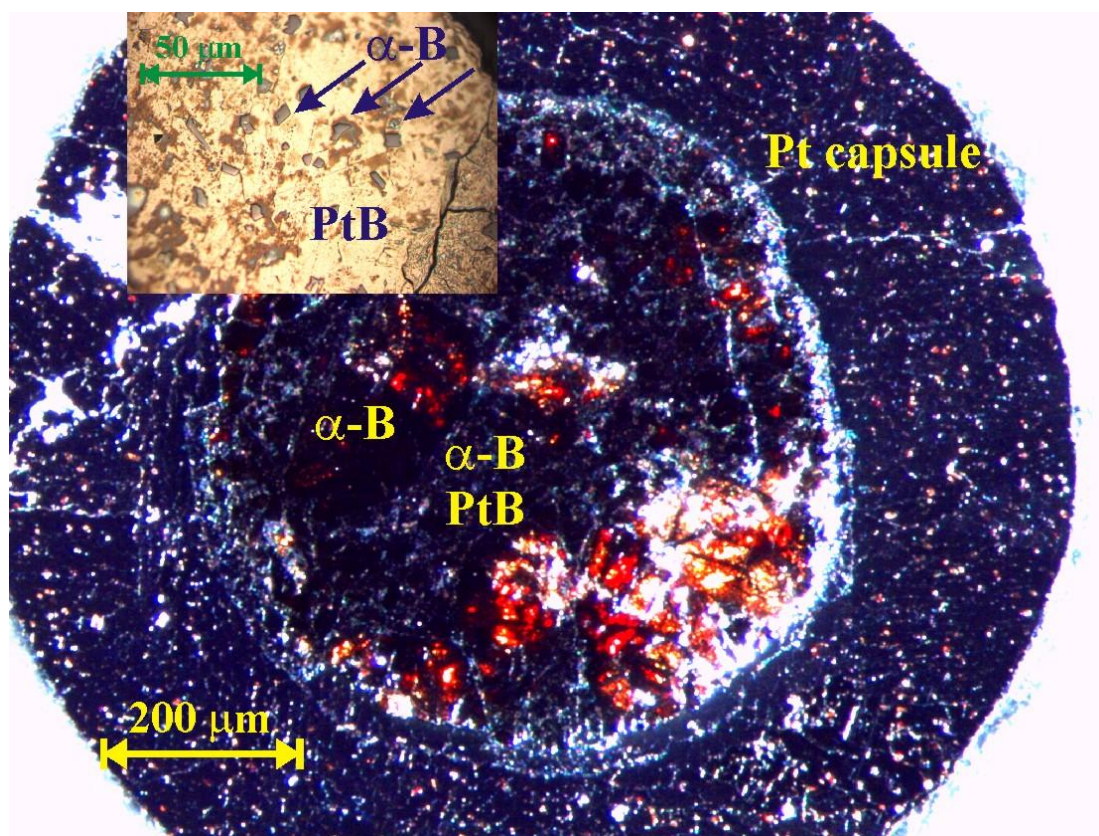


**Figure 4.3.3.1.2** Cross section of the capsule recovered after the experiment at 7 GPa and 1573 K. Bright orange-red  $\alpha$ -boron crystals were crystallised from Pt-PtB flux. The insert shows an enlarged area containing platinum boride and small  $\alpha$ -B crystals.

Dependent on the pressure-temperature conditions, the experiments resulted in formation of the following pure boron phases:

(1) *Re-crystallised  $\beta$ -B*, which is different from the precursor polycrystalline  $\beta$ -B. It forms black or slightly reddish in thin sections single crystals of an irregular or sometimes hexagonal shape (Fig. 4.3.3.1.1), gives a typical for single crystals diffraction pattern consisting of spots (Fig. 4.3.3.1.3) (space group  $R\bar{3}m$ ,  $a = 10.965(2)$  Å,  $c = 23.859(4)$  Å). Its Raman spectrum is distinctly different from that of the precursor and characterised by much sharper peaks compared to the latter (Fig. 4.3.3.1.4);

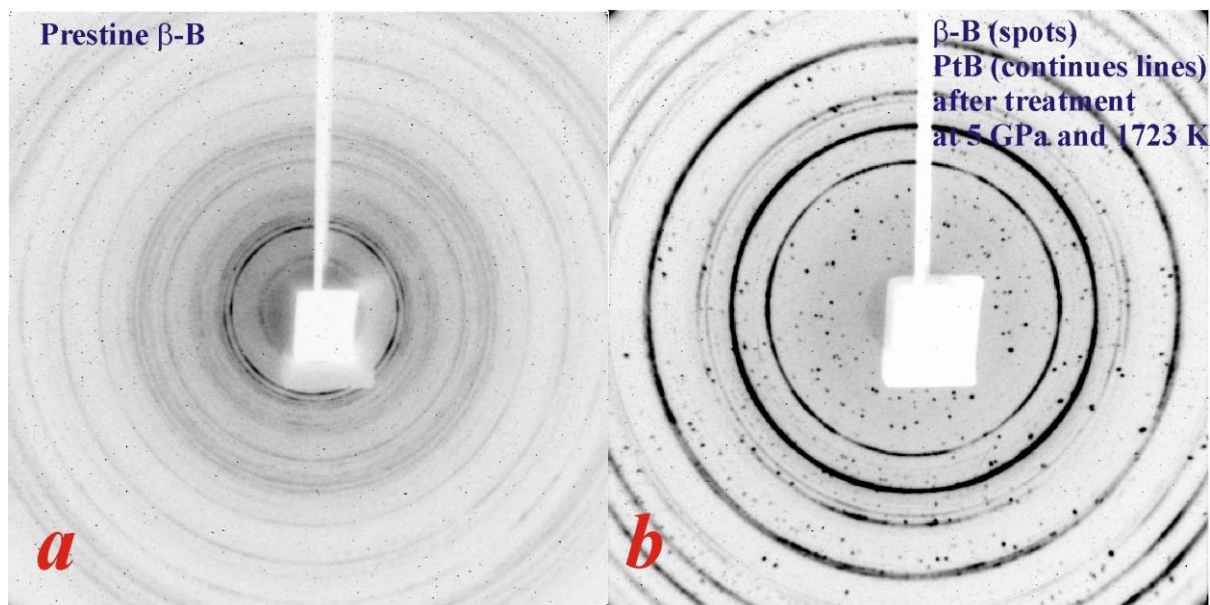


**Fig. 4.3.3.1.3 2D rotational X-ray diffraction patterns** of (a) polycrystalline  $\beta$ -B used as starting material and (b) re-crystallized  $\beta$ -B single crystals consisting of diffraction spots.

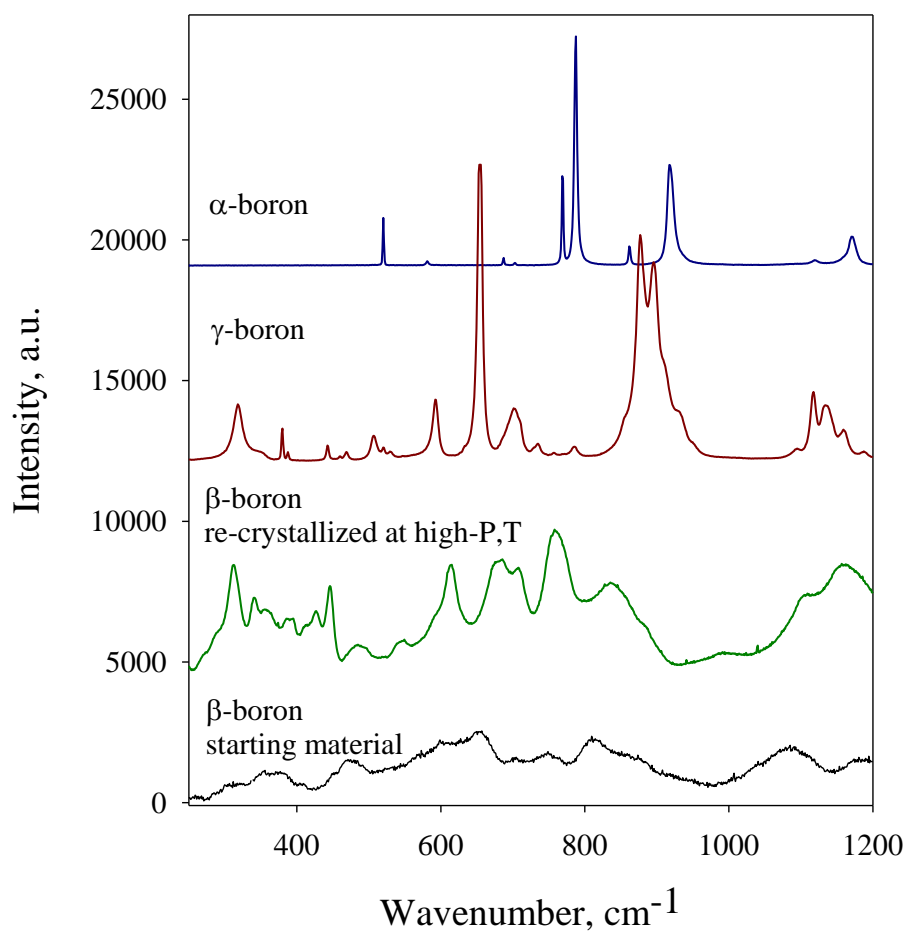


**Figure 4.3.3.1.4 Representative Raman spectra of boron phases.** All spectra were collected for 10 sec except the one spectrum of starting polycrystalline  $\beta$ -boron collected for 60 min.

(2)  $\gamma$ -B, which appears as purple elongated prismatic crystals, gives the characteristic strong Raman spectra (Figs. 4.3.3.1.1, 4.3.3.1.4) and the X-ray diffraction pattern (space group  $Pn\bar{m}$ ,  $a = 5.0576(4)$  Å,  $b = 5.6245(8)$  Å,  $c = 6.9884(10)$  Å). This material is identical to that described in our previous works<sup>5,9,26</sup>.

(3)  $\alpha$ -B. It forms single crystals of semi-transparent orange-red colour and relatively isometric shape (Fig. 4.3.3.1.1, 4.3.3.1.2). Like other boron phases,  $\alpha$ -B is easily identified by the Raman spectrum<sup>14,27</sup> (Fig. 4.3.3.1.4) and X-ray diffraction (space group  $R\bar{3}m$ ,  $a = 4.9065(4)$  Å,  $c = 12.5658(5)$  Å).

The SEM (EDX), microprobe (WDX), and EELS data have shown that boron phases obtained from crystalline  $\beta$ -boron powders are not contaminated independently on the type of the capsule material or pressure-temperature conditions (Fig. 4.3.3.1.5). SEM images of the sample surfaces in backscattered electrons demonstrate homogeneity of the synthesized at HPHT boron phases. High resolution transmission electron microscopy (HRTEM) images of  $\alpha$ -B, for example, reveal almost dislocation free regular packing of spheres (Fig. 4.3.3.1.5) with a diameter of 3.3-3.4 Å, comparable with that of a circumscribed circle around the B<sub>12</sub> icosahedron (3.34 Å)<sup>28</sup>.

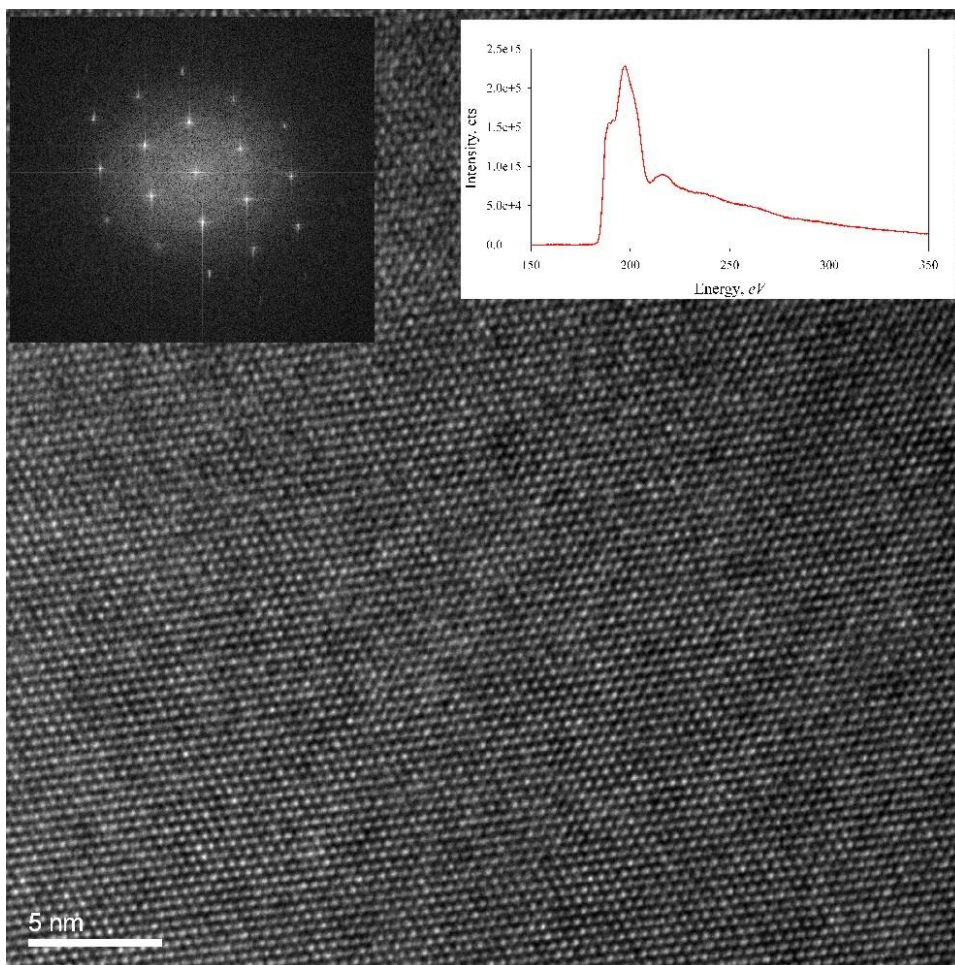


**Figure 4.3.3.1.5 High resolution TEM image of the  $\alpha$ -boron crystal synthesized from platinum flux at 7 GPa and 1573 K.** The insert in the left upper corner is a Fast Fourier Transform (FFT) pattern showing characteristic  $\alpha$ -B reflections 4.16 Å, 4.02 Å, and 2.52 Å. The insert in the right upper corner is a core-loss EELS spectrum of the B-K edge confirming the absence carbon contaminations at about 284 eV the onset of the C-K edge. The spectrum has been gain-normalized and deconvoluted using the low-loss spectrum.

#### 4.3.3.2 Boron phase diagram

Proven chemical and phase purity of boron crystals obtained at different pressure-temperature condition creates a basis for construction of the experimental phase diagram. Different runs resulted in crystallization of one, two or even all three boron phases simultaneously (Fig. 4.3.3.1.1, Table 4.3.3.1.1) that allows defining stability fields of the  $\alpha$ -B,  $\beta$ -B, and  $\gamma$ -B phases. The phase boundary separating the  $\beta$ -B and  $\gamma$ -B phase stability fields agrees well with the phase relations experimentally found in our previous work<sup>5</sup>. The other two phase boundaries ( $\alpha$ -/ $\beta$ -B, and  $\alpha$ -/ $\gamma$ -B) have not been reported so far based on experimental data. We argue that the  $\alpha$ -B has the thermodynamic stability field, because its crystallization is controlled only by pressure and temperature conditions of the experiments independently on the type of metallic solvent (Au or Pt, Table 4.3.3.1.1). Observation of

simultaneous crystallization of chemically pure  $\alpha$ - and  $\beta$ -B (at 5 GPa and 1520 K, for example) or  $\alpha$ - and  $\gamma$ -B (at 8 GPa and 1570 GPa, for example) demonstrates the existence of monovariant boundaries in the pressure-temperature phase diagram. The invariant (triple) point in the phase diagram could be determined by intersections of  $\alpha$ -/ $\beta$ -B,  $\alpha$ -/ $\gamma$ -B, and  $\beta$ -/ $\gamma$ -B boundaries. The all three lines cross at 7.6(5) GPa and 1880(50) K (Fig. 4.3.3.1.1). Indeed, at 7.5 GPa and 1920 K we observed simultaneous crystallisation of all  $\alpha$ -,  $\beta$ -, and  $\gamma$ -boron phases (Table 4.3.3.1.1, Fig. 4.3.3.1.1).

The transition of  $\alpha$ -to- $\beta$  boron upon heating at ambient pressure was already reported in literature<sup>20,21</sup>. In a diamond anvil cell (DAC) experiment (see Methods Summary) we loaded two pre-synthesized  $\alpha$ -B crystals into the sample chamber along with sodium chloride, NaCl, acting as a pressure transmitting medium and thermal insulator. One of the crystals was laser-heated at 4.7(3) GPa and 1600(100) K and another one at 11.5(5) GPa and 1550(100) K. In the first case we observed formation of  $\beta$ -B, while at higher pressure  $\alpha$ -B transformed directly into the  $\gamma$ -phase (Fig. 4.3.3.2.1). One more DAC experiment was conducted at 7 GPa and 1370 K, i.e. at temperature lower than that necessary for eutectic melting of platinum and boron. As in other experiments  $\beta$ -B was used as starting material, but in the recovered sample we found polycrystalline  $\alpha$ -B. Direct solid-solid phase transformation of  $\beta$ -to- $\alpha$  phase proves that  $\alpha$ -boron is a thermodynamically stable phase at certain PT conditions (Fig. 4.3.3.1.1).

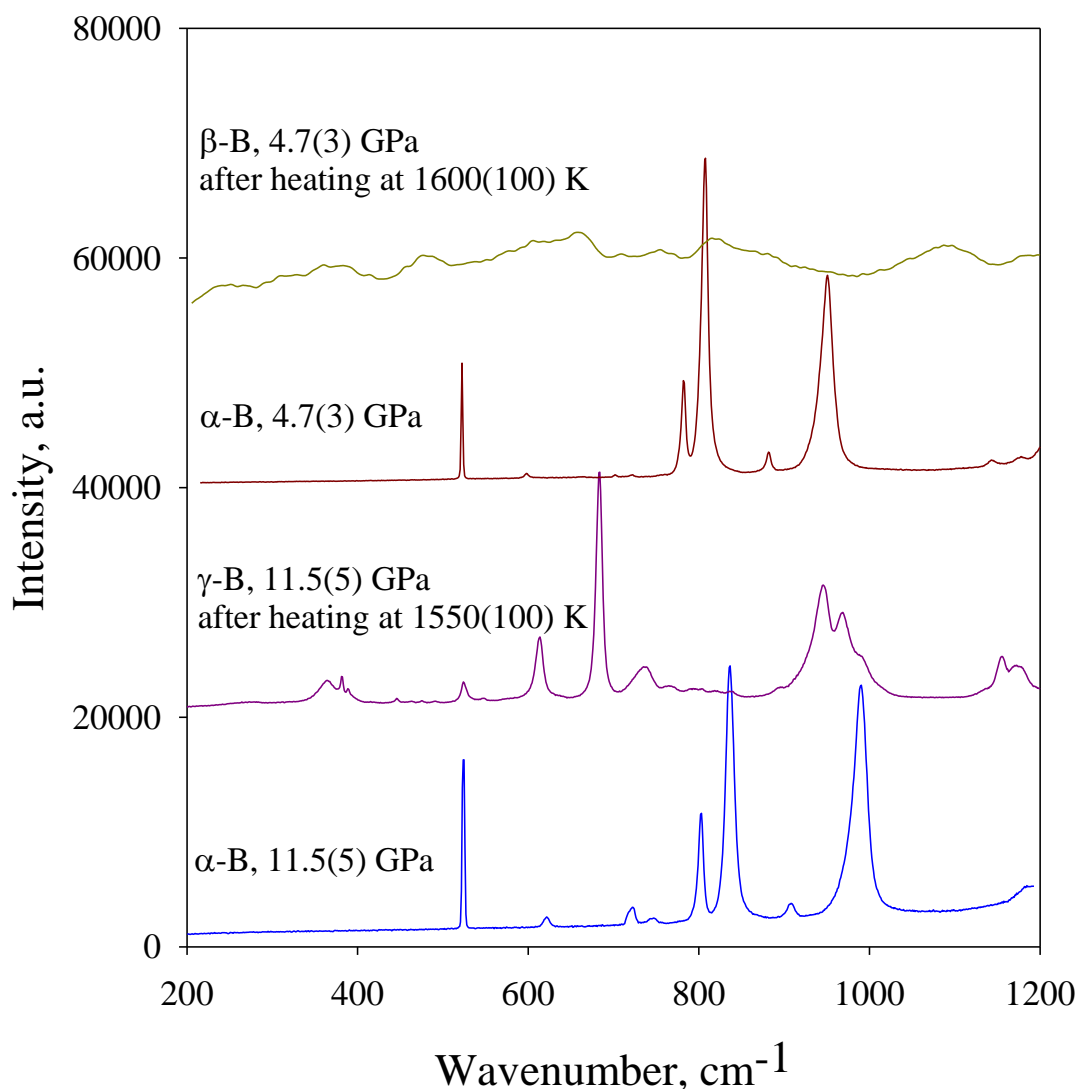


**Figure 4.3.3.2.1 Raman spectra of pre-synthesized  $\alpha$ -B crystals taken *in situ* in a diamond anvil cell experiments at various PT conditions.** From the bottom to the top: before and after laser heating at 11.5(5) GPa and 1550(100) K and at 4.7(3) GPa and 1600(100) K. At higher pressure we observed formation of  $\gamma$ -B, while at lower pressure  $\alpha$ -B transformed directly in to the  $\beta$ -phase. (NaCl in the DAC experiments was used as a pressure transmitting medium and a thermal insulator.)

#### 4.3.4 Discussion

Extrapolation of the  $\alpha$ -/ $\beta$ -B boundary to ambient pressure (Fig. 4.3.3.1.1) suggests that  $\alpha$ -boron is the thermodynamically stable low-temperature boron phase below  $\sim 933(50)$  K. Indeed, in 1960s and 1970s arguments were raised<sup>20,29-33</sup> that crystallization of small crystals of  $\alpha$ -B from different metallic solvents (Pt, Au, Ag, Cu, Cu-Ni, etc.) at temperature around 1100–1200 K may indicate stability of the  $\alpha$ -polymorph at temperatures below these values. However, inability to grow larger crystals of  $\alpha$ -B, its crystallization simultaneously with the  $\beta$ -form, and failure to transform  $\beta$ -B into the  $\alpha$ -phase or to synthesize  $\alpha$ -B from an

amorphous boron precursor supports arguments that  $\alpha$ -B may be just a metastable, or even monotropic, form of boron. In our experiments at appropriate pressure-temperature conditions (Fig. 4.3.3.1.1)  $\alpha$ -B crystals grow at the expense of  $\beta$ -B and in some runs (Table 4.3.3.1.1) all starting  $\beta$ -boron transforms into the  $\alpha$ -phase. Moreover, we observed direct transformation of  $\beta$ -B into  $\alpha$ -B. All mentioned observations prove that  $\alpha$ -boron is a thermodynamically stable phase. Previously reported difficulties and even failure to synthesized  $\alpha$ -B at ambient pressure could be explained based on the phase diagram we have experimentally constructed (Fig. 4.3.3.1.1):  $\alpha$ -B is stable below about 1000 K and strictly speaking, should not crystallize from metallic fluxes with the eutectic point at temperature above  $\sim 1100$  K. However, according to the Ostwald step rule at conditions not far from equilibrium not the most stable but the least stable polymorph that crystallizes first<sup>34</sup>, so that  $\alpha$ -B may appear if a boron-rich metallic flux solidified at relatively low temperature<sup>20</sup>. Transformation of  $\beta$ -B or amorphous boron into the  $\alpha$ -phase requires very significant rearrangement and/or rupture of  $B_{12}$  icosahedra. It is impossible to activate such a rearrangement at relatively low temperatures (below 1000 K) in the field of stability of  $\alpha$ -B. With a pressure increase the temperature stability field of  $\alpha$ -boron increases and, as we demonstrated in a DAC experiment, it becomes possible to realize the direct  $\beta$ -to- $\alpha$ -B transition.

Theoretical works<sup>7,15,22,25</sup> suggesting that  $\beta$ -B is the ground state of boron are not supported by our experimental results. The phase diagram drawn by Oganov *et al.*<sup>35</sup> is schematic and based on only a few experimental points related to the HPHT synthesis conditions of  $\beta$ -B. The authors<sup>35</sup> sketched the  $\alpha$ -/ $\beta$ -B phase boundary in accordance with the theoretical data of van Setten *et al.*<sup>7</sup> and consequently suggested that  $\beta$ -B is stable down to 0 K at ambient pressure at odds with our conclusions. Combining *ab initio* pseudopotential calculations and some experimental data (Grüneisen parameters, particularly), Masaga *et al.*<sup>6</sup> and Shirai *et al.*<sup>23</sup> estimated the phase boundary between  $\alpha$ - and  $\beta$ -phases and apparently found that  $\alpha$ -B is more stable below about 1000 K, in good agreement with our experimental results. However, these authors<sup>6,23</sup> calculated total energy of  $\beta$ -B using an ideal, defects free structural model which contradicts available experimental crystallographic data. Such a simplification of the structure of  $\beta$ -B in calculations could result in “underestimating”  $\beta$ -boron stability compared to other calculations<sup>7</sup>; i.e. the agreement with the experimental results could be reached just by chance, because indeed, according to Refs. 7, 15, 22, and 25 structural defects in  $\beta$ -B play key role in stabilization of the phase. Thus, our results call for further detailed theoretical investigations related to stability of boron polymorphs.

Boron has been for a long time known as prospective material<sup>4,5</sup> for numerous applications.  $\alpha$ -boron demonstrates a truly spectacular combination of properties – it is a direct band gap semiconductor (with the reported band gap of 2.0 eV (Ref. 36), 2.4 eV (Ref. 37), or 2.15(2) eV as derived by us from EELS data), has a very high hardness (we measured the Vickers hardness of 38(2) GPa on polycrystalline aggregates), thermally and chemically highly resistive, and quite light (the density of  $\alpha$ -B is 2.46 g/cm<sup>3</sup> vs 4.89 g/cm<sup>3</sup> of CdS or 6.11 g/cm<sup>3</sup> of GaN having comparable band gaps). Such properties may make  $\alpha$ -B material of choice in many industrial semiconductors applications, and, especially, as a working element of solar cells with high efficiency of sun light conversion into electrical power. So far research and development on potential applications of  $\alpha$ -boron were hindered by concerns of its thermodynamic instability and the absence of a reliable way of synthesis of single crystals. A phase diagram, as a projection of the fundamental property diagram, allows materials scientist indirect use of thermodynamics<sup>38</sup>. It can be utilized to understand materials behaviour and propose optimal ways of their synthesis. The phase diagram of boron (Fig. 4.3.3.1.1) shows that  $\alpha$ -B is not only thermodynamically stable phase in a large pressure-temperature range, but it also can be reproducibly synthesized<sup>14</sup> at conditions readily accessible by modern industry for large-scale production (like synthetic diamonds, for example).

Summarising, our serial exploration of the pressure-temperature field using the large volume press synthesis technique resulted in establishing the phase diagram of boron in the pressure interval of 3 GPa to 14 GPa at temperatures between 1073 K and 2423 K. Based on our experimental data and linear extrapolation of the  $\alpha/\beta$  phase boundary down to ambient pressure we could resolve a long-standing controversy on the ground state of boron in favour of the  $\alpha$ -B phase.

## Methods

Polycrystalline  $\beta$ -boron (purity of 99.9995 at.%, grain size of <1000 microns), purchased from *Chempur Inc.*, was used as a boron source material.

### High-pressure techniques

Experiments in multianvil apparatuses were conducted in installed at BGI 1000-ton (Hymag) and 1200-ton (Sumitomo) hydraulic presses<sup>37</sup>. The Kawai-type multi-anvil system employs six tool-steel outer-anvils and eight tungsten carbide cubic inner-anvils to focus an applied load on an octahedral high-pressure chamber formed as a result of corner truncations on the inner-anvils. By varying the corner truncation size of the inner-anvils, various sample-pressure ranges can be attained. An octahedron made of magnesium oxide that matches the

pressure chamber was used as a pressure medium. In our experiments 18/11 (the edge-length of an octahedron /anvil truncation edge-length, in millimeters) assemblies for pressures of 7-11 GPa and 25/15 assemblies for pressures of 5-8 GPa were used. Although an indubitable advantage of using large assemblies is the increase of the amount of synthesized material, reaching highest temperatures in big assemblies is more difficult. Temperature in our experiments was increased stepwise with a speed of about 80 K/min. Duration of heating was 5 or 3 minutes. Then the samples were either gradually cooled with a speed  $\sim 10$  K/min, or quenched. “Pressure in chamber” vs “hydraulic oil pressure” in experiments was calibrated by observations of phase transitions in standard materials, and temperature determined using  $W_3Re/W_{25}Re$  thermocouple. Uncertainties estimated in pressure 0.5 GPa and in temperature 50 K.

Experiments at pressures below 4 GPa were conducted using an end-loaded piston-cylinder type apparatus<sup>38</sup>. The sample material was loaded into 6 mm diameter, 13 mm long Pt capsules (sample area 3 mm diameter, 6 mm long) which were placed into  $\frac{1}{2}$  inch talc-pyrex sample assemblies. These sample assemblies contained an internal, tapered, graphite resistance furnace to ensure minimal temperature gradients along the length of the capsule. Temperature gradients are estimated to be less than 25°C for the experimental conditions used. Pressure was calibrated against the quartz-coesite and kyanite-sillimanite transitions, as well as the melting point of diopside, and pressures are considered accurate to within less than  $\pm 5\%$  of the stated value. Temperatures were measured with a Pt-Pt10%Rh thermocouple. Run pressures and temperatures were continually monitored and maintained for the duration of the runs. Experiments were quenched isobarically by turning off power to the heating circuit.

Diamond anvil cell experiments we conducted using diamond anvils with the culet diameter of 300  $\mu m$ . Pre-synthesized  $\alpha$ -B and NaCl (used as a pressure medium and thermal insulating material) were loaded into the pressure chamber in the Re gasket preindented to about 45  $\mu m$  thickness with the hole of 125  $\mu m$  in diameter. Several ruby chips were placed into the sample chamber for pressure measurements. For double-side laser heating we employed two UniHead systems installed at BGI<sup>39</sup>. The size of the laser beam was of about 30  $\mu m$  in diameter with a temperature variation of  $\pm 50$  K within the beam. The heating duration was about 5 minutes. Temperature was measured by means of multiwavelength spectroradiometry.

## Analytical techniques

For the phase identification, selection of single crystals, and preliminary structural analysis a high-brilliance Rigaku diffractometer (Mo- $K\alpha$  radiation) equipped with Osmic focusing X-ray optics and Bruker Apex CCD detector was used. The diffraction patterns were processed using Fit2D software.

A LabRam spectrometer (with a resolution of  $2\text{ cm}^{-1}$ ), a He-Ne laser (632.8 nm) with a power of 15 mW for excitation, and a 50 $\times$  objective were used for the Raman scattering experiments.

The morphology and chemical composition of the synthesized samples of single crystals were studied by means of the scanning electron microscopy (SEM) (LEO-1530). Chemical purity of the samples was confirmed using WDX microprobe analysis (JEOL JXA-8200; focused beam; 20 keV, 20 nA).

Electron transparent foils were prepared by focused ion beam (FIB) techniques. FIB allows preparation of site-specific TEM foils with typical dimensions of 15–20  $\mu\text{m}$  wide, by approximately 10  $\mu\text{m}$  high and approx. 0.150  $\mu\text{m}$  thick<sup>40</sup>.

TEM investigations were performed with a TECNAI F20 XTWIN transmission electron microscope operating at 200 kV with a field emission gun electron source. The TEM is equipped with a Gatan Tridiem™ filter, an EDAX Genesis™ X-ray analyzer with ultra thin window and a Fishione high angle annular dark field detector (HAADF). The Tridiem filter was used for the acquisition of energy-filtered images applying a 20 eV window to the zero loss peak. EEL spectra were acquired with a dispersion of 0.1 eV/channel and an entrance aperture of 2 mm. The resolution of the filter was 0.9 eV at FWHM of the zero loss peak. Acquisition time was 1 second. Spectra of the different K-edges (B, C, N, O) were acquired in diffraction mode with a camera length of 770 mm. Spectra processing (background subtraction, removal of plural scattering, quantification) was performed using the DigitalMicrograph software package. EDX spectra were usually acquired in the scanning transmission mode (STEM) using the TIA™ software package of the TEM. Significant mass loss during analysis was avoided by scanning the beam in a pre-selected window (20 x 20 nm or larger). Spot size was approx. 1 nm, and acquisition time 60 seconds at an average count rate of 60 – 80 counts/second. This resulted in a counting error of about 4 -5% at a  $3\sigma$  level.

## References

1. Garrett, D. E. Borates: handbook of deposits, processing, properties, and use. *Academic Press* (1998).
2. Perkins, G. L. Boron: Compounds, Production and Application. *Nova Science Pub Inc.* (2011).
3. Braccini, V., Nardelli, D., Penco, R., Grasso, G. Development of ex situ processed MgB<sub>2</sub> wires and their applications to magnets. *Physica C: Superconductivity* **456** (1–2): 209–217 (2007).
4. Albert, B., Hillebrecht, H. Boron: elementary challenge for experimenters and theoreticians. *Angew. Chem. Int. Ed.* **48** (46), 8640–8668 (2009).
5. Zarechnaya, E.Yu., Dubrovinsky, L., Dubrovinskaia, N., Filinchuk, Y., Chernyshov, D., Dmitriev, V., Miyajima, N., El Goresy, A., Braun, H.F., Van Smaalen, S., Kantor, I., Kantor, A., Prakapenka, V., Hanfland, M., Mikhaylushkin, A.S., Abrikosov, I.A., Simak, S.I. Superhard semiconducting optically transparent high pressure phase of boron. *Phys. Rev. Lett.* **102**, 185501 (2009).
6. Masago, A., Shirai, K., Katayama-Yoshida, H. Crystal stability of  $\alpha$ - and  $\beta$ -boron. *Phys. Rev. B* **73**, 104102 (2006).
7. Van Setten, M.J., Uijtewaal, M.A., de Wijs, G.A. & de Groot, R.A. Thermodynamic stability of boron: The role of defects and zero point motion. *J. Am. Chem. Soc.* **129**, 2458–2465 (2007).
8. Eremets, M.I., Struzhkin, V.V., Mao, H., Hemley, R.J. Superconductivity in boron. *Science* **293**, 272–274 (2001).
9. Mondal, S., van Smaalen, S., Schönleber, A., Filinchuk, Y., Chernyshov, D., Simak, S.I., Mikhaylushkin, A.S., Abrikosov, I.A., Zarechnaya, E.Yu., Dubrovinsky, L., Dubrovinskaia, N. Electron deficient and multicenter bonds in the high-pressure  $\gamma$ -B28 phase of boron. *Phys. Rev. Lett.* **106**, 215502 (2011).
10. Zhou, W., Sun, H., Chen, C. Soft bond-deformation paths in superhard gamma-boron. *Phys. Rev. Lett.* **105**, 215503 (2010).
11. Brazhkin, V. V., Taniguchi, T., Akaishi, M., Popova, S. V. Fabrication of  $\beta$ -boron by chemical-reaction and melt-quenching methods at high pressures. *J. Mat. Res.* **19**, 1643–1648 (2004).

12. Zarechnaya, E.Yu., Dubrovinsky, L., Dubrovinskaia, N., Filinchuk, Y., Chernyshov, D., Dmitriev, V. Growth of singlecrystals of B28 at high pressures and high temperatures. *J. Cryst. Growth* **312**, 3388–3394 (2010).
13. Zarechnaya, E.Yu., Dubrovinskaia, N., Caracas, R., Merlini, M., Hanfland, M., Filinchuk, Y., Chernyshov, D., Dmitriev, V., Dubrovinsky, L. Pressure-induced isostructural phase transformation in  $\gamma$ -B28. *Phys. Rev. B* **82**, 184111 (2010).
14. Parakhonskiy, G., Dubrovinskaia, N., Dubrovinsky, L., Mondal, S., van Smaalen, S. High pressure synthesis of single crystals of  $\alpha$ -boron. *J. Cryst. Growth* **321**, 162-166 (2011).
15. Widom, M., Mihalcovic, M. Symmetry-broken crystal structure of elemental boron at low temperature. *Phys. Rev. B* **77**, 064113 (2008).
16. Slack, G.A., Hejna, C.I., Garbaskas, M.F., Kasper, J.S. *J. Sol. Stat. Chem.* **76**, 52-63 (1988).
17. Decker, B.F., Kasper, J.S. The crystal structure of simple rhombohedral form boron. *Acta Cryst.* **12**, 503–506 (1959).
18. Cueilleron, J., Viala, J.C. The Chemical and Pyrometallurgical Purification of  $\beta$ -Rhombohedral Boron. *J. Less-Com. Met.*, **67**, 333-337 (1979).
19. Greenwood, N.N., in Bailar, J.C. (ed.). *Comprehensive Inorganic Chemistry. Pergamon Press, Oxford-New York* **1**, 680–689 (1973).
20. Wald, F. On the stability of the red  $\alpha$ -rhombohedral boron modification, *Elec. Tech.* **3**, 103-108 (1970).
21. Shalamberidze, S.O., Kalandadze, G.I., Khuedze, D.E., Tsurtsunia, B.D. Production of  $\alpha$ -rhombohedral boron by amorphous boron crystallization. *J. Sol. St. Chem.* **154**, 199-203 (2000).
22. Ogitsu, T., Gygi, F., Reed, J., Motome, Y., Schwergler, E., Galli, G. Imperfect crystal and unusual semiconductor element. *J. Am. Chem. Soc.* **131(5)**, 1903–1909 (2009).
23. Shirai, K., Masago, A., Katayama-Yoshida, H. High-pressure properties and phase diagram of boron. *Phys. Stat. Sol. (b)* **244 (1)**, 303-308 (2007).
24. Shang, S., Wang, Y., Arroyave, R., Liu, Z.-K. Phase stability in alfa and beta-rhombohedral boron. *Phys. Rev. B.* **75**, 092101 (2007).
25. Ogitsu, T., Gygi, F., Reed, Udagawa, M., Motome, Y., Schwergler, E., Galli, G. Geometrical frustration in an elemental solid: An Ising model to explain the defect structure of  $\beta$ -rhombohedral boron. *Phys. Rev. B* **81**, 020102R (2010).
26. Zarechnaya, E., Dubrovinskaia, N., Dubrovinsky, L. Polarized Raman spectroscopy of high pressure orthorhombic boron phase. *J. High Pressure Research* **29 (4)**, 530-535 (2009).

27. Polian, A., Ovsyannikov, S., Gauthier, M., Munsch, P., Chervin, J.C., Lemarchand, G. High pressure crystallography: from fundamental phenomena to technological applications, in: E.Boldyreva, P. Dera (Eds.). *NATO Science for Peace and Security SeriesB: Physics and Biophysics XIV, Springer, Dordrecht, Netherlands, 241–250* (2010).
28. Zarechnaya, E.Yu., Dubrovinsky, L., Dubrovinskaia, N., Miyajima, N., Filinchuk, Y., Chernyshov, D., Dmitriev, V. Synthesis of an orthorhombic high pressure boron phase. *Sci. Technol. Adv. Mater.* **9**, 044209 (2008).
29. Hoard, F.L., Hughes, R.E. The chemistry of boron and its compounds. *John Wiley and Sons Inc.* 25-98 (1967).
30. Horn, F.H. “Boron” synthesis, structure, and properties. *Plenum Press Inc.* 110-115 (1960).
31. Horn, F.H., Taft, E.A., Oliver, D.W. Boron, 2, preparation, properties and applications. *Plenum Press Inc.* 231-234 (1965).
32. Niemyski, T., Zawadzki, W. Some properties of pure polycrystalline boron. *Phys. Let.* **2**, 30 (1962).
33. Wald, F., Rosenberg, J.A., Constitutional investigations in the boron-platinum system. *Trans. Met. Soc. AIME*, **233**, 796 (1965).
34. Van Santen, R. A. The Ostwald step rule, *J. Phys. Chem.*, **88(24)**, 5768–5769 (1984)
35. Oganov, A.R., Chen, J., Gatti, C., Ma, Y., Ma, Y., Glass, C.W., Liu, Z., Yu, T., Kurakevych, O.O., Solozhenko, V.L. Ionic high-pressure form of elemental boron. *Nature letters* **457**, 863-867 (2009); **460**, 292 (2009).
36. Horn., F. Some electrical and optical properties of simple rhombohedral boron. *J. Appl. Phys.* **30**, 1611-1613 (1959).
37. Terauchi, M., Kawamata, Y., Tanaka, M., Takeda, M., Kimura, K. Electron energy-loss spectroscopy study of the electronic structure of  $\alpha$ -rhombohedral boron. *J. Sol. State Chem.* **133**, 156-159 (1997).
38. Hillert, M. Phase equilibria, phase diagrams and phase transformations: their thermodynamic basis. *Cambridge Univ. Press* (2007).
39. Dubrovinskaia, N., Dubrovinsky, L., Miyajima, N., Langenhorst, F., Crichton, W.A., Braun H. F. High-pressure high-temperature synthesis and characterization of boron-doped diamond. *Zeitschrift für Naturforschung* **61b**, 1561-1565, (2006).
40. Dubrovinskaia, N., Dubrovinsky, L., McCammon, C. Iron-magnesium alloying at high pressures and temperatures. *J. of Physics: Condensed Matter*, **16**, S1143 -S1150 (2004).

41. Dubrovinsky, L., Glazyrin, K., McCammon, C., Narygina, O., Greenberg, E., Uebelhack, S., Chumakov, A. I., Paskarelli, S., Prakapenka, V., Bock, J., Dubrovinskaia, N. Portable laser-heating system for diamond anvil cells. *J. Synchrotron Rad.*, **16**, 737-741 (2009).
42. Wirth, R. Focused Ion Beam (FIB): A novel technology for advanced application of micro- and nanoanalysis in geosciences and applied mineralogy. *Eur. Journal Mineralogy*, **16**, 863-877 (2004).

### **Acknowledgments**

The work was supported by the German Research Foundation (DFG) through the DFG Priority Program 1236. N.D. thanks DFG for the financial support through the Heisenberg Program.

### **Author Contributions**

L.D. and N.D. designed research; G.P., N.D., L.D., E.B., and R.W. performed research and analyzed data; G.P., L.D. and N.D. wrote the paper.

### **Competing financial interests**

The authors declare no competing financial interests.

## **4.4 High pressure synthesis and investigation of single crystals of metastable boron phases**

Gleb Parakhonskiy<sup>a,b</sup>, Natalia Dubrovinskaia<sup>\*b</sup>, Elena Bykova<sup>a,b</sup>, Richard Wirth<sup>c</sup>, Leonid Dubrovinsky<sup>a</sup>

<sup>a</sup> *Bayerisches Geoinstitut, Universität Bayreuth, D-95440 Bayreuth, Germany*

<sup>b</sup> *Materialphysik und Technologie bei extremen Bedingungen, Lehrstuhl für Kristallographie, Universität Bayreuth, D-95440 Bayreuth, Germany*

<sup>c</sup> *GeoForschungsZentrum Potsdam, Experimental Geochemistry and Mineral Physics, 14473 Potsdam, Germany*

### **4.4.1 Abstract**

In the present work we have confirmed the existence of the tetragonal boron phase T-50 that was disputed for more than a half of a century. This phase was reproducibly synthesised at high pressures and high temperatures (HPHT) in form of single crystals and its structure was refined based on single crystal synchrotron X-ray diffraction data. We also present here a previously unknown rhombohedral boron phase synthesised in a limited HPHT field. Its structure was solved based on in house single crystal X-ray diffraction data and found to be similar to that of boron carbide. After hitherto known stable  $\alpha$ -B,  $\beta$ -B, and  $\gamma$ -B polymorphs, T-50 and the newly obtained rhombohedral boron phases were designated in the present work as  $\delta$ -B and  $\varepsilon$ -B, correspondingly. Issuing from the experimental evidences, the both phases are considered as metastable.

### **4.4.2 Introduction**

The synthesis and structure of tetragonal boron t-I (also referred to as  $\alpha$ -tetragonal boron, or T-50 on the number of atoms distributed among four icosahedra and two interstitial positions in the unit cell (space group  $P4_2/nm$ ), according to the original study [1-3]) has been a long standing controversy [4]. Further we will call this phase T-50. Despite theoretical calculations [5] showed that T-50 has an unstable electronic configuration, it was considered the first known crystal structure of a boron allotrope [4] until Will & Ploog refuted this [6]. Will & Ploog [6] failed to reproduce the crystals using the chemical preparative technique described in Ref. 1, but developed methods allowing yielding boron-rich carbide  $B_{25}C$  and nitride  $B_{25}N$  with the structure previously reported [1-3] for the tetragonal boron polymorph. The argument of irreproducibility of the previously reported synthesis [1] along with a

possibility to explain stabilisation of the otherwise theoretically unstable T-50 structure due to the presence of carbon and nitrogen [6] led to a long-time rejection of the existence of T-50 as a boron polymorph [4].

Synthesis of boron nanoribbons [7] and nanowire boron bundles [8] with the T-50 structure has been reported in literature relatively recently and the DFT based calculations [9] showed that T-50 can be stabilized compared to  $\alpha$ -B and  $\beta$ -B if one takes into consideration the surface energy. However, all the available experimental information summarised in the recent review article (see Ref. 4 and references therein) allowed the authors [4] to conclude that the question of the real composition and structure of T-50 can still not be answered. Although recently there were reports on synthesis of polycrystalline T-50 [10, 11, 12], there have not been unambiguous synthesis of T-50 in the form of single crystals, hence the efforts to do this to prove the existence of this phase are totally justified.

Following our successful experience on HPHT synthesis of single crystals of  $\alpha$ -B and  $\gamma$ -B [13-16], in the present work we systematically explored the PT phase diagram of boron in the region of pressures of 7.5 to 18 GPa and temperatures of 1373 to 2373 K to study the relations between boron stable phases and to reveal possible metastable phases. In a series of experiments we synthesized single crystals of the T-50 boron phase (later designated as  $\delta$ -B) and a new, previously not reported in literature, rhombohedral boron phase (later designated as  $\varepsilon$ -B) using  $\beta$ -boron as a starting material. Single crystals of the both phases were investigated by means of X-ray diffraction and spectroscopic techniques at variable PT conditions. The implications of the experimental results for the PT phase diagram of boron have been outlined.

#### 4.4.3 Experimental details

Highly crystalline  $\beta$ -boron (purity of 99.995 at.%, grain size of  $<1000 \mu\text{m}$ ), purchased from *Chempur Inc.*, was used as a source of boron. Pure  $\beta$ -B was loaded into a Pt or Au capsules made from the metal tubes. The capsules along with  $\text{LaCrO}_3$  heaters, isolated from each other by the MgO tubes, were enclosed into magnesium oxide ( $\text{MgO}+5 \text{ wt\% Cr}_2\text{O}_3$ ) octahedron which served as a pressure transmitting medium.

Synthesis was realised at various PT conditions using 1000-ton (Hymag) and 1200-ton (Sumitomo) multi-anvil hydraulic presses as described elsewhere [13-17]. The Kawai-type multi-anvil system was employed. In our experiments 18/11 (octahedron edge/anvil truncation length in mm), 14/8, and 10/5 assemblies were used to achieve pressures of 7-11 GPa, 11-15,

and 14-20 GPa, correspondingly. Temperature was measured using a W3%Re-W25%Re thermocouple located axially with respect to the heater (without corrections for the pressure effect on the thermocouple's emf). It was increased stepwise with a speed of about 80 K/min. In all the experiments, the uncertainties in pressure and temperature determination were estimated to be 1 GPa and 100 K, respectively. Duration of heating was 5 minutes, then the sample was quenched. After decompression, the synthesis products were extracted and crystals were taken out of the capsule with a needle and carefully washed first in *aqua regia* at 100 °C and then in water.

For the phase identification, selection of single crystals, and preliminary structural analysis a high-brilliance Rigaku diffractometer (Mo K $\alpha$  radiation) equipped with Osmic focusing X-ray optics and Bruker Apex CCD detector was used. The diffraction patterns were processed using Fit2D software [18].

A LabRam spectrometer (with a resolution of 2 cm<sup>-1</sup>), a He-Ne laser (632.8 nm) with a power of 15 mW for excitation, and a 50 $\times$  objective were used for the Raman spectroscopy experiments.

The morphology and chemical composition of the synthesized single crystals were characterised by means of the scanning electron microscopy (SEM) (LEO-1530). Chemical composition of the samples was investigated using WDX microprobe analysis (JEOL JXA-8200; focused beam; 20 keV, 20 nA).

Electron transparent foils were prepared by focused ion beam (FIB) techniques. FIB allows preparation of site-specific TEM foils with typical dimensions of 15–20  $\mu$ m wide, by approximately 10  $\mu$ m high and approx. 0.150  $\mu$ m thick [19].

TEM investigations were performed with a TECNAI F20 XTWIN transmission electron microscope operating at 200 kV with a field emission gun electron source. The TEM is equipped with a Gatan Tridiem<sup>TM</sup> filter, an EDAX Genesis<sup>TM</sup> X-ray analyzer with ultra thin window and a Fishione high angle annular dark field detector (HAADF). The Tridiem filter was used for the acquisition of energy-filtered images applying a 20 eV window to the zero loss peak. EELS spectra were acquired with a dispersion of 0.1 eV/channel and an entrance aperture of 2 mm. The resolution of the filter was 0.9 eV at full width, at half maximum of the zero loss peak. Acquisition time was 1 second. Spectra of the different K-edges (B, C, N, O) were acquired in diffraction mode with a camera length of 770 mm. Spectra processing (background subtraction, removal of plural scattering, quantification) was performed using the DigitalMicrograph software package. EDX spectra were usually acquired in the scanning transmission mode (STEM) using the TIA<sup>TM</sup> software package of the TEM. Significant mass

loss during analysis was avoided by scanning the beam in a pre-selected window (20 x 20 nm or larger). Spot size was approx. 1 nm, and acquisition time 60 seconds at an average count rate of 60 – 80 counts/second. This resulted in a counting error of about 4 -5% at a  $3\sigma$  level.

Single-crystal X-ray diffraction data of the  $\epsilon$ -B crystal was collected at ambient temperature using four-circle Oxford Diffraction Xcalibur diffractometer ( $\lambda = 0.7107 \text{ \AA}$ ) equipped with an Xcalibur Sapphire 2 CCD detector. The reflection intensities were measured by omega scanning of narrow ( $0.5^\circ$ ) frames. The data collection and further integration were performed with CrysAlis CCD and CrysAlis RED software [20], respectively. Empirical absorption correction using spherical harmonics, implemented in SCALE3 ABSPACK scaling algorithm which is included to the CrysAlis RED software [20]. The structure was solved by the direct method and refined by full matrix least-squares in the anisotropic approximation for all atoms using the SHELX-97 program package[21].

Due to a small size of the  $\delta$ -B crystal X-ray diffraction experiment has been performed on synchrotron (Swiss-Norwegian beamline BM01A, ESRF). The data were collected at ambient temperature using a six-circle KUMA6 diffractometer ( $\lambda = 0.7006 \text{ \AA}$ ) equipped with a MAR345 image plate detector. The reflection intensities were measured by omega-scanning of narrow ( $0.5^\circ$ ) frames. The data collection and further integration were performed with CrysAlis CCD and CrysAlis RED [20] software, respectively. The absorption corrections were applied empirically by the SADABS program [22,23]. The structure was solved by the direct method and refined by full matrix least-squares in the isotropic approximation for all atoms. The DIAMOND software [24] was used to create molecular graphics.

Diamond anvil cell (DAC) experiments were conducted using diamond anvils with the culet size of 250  $\mu\text{m}$ . A hole of 120  $\mu\text{m}$  in diameter was drilled in the Re gasket pre-indented to about 30  $\mu\text{m}$  thickness to serve as a pressure chamber. Neon was used as a pressure transmitting medium. A ruby gauge was used for pressure determination. For double-side laser heating in DAC we employed two UniHead systems [25] installed at Bayerisches Geoinstitut. The size of the laser beam was of about 30  $\mu\text{m}$  in diameter with a temperature variation of  $\pm 50 \text{ K}$  within the beam. The heating duration was about 5 minutes. Temperature was measured by means of multiwavelength spectroradiometry.

#### 4.4.4 Results and discussion

##### *HP synthesis and characterisation of single crystals of the tetragonal metastable boron phase ( $\delta$ -boron)*

At pressures above 9 GPa, characteristic needle-shaped grey-reddish semitransparent crystals were found among other synthesis products (Figure 4.4.4.1a). Their size varied from  $30 \times 2 \times 2 \mu\text{m}^3$  to  $150 \times 5 \times 5 \mu\text{m}^3$ .

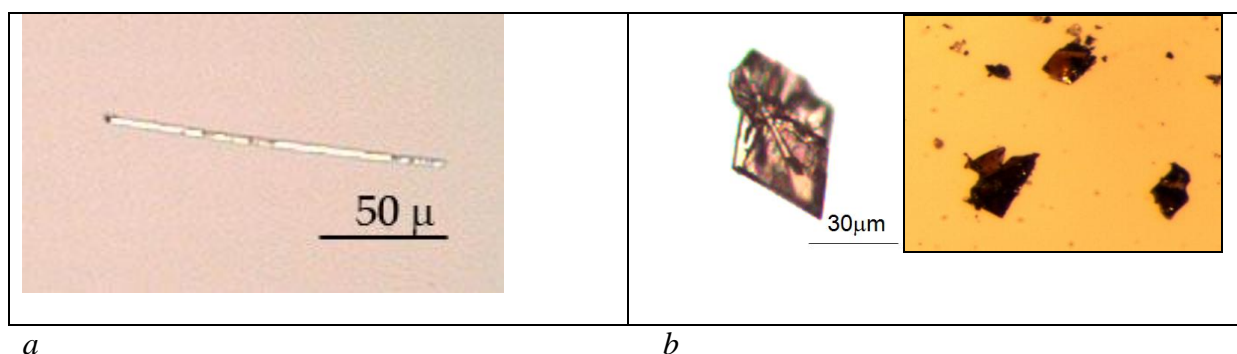
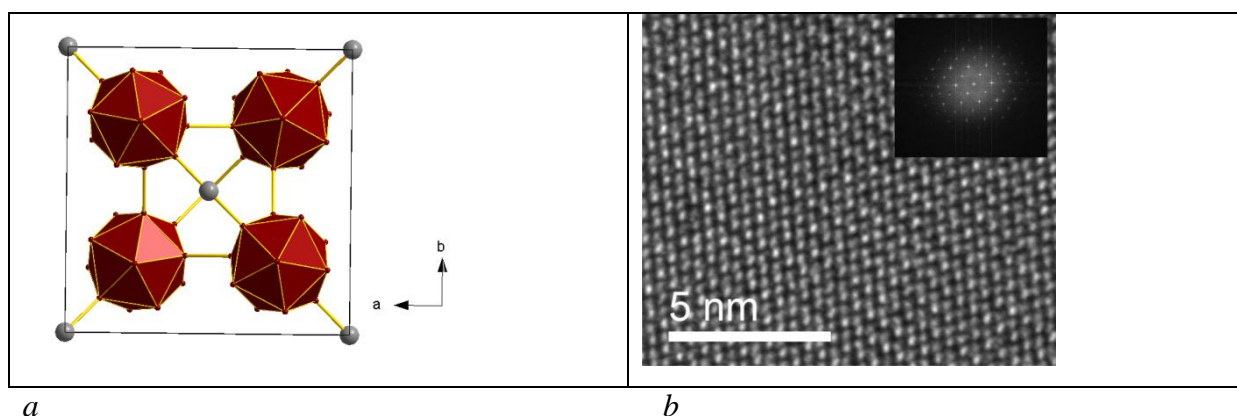


Figure 4.4.4.1. Single crystal of (a) T-50 (designated as  $\delta$ -B later in this work) and (b) the newly synthesised boron phase (designated as  $\epsilon$ -B later in this work).

On the X-ray diffraction the phase was identified as the tetragonal (T-50) boron [2,3] (Figure 4.4.4.2a) in good agreement with the results of HRTEM and electron diffraction (Figure 2b). Experimental parameters and single crystal synchrotron X-ray diffraction data are presented in Table 4.4.4.1. The refined unit cell parameters are in agreement with those determined by Hoard et al. [2] (Table 4.4.4.2). Interatomic B-B distances in B<sub>12</sub> icosahedra vary from 1.66 to 1.87 Å and correspond to those in other icosahedral boron structures, like  $\alpha$ -boron (B<sub>12</sub>) (1.74-1.81 Å) and  $\gamma$ -boron (B<sub>28</sub>) (1.76-1.88 Å) [13,16].



**Figure 4.4.4.2** Structure of T-50 ( $\delta$ -B). (a) Structure of  $\delta$ -B in polyhedra; (b) HRTEM image of  $\delta$ -B. On electron diffraction pattern all reflections correspond to  $\delta$ -B.

**Table 4.4.4.1** Experimental single crystal X-ray diffraction data for T-50 ( $\delta$ -B).

Name	B <sub>50</sub>
Formula weight	540.50
Temperature	296(2) K
Wavelength	0.7 Å
Crystal system	Tetragonal
Space group	<i>P4<sub>2</sub>/nnm</i>
Unit cell dimensions	<i>a</i> = 8.708(9) Å <i>c</i> = 5.0750(8) Å
Volume	384.8(6) Å <sup>3</sup>
Z	1
Density (calculated)	2.332 g/cm <sup>3</sup>
Absorption coefficient	0.086 mm <sup>-1</sup>
F(000)	250
Crystal size	0.100x0.02x0.002 mm <sup>3</sup>
Theta range for data collection	3.26 to 21.07°
Index ranges	-8 ≤ <i>h</i> ≤ 8, -8 ≤ <i>k</i> ≤ 8, -5 ≤ <i>l</i> ≤ 5
Reflections collected	2816
Independent reflections	119 [ <i>R</i> <sub>(int)</sub> = 0.056]
Completeness to theta = 21.07°	96.9 %
Refinement method	Full-matrix least-squares on F <sup>2</sup>
Data / restraints / parameters	119 / 0 / 16
Goodness-of-fit on F <sup>2</sup>	1.003
Final <i>R</i> indices [ <i>I</i> > 2σ( <i>I</i> )]	<i>R</i> <sub>1</sub> = 0.094, <i>wR</i> <sub>2</sub> = 0.246
<i>R</i> indices (all data)	<i>R</i> <sub>1</sub> = 0.095, <i>wR</i> <sub>2</sub> = 0.247
Largest diff. peak and hole	0.058 and -0.27 e·Å <sup>-3</sup>

**Table 4.4.4.2** The data on the crystal structure of  $\delta$ -B obtained in the present work in comparison with the literature data.

	This work	Hoard et al. (Ref. 2)
<i>a</i> , Å	8.708(9)	8.743(15)
<i>c</i> , Å	5.0750(9)	5.030(3)
<i>V</i> , Å <sup>3</sup>	384.8(6)	384.493
B1, 2b	0, 0, 1/2	0, 0, 1/2
B1, 8m	0.1239(7) 0.1239(7) 0.3685(18)	0.1195, 0.1195, 0.3780
B3, 8m	0.2458(8) 0.2458(8) 0.5897(17)	0.2423, 0.2425, 0.5815
B4, 16n	0.3161(7) 0.1042(8) 0.3907(14)	0.3253, 0.0883, 0.3985
B5, 16n	0.2288(7) 0.0827(7) 0.0819(13)	0.2272, 0.0805, 0.0685
<i>R</i> <sub>1</sub>	9.4%	11.4%

The Raman spectrum of the synthesized crystals is drastically distinct from those of other boron polymorphs (Figure 4.4.4.3a). It has one dominating intense Raman peak at 491

$\text{cm}^{-1}$ , which is also characteristic for the spectrum of tetragonal boron nanoribbons reported by Xu *et al.* [7]. The Raman spectrum reported by Qin *et al.* [10] does not correspond to the spectra obtained both in the present work and Ref. 7.

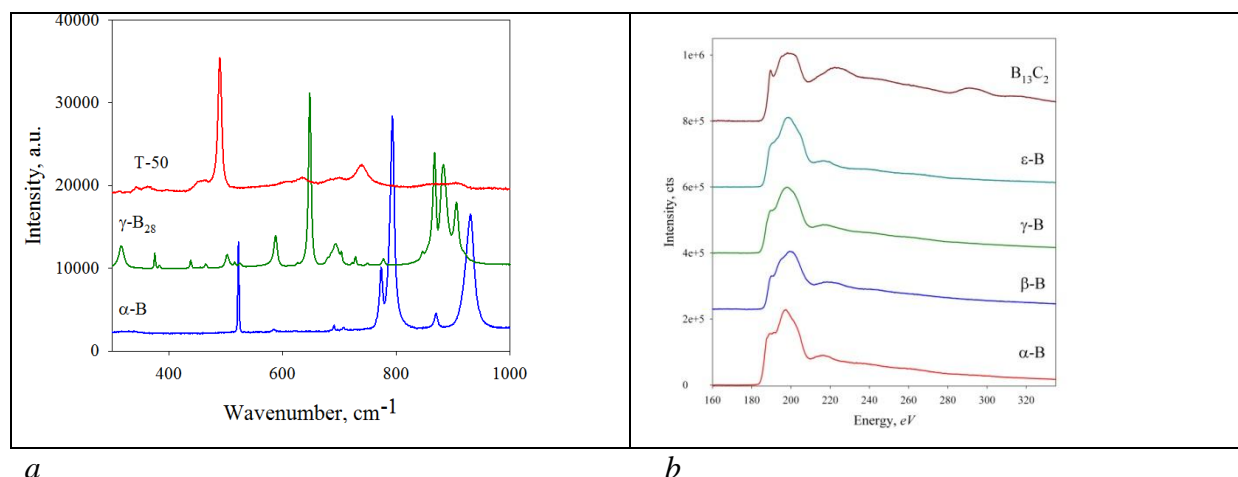


**Figure 4.4.4.3** Raman and EELS spectra of boron polymorphs. (a) Raman spectrum of T-50 ( $\delta\text{-B}$ ) compared to those of  $\alpha\text{-B}$  and  $\gamma\text{-B}$ . (b) EELS spectra of boron polymorphs compared to that of boron carbide.

Thus, in the present work T-50 was for the first time synthesised at HPHT conditions in form of single crystals and its structure was refined based on synchrotron X-ray diffraction data. Diffraction data provide no sign of any contamination. The presence of carbon or nitrogen in the structure was also excluded, because the chemical purity of the T-50 phase was proven by EELS (Figure 4.4.4.3b). Therefore, the long standing controversy, if the “theoretically unstable” [5, 26] T-50 phase can be synthesised as a bulk material without stabilisation due to the surface energy in nanostructures, or by the presence of carbon or nitrogen [6], has been experimentally resolved. This means that T-50 can be designated as  $\delta\text{-B}$  in a row of the known stable  $\alpha\text{-B}$ ,  $\beta\text{-B}$ , and  $\gamma\text{-B}$  polymorphs. The fact that the  $\delta\text{-B}$  crystals never appeared as a single phase in the process of HPHT synthesis, but always in the presence of other boron polymorphs, points towards metastability of  $\delta\text{-B}$ .

#### ***HP synthesis and characterisation of single crystals of the new rhombohedral metastable boron phase ( $\epsilon\text{-boron}$ )***

In course of our experiments at P-T conditions of 8.5-9 GPa and 1873-2073 K, except known boron phases, some other yellow-reddish-orange, transparent, plate-shaped crystals were found (Figure 4.4.4.2b). The length of these crystals varied from 20  $\mu\text{m}$  to 150  $\mu\text{m}$ . Their Raman spectrum is characterized by the following peak positions: 336  $\text{cm}^{-1}$ , 484  $\text{cm}^{-1}$ , 537  $\text{cm}^{-1}$ , 732  $\text{cm}^{-1}$ , 807  $\text{cm}^{-1}$  and 1086  $\text{cm}^{-1}$ . It is different from the spectra of any other boron

polymorphs, but akin to that of boron carbide  $B_{13}C_2$  with a small shift of about  $5\text{ cm}^{-1}$  (Figure 4). The transparency of the new crystals compared to always black boron carbide also gives evidence to their different chemical nature. EELS measurements on the new phase revealed the absence of carbon (Figure 4.4.4.3b) or any other atoms except boron. Taking into account that the crystals appeared only in the presence of the other boron phases, this phase is likely metastable. After  $\delta$ -B it will be called  $\varepsilon$ -B further in the paper.

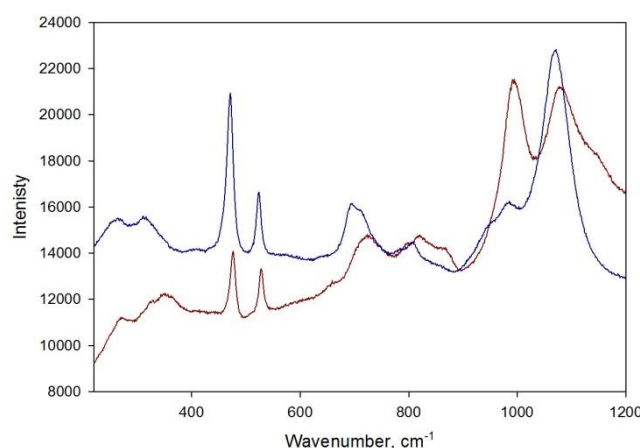


**Figure 4.4.4.4** Raman spectrum of the newly synthesised phase (later in this work designated as  $\varepsilon$ -B) (lower curve) compared to that of boron carbide  $B_{13}C_2$  (upper curve). Both spectra were collected on the same instrument at one experimental session that excludes a possibility of the shift because of the calibration problem.

Single crystal X-ray diffraction (Table 4.4.4.3) revealed that this phase is isostructural to  $B_{13}C_2$  [27], whose arrangement of B12 icosahedra is analogous to that of the  $\alpha$ -B structure. The rhombohedral unit cell of  $B_{13}C_2$  contains three-atomic (or two-atomic in case of the presence of a vacancy) linear groups of carbon and boron atoms oriented along the main diagonal of the unit cell. In the newly synthesised boron phase there are only three-atomic linear groups consisting of boron atoms (Figure 4.4.4.5). The unit cell parameters are:  $a = 5.5940(7)\text{ \AA}$ ,  $c = 12.0756(16)\text{ \AA}$  (hexagonal setting); the space group is  $R\bar{3}m$ . We must note that upon refinement of the structure, a residual electron density peak of  $0.54\text{ e}^*\text{ \AA}^{-3}$  appears in  $0.47\text{ \AA}$  from B4, while the absolute value of the largest hole is smaller,  $-0.27\text{ e}^*\text{ \AA}^{-3}$ . In addition, an equivalent isotropic thermal parameter of B4 is much smaller ( $0.0028(8)\text{ \AA}^2$ ) in comparison with that for B1, B2, B3 atoms ( $0.0113(13)$ ,  $0.0074(6)$ ,  $0.0078(6)\text{ \AA}^2$ ). The quality of the refinement can be improved due to placing one carbon atom instead of B4, then the  $R_1$  value decreases from 5.01 to 3.83 % (contrary, placing nitrogen instead of boron increases the  $R_1$  value to  $\sim 7.5\%$ ). The highest residual density peak and hole have very close absolute values,  $0.278$  and  $-0.274\text{ e}^*\text{ \AA}^{-3}$ . The thermal parameter of C4 ( $0.0083(7)\text{ \AA}^2$ ) becomes closer to B2, B3 ( $0.0075(5)$ ,  $0.0079(5)\text{ \AA}^2$ ). In both models the isothermal parameter

of B1 is larger,  $\sim 0.011 \text{ \AA}^2$  which is the most likely due to a disorder of the boron atom in this position. However, taking into account the confirmed by EELS and EDX absence of any contaminations in the material, the presently available experimental data can be interpreted only as described above and presented in Table 4.4.4.3 and Table 4.4.4.4.

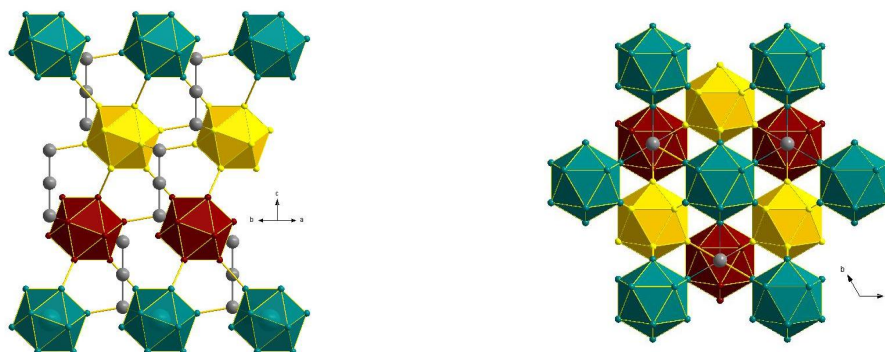


**Figure 4.4.4.5** Crystal structure of  $\epsilon$ -B.

**Table 4.4.4.3** Experimental single crystal X-ray diffraction data for  $\epsilon$ -B.

Name	$B_{15}$
Formula weight	162.15
Temperature	296(2) K
Wavelength	0.71073 $\text{\AA}$
Crystal system	Trigonal
Space group	$R\bar{3}m$
Unit cell dimensions	$a = 5.5940(7) \text{ \AA}$ $c = 12.0756(16) \text{ \AA}$
Volume	327.25(7) $\text{\AA}^3$
Z	3
Density (calculated)	2.468 $\text{g/cm}^3$
Absorption coefficient	0.091 $\text{mm}^{-1}$
F(000)	225
Crystal size	0.05 x 0.03 x 0.01 $\text{mm}^3$
Theta range for data collection	4.53 to 31.12 $^\circ$
Index ranges	$-7 \leq h \leq 8, -8 \leq k \leq 6, -13 \leq l \leq 17$
Reflections collected	978
Independent reflections	148 [ $R_{\text{int}} = 0.0863$ ]
Completeness to theta = 25.00 $^\circ$	94.4 %
Max. and min. transmission	0.9991 and 0.9955
Refinement method	Full-matrix least-squares on $F^2$
Data / restraints / parameters	148 / 0 / 18
Goodness-of-fit on $F^2$	1.185
Final R indices [ $I > 2 \sigma(I)$ ]	$R_1 = 0.0501, wR_2 = 0.1254$
R indices (all data)	$R_1 = 0.0590, wR_2 = 0.1292$
Largest diff. peak and hole	0.540 and $-0.327 \text{ e} \cdot \text{\AA}^{-3}$

**Table 4.4.4.4** Atomic coordinates and equivalent isotropic displacement parameters for  $\epsilon$ -B.  $U_{\text{eq}}$  is defined as one third of the trace of the orthogonalized  $U_{ij}$  tensor.

Atom	Wyckoff position	$x/a$	$y/b$	$z/c$	$U_{\text{eq}}, \text{\AA}^2$
B(1)	$3b$	0	0	1/2	0.011(1)
B(2)	$18h$	0.1626(3)	0.8374(3)	0.6413(2)	0.007(1)
B(3)	$18h$	0.2255(3)	0.7745(3)	0.7805(2)	0.008(1)
B(4)	$6c$	0	0	0.6192(3)	0.003(1)

To study phase transformations of  $\epsilon$ -B in the field of stability of  $\gamma$ -B, a crystal of  $\epsilon$ -B along with a  $\beta$ -B crystal was loaded into a DAC. Neon was used as a pressure transmitting medium and ruby as a pressure gauge. After pressurising to 11 GPa, both crystals were heated by laser at 2300 K. According to the phase diagram [13], at such PT conditions boron must transform to the  $\gamma$ -B phase. After heating the Raman spectra were measured again. As expected, both  $\beta$ -B and  $\epsilon$ -B fully transformed to  $\gamma$ -B (Figure 4.4.4.6) that may also serve as an additional evidence of the pure-boron composition of the  $\epsilon$ -B phase.

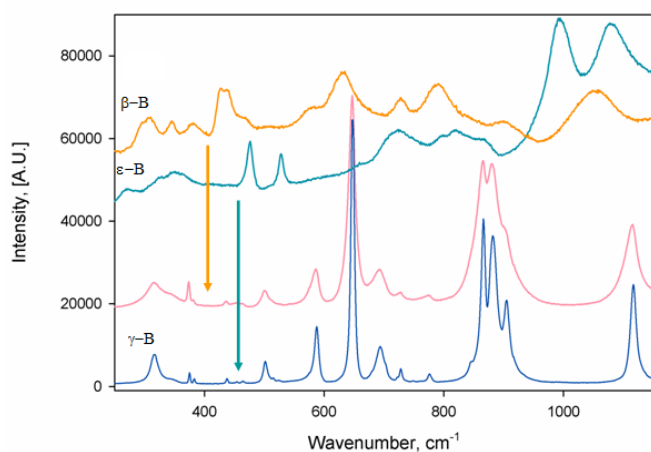


**Figure 4.4.4.6** Raman spectra of  $\epsilon$ - and  $\beta$ -boron crystals taken in a DAC before (upper two curves) and after (lower two curves) laser heating at 2300 K at 11 GPa.

Stability of  $\epsilon$ -B under compression at room temperature was investigated by pressurising a crystal of  $\epsilon$ -B isothermally in a DAC to 62 GPa. During the compression, a monotonous shift of the Raman peak positions toward higher wavenumbers was observed.

The Raman spectroscopy investigation revealed the absence of any phase transitions in  $\epsilon$ -B under compression up to 62 GPa at room temperature.

At 30, 40 and 62 GPa, the crystal of  $\epsilon$ -boron was heated by laser at 2000 K for 5 min. The Raman spectra did not change after heating. Similar experiments at 11 GPa and 2300 K led to a transition of  $\epsilon$ -boron to  $\gamma$ -boron that may be an evidence of the increasing kinetic stability of  $\epsilon$ -B with pressure. It is interesting to note, that at 62 GPa, the crystal of  $\epsilon$ -boron became colorless and totally optically transparent (Figure 7).

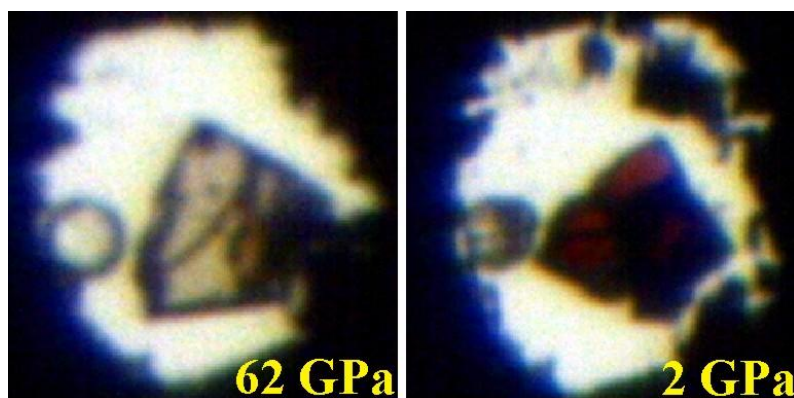


**Figure 4.4.4.7** Photograph of  $\epsilon$ -B crystal in the DAC upon 62 and 2 GPa.

Measured microhardness of  $\epsilon$ -boron is  $H_V \sim 55$ -60 GPa that is similar to that of single crystal  $\gamma$ -B ( $\sim 60$  GPa) [16] and higher than that of boron carbide (38 GPa) and of other boron polymorphs,  $\alpha$ -B (42 GPa) and  $\beta$ -B (45 GPa) [27].

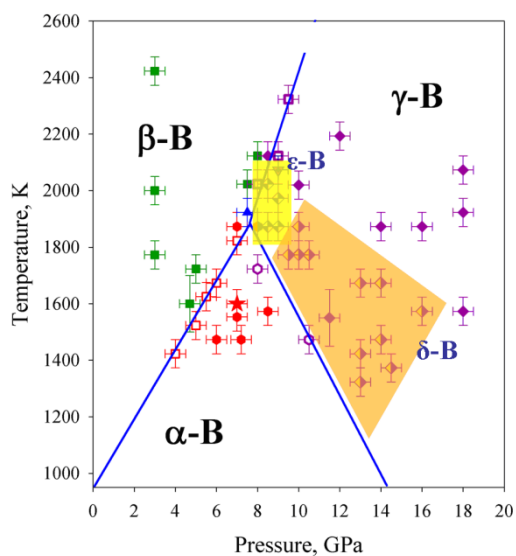
#### *The implications of the experimental results for the HP phase diagram of boron*

Table 4.4.4.5 summarizes the HPHT experiments conducted with the purpose of synthesis of metastable boron phases. Based on these results, the PT phase diagram of boron [13] can be complemented with the fields of the occurrence of metastable phases,  $\epsilon$ -B and  $\delta$ -B (Figure 4.4.4.8).

**Table 4.4.4.5** Summary of HPHT experiments on boron, conducted in multi-anvil apparatus. Heating duration in every experiment was 5 minutes. (Typical uncertainty in temperature is  $\pm 50$ K and  $\pm 0.5$  GPa in pressure. In synthesis products initial non-transformed  $\beta$ -boron powder and platinum boride are not mentioned).

Experiment	Starting material	Experimental conditions			Synthesis results
		capsule material	temperature, K	Pressure, GPa	
S4805	85 at.% $\beta$ -B + 15 at.% Pt	Au	1773	9.5	$\gamma$ -B, $\delta$ -B

H3154	85 at.% $\beta$ -B + 15 at.% Pt	Au	1773	10.5	$\gamma$ -B, $\delta$ -B
H3244	$\beta$ -B	Pt	1873	14	$\gamma$ -B
S5064	$\beta$ -B	Pt	1923	7.5	$\alpha$ -B, $\gamma$ -B, recryst. $\beta$ -B
S5110	$\beta$ -B	Pt	1373	14.5	$\delta$ -B, $\gamma$ -B
H3191	$\beta$ -B	Pt	2193	12	$\gamma$ -B
S5150	$\beta$ -B	Pt	1673	13	$\delta$ -B, $\gamma$ -B
S5166	$\beta$ -B	Pt	1673	14	$\delta$ -B, $\gamma$ -B
S5231	$\beta$ -B	Pt	1573	16	$\delta$ -B, $\gamma$ -B
S5225	$\beta$ -B	Pt	1873	16	$\gamma$ -B
S5194	$\beta$ -B	Pt	1573	18	$\gamma$ -B
S5206	$\beta$ -B	Pt	1923	18	$\gamma$ -B
S5187	$\beta$ -B	Pt	2073	18	$\gamma$ -B
S5063	$\beta$ -B	Pt	1873	8.5	$\gamma$ -B, $\epsilon$ -B
S5053	$\beta$ -B	Pt	2023	8.5	$\gamma$ -B, $\epsilon$ -B
S5027	$\beta$ -B	Pt	1873	9	$\gamma$ -B, $\epsilon$ -B
S5062	$\beta$ -B	Pt	1973	9	$\gamma$ -B, $\epsilon$ -B
S5084	$\beta$ -B	Pt	2073	9	$\gamma$ -B, $\beta$ -B, $\epsilon$ -B
S5080	$\beta$ -B	Pt	2123	9	$\gamma$ -B, $\beta$ -B
S5060	$\beta$ -B	Pt	2123	8	$\beta$ -B
S5090	$\beta$ -B	Pt	2023	10	$\gamma$ -B
S5095	$\beta$ -B	Pt	1873	10	$\gamma$ -B, $\delta$ -B
S5103	$\beta$ -B	Pt	1773	10	$\gamma$ -B, $\delta$ -B
S5148	$\beta$ -B	Pt	1423	13	$\gamma$ -B, $\delta$ -B
S5123	$\beta$ -B	Pt	1323	13	$\gamma$ -B, $\delta$ -B
S5169	$\beta$ -B	Pt	1473	14	$\gamma$ -B, $\delta$ -B
S5073	$\beta$ -B	Pt	2323	9.5	$\gamma$ -B, $\beta$ -B



**Figure 4.4.4.8. The PT phase diagram of boron** [13]. The PT fields where metastable phases of  $\epsilon$ -B and  $\delta$ -B were observed along with other boron phases are shadowed. The conditions at which crystallisation of various boron phases occurred are marked by different signs: solid green squares -  $\beta$ -B; solid purple diamonds -  $\gamma$ -B; solid red hexagons -  $\alpha$ -B; open red squares -  $\alpha$ -B and  $\beta$ -B; open purple squares -  $\beta$ -B and  $\gamma$ -B; open purple hexagons -  $\alpha$ -B and  $\gamma$ -B; blue solid triangle -  $\alpha$ -B,  $\beta$ -B, and  $\gamma$ -B; red inverted triangle -  $\epsilon$ -B,  $\beta$ -B, and  $\gamma$ -B; red star marks the conditions of the multi-anvil experiment which led to the solid-solid  $\beta$ -B-to- $\alpha$ -B phase transition; continues blue lines show apparent phase boundaries. Hour-glass rhombuses in the shadowed yellow area and semi-filled rhombuses in the shadowed orange area mark PT conditions of experiments when correspondingly single crystals of  $\epsilon$ -B and  $\delta$ -B were synthesized.

The PT phase diagram (Figure 4.4.4.8) is quite different from that one recently proposed in Qin et al. [10]. In particular, the diagram of Qin et al. [10] does not contain any information about the field of stability of  $\alpha$ -B and the phase boundaries do not agree with those shown in Figure 8. The discrepancies and the mismatch of the diagrams can be explained as follows. Our exploration of the boron phase diagram [13] was based on the same principles used for establishing the carbon phase diagram [28, 29] and crystallisation at various PT conditions was realised from the melt both in Ref. 13 and in the present work. This technique allows establishing equilibrium phase boundaries [28, 29]. Qin et al. [10] studied solid-state transformations which require high activation energies. The specific effects of transformation paths, pointed out as an additional factor for formation of metastable forms in the carbon system [29], play equally important role for boron as well, when metastable phases are quenched-in to survive metastably. This explains why the metastable T-50 ( $\delta$ -B) phase was observed at quite different PT conditions in the present work and in Qin et al. [10], but always in the presence of other boron polymorphs.

It should be noticed that in no one HPHT experiment we observed the T-192 phase [30, 31], although our PT experimental conditions covered the field where the T-192 was previously reported [30]. Studying solid-state transformations, Qin et al. [10] also did not see the T-192 phase, thus its existence still has not been confirmed experimentally.

#### **4.4.5 Conclusion**

In a series of experiments we have shown a feasibility of synthesis of single crystals of the tetragonal boron phase  $\delta$ -B (previously called T-50) at high PT conditions. The structure of  $\delta$ -B was refined based on single crystal X-ray diffraction in good agreement with the literature data. A new, previously not observed rhombohedral boron phase  $\varepsilon$ -B was synthesised at pressures above 8.5 GPa in form of single crystals and found to be isostructural with boron carbide. Chemical purity of the investigated crystals was proven by EELS. At ambient temperature  $\varepsilon$ -B was found to be stable at least up to 62 GPa. The measured Vickers hardness of the newly synthesised  $\varepsilon$ -B phase is about 55 GPa that places it in the row of superhard materials.

#### **Acknowledgments**

The work was supported by the German Research Foundation (DFG) through the DFG Priority Program 1236. N.D. thanks DFG for the financial support through the Heisenberg

Program. Help of Y. Filinchuk, D. Chernyshov, and V. Dmitriev in the synchrotron X-ray diffraction data collection is gratefully acknowledged.

## References

1. Laubengayer, A. & Hurd, D. Boron. I. *Preparation and properties of pure crystalline boron*. J. Am. Chem. Soc. 65 (1943), pp. 1924–1931.
2. Hoard, J., Hughes, R. & Sands, D.E. *The structure of tetragonal boron*. J. Am. Chem. Soc. 80 (1958), pp. 4507–4515.
3. Hoard, J., Geller, S. & Hughes, R. *On the structure of elementary boron*. J. Am. Chem. Soc. 73 (1951), pp. 1982–1983.
4. Albert, B., Hillebrecht, H. *Boron: elementary challenge for experimenters and theoreticians*. Angew. Chem. Int. Ed. 48 (46) (2009), pp. 8640–8668.
5. Longuet-Higgins, H.C. & Roberts, de V.M. *The electronic structure of the borides MB<sub>6</sub>*. P. Roy. Soc. A. Mat. 224 (1954), pp. 336–347.
6. Will, G. & Ploog, K. *Crystal structure of I-tetragonal boron*. Nature 251 (1974), pp. 406–408.
7. Xu, T.T., Zheng, J-G., Nicholls, A.W., Roth, J.R., Dikin, D. A. & Ruoff, R.S. *Crystalline boron nanoribbons: synthesis and characterization*. Nano Lett. 4 (2004), pp. 963–968.
8. Liu, F., Liang, W.J., Su, Z.J., Xia, J.X., Deng, S.Z., Chen, J., She, J.C., Xu, N.S., Tian, J.F., Shen, C.M. & Gao, H.-J. *Fabrication and field emission properties of boron nanowire bundles*. Ultramicroscopy 109 (2009), pp. 447–50.
9. Hayami, W. & Otani, S. *The role of surface energy in the growth of boron crystals*. J. Phys. Chem. C 111 (2007), pp. 688–692.
10. Qin, J., Irifune, T., Dekura, H., Ohfuji, H., Nishiyama, N, Lei, L. & Shinmei, T. *Phase relations in boron at pressures up to 18 GPa and temperatures up to 2200 °C*. Phys. Rev. B 85 (2012), pp. 014107-1-5.
11. Ekimov, E.A. & Zibrov, I.P. *High-pressure high-temperature synthesis and structure of α-tetragonal boron*. Sci. Technol. Adv. Mater. 12 (2011) pp. 055009-1-5.
12. Ekimov, E.A., Zibrov, I.P. & Zoteev, A.V. *Preparation of boron microcrystals via high-pressure, high-temperature pyrolysis of decaborane, B<sub>10</sub>H<sub>14</sub>*. Inorg. Chem. 47 (2011), pp. 1194-1198.
13. Parakhonskiy, G., Dubrovinskaia, N., Dubrovinsky, L., Mondal, S. & van Smaalen, S. *High pressure synthesis of single crystals of α-boron*. J. Cryst. Growth 321 (2011), pp. 162–166.
14. Parakhonskiy, G., Dubrovinskaia, N., Bykova, E., Wirth, R. & Dubrovinsky, L. *Experimental pressure-temperature phase diagram of boron: resolving the long-standing enigma*. Sci. Rep. 1, 96 (2011), DOI:10.1038/srep00096, pp 1–7.
15. Zarechnaya, E.Yu., Dubrovinskaia, N., Dubrovinsky, L., Filinchuk, Y., Chernyshov, D. & Dmitriev, V. *Growth of single crystals of B<sub>28</sub> at high pressures and high temperatures*. J. Cryst. Growth 312 (2010), pp. 3388–3394.
16. Zarechnaya, E.Yu., Dubrovinsky, L., Dubrovinskaia, N., Filinchuk, Y., Chernyshov, D., Dmitriev, V., Miyajima, N., El Goresy, A., Braun, H.F., Van Smaalen, S., Kantor, I., Kantor, A., Prakapenka, V., Hanfland, M., Mikhaylushkin, A.S., Abrikosov, I.A. & Simak, S.I. *Superhard semiconducting optically transparent high pressure phase of boron*. Phys. Rev. Lett. 102 (2009), pp. 185501.
17. Zarechnaya, E., Dubrovinsky, L., Dubrovinskaia, N., Miyajima, N., Filinchuk, Y., Chernyshov, D. & Dmitriev, V. *Synthesis of an orthorhombic high pressure boron phase*. Sci. Technol. Adv. Mat. 9 (2008), pp. 044209.
18. Hammersley, A.P., ESRF98HA01T, FIT2D V9.129 Reference Manual, vol. 3.1, 1998 (Internal Report).
19. Wirth, R. *Focused Ion Beam (FIB): A novel technology for advanced application of micro- and nanoanalysis in geosciences and applied mineralogy*. European J. Mineral. 16 (2004), pp. 863–876.
20. Oxford Diffraction CrysAlis CCD. (2006) ; Oxford Diffraction CrysAlis RED. (2006).
21. Sheldrick, G. M. SHELXL97. (1997).
22. Blessing, R. H. *DREADD – data reduction and error analysis for single crystal diffractometer data*. J. Appl. Crystallogr. 22 (1989) 396–397.
23. Sheldrick, G.M. (2003). SADABS. University of Göttingen, Germany.
24. Brandenburg, K. (1999). DIAMOND. Crystal Impact GbR, Bonn, Germany.
25. Dubrovinsky, L., Glazyrin, K., McCammon, C., Narygina, O., Greenberg, E., Uebelhack, S., Chumakov, A. I., Paskarelli, S., Prakapenka, V., Bock, J. & Dubrovinskaia, N. *Portable laser-heating system for diamond anvil cells*. J. Synchrotron Rad., 16 (2009), pp. 737-741.
26. Lee, S., Bylander, D.M., Kim, S.W. & Kleinman, L. *Computational search for the real tetragonal B<sub>50</sub>*. Phys. Rev. B 45 (1992), pp. 3248-3251.

27. Amberger, E. & Stumpf, W. *Boron*, *Gmelin Handbook of Inorganic Chemistry*, Berlin: Springer-Verlag, 112–238 (1981).
28. Bandy F.P., Bovenkerk H.P., Strong H.M. & Wentorf, Jr. R.H. *Diamond-graphite equilibrium line from growth and graphitization of diamond*. *J. Chem. Phys.* 35 (1961), pp. 383-391.
29. Bandy F.P., Bassett W.A., Weathers M.S., Hemley R.J., Mao H.K. & Goncharov A.F. *The pressure-temperature phase and transformation diagram for carbon; updated through 1994*. *Carbon* 34 (1996), pp. 141-153.
30. Ma, Y., Prewitt, C., Zou, G., Mao, H. & Hemley, R. High-pressure high-temperature x-ray diffraction of  $\beta$ -boron to 30 GPa. *Phys. Rev. B* 67, 174116 (2003).
31. Oganov, A.R., Chen, J., Gatti, C., Ma, Y., Ma, Y., Glass, C.W., Liu, Z., Yu, T., Kurakevych, O.O., Solozhenko, V.L. *Ionic high-pressure form of elemental boron*. *Nature* 457 (2009), pp. 863-867.

## **FULL LIST OF PUBLICATIONS (WITH PAPERS NOT INCLUDED INTO THE THESIS)**

G. Parakhonskiy, N. Dubrovinskaia, L. Dubrovinsky, S. Mondal, and S. van Smaalen. “High pressure synthesis of single crystals of  $\alpha$ -boron” *J. Cryst. Growth* **321**, 162-166 (2011).

G. Parakhonskiy, N. Dubrovinskaia, E. Bykova, R. Wirth, and L. Dubrovinsky. “Experimental pressure-temperature phase diagram of boron: resolving the long-standing enigma” *Sci. Rep.* **1**, 1-7 (2011).

G. Parakhonskiy, V. Vtech, N. Dubrovinskaia, R. Caracas and L. Dubrovinsky. “Raman spectroscopy investigation of  $\alpha$ -boron at elevated pressures and temperatures.” *J. Sol. State Com.*, **154**, 34-39 (2013).

G. Parakhonskiy, N. Dubrovinskaia, E. Bykova, R. Wirth, and L. Dubrovinsky. “High pressure synthesis and investigation of single crystals of metastable boron phases.” *Submitted to J. High Press. Res.*

E. Bykova, G. Parakhonskiy, N. Dubrovinskaia and L. Dubrovinsky. “The crystal structure of  $\beta$ -rhombohedral boron doped by aluminium.” *J. Sol. State Chem.*, **194**, 188-193 (2012).

S. Mondal, S. van Smaalen, G. Parakhonskiy, S.J. Prathapa, L. Noohinejad, E. Bykova, N. Dubrovinskaia, D. Chernyshov, and L. Dubrovinsky. “Experimental evidence of orbital order in  $\alpha$ -B<sub>12</sub> and  $\gamma$ -B<sub>28</sub> polymorphs of elemental boron. *Submitted to J. Am. Chem. Soc.*

N. Norrby, H. Lind, G. Parakhonskiy, M. Johansson, F. Tasnadi, L. Dubrovinsky, N. Dubrovinskaia, I. Abrikosov, and M. Oden. “High pressure and high temperature behaviour of Ti<sub>0.60</sub>Al<sub>0.40</sub>N. *J. Appl. Phys.* **113** (5), 053515 (2013).

Parakhonskiy B.V., Bukreeva T.V., Parakhonskiy G.V, Skirtach A.G., Sukhorukov G.B., Khlebtsov N.G., Feigin L.A., and Kovalchuk M.V. “Permeability adjustment of polyelectrolyte micro- and nanocapsules by laser irradiation” *Proc. SPIE.* **6536**, 653605 (2007).



## 5 BIBLIOGRAPHY

- Albert, B., and H. Hillebrecht. 2009. "Boron: Elementary Challenge for Experimenters and Theoreticians." *Ang. Chem. (Int. Ed.)* 48 (46): 8640–8668.
- Amberger, E., and W. Dietze. 1964. "Zur Bildung von Alpha-rhomboedrischem, Rotem Bor." *Z. Anorg. Allg. Chem* 38: 131–139.
- Becher, H.J., and H. Neidhard. 1968. "Siliziumhaltiges  $\beta$ -AlB<sub>12</sub> Und AlBeB<sub>24</sub> vom Typ Des BeB<sub>12</sub>." *Acta Crystallogr. B* 24: 280–281.
- Becher, H.J. 1960. "Über das Berylliumborid BeB<sub>12</sub> mit  $\beta$ -Bor-Struktur." *Z. Anorg. Allgem. Chem.* 306 (5-6): 266–272.
- Braccini, V., Davide, N., Roberto, P., and G. Giovanni. 2007. "Development of Ex Situ Processed MgB<sub>2</sub> Wires and Their Applications to Magnets." *Physica C.* 456 (1-2): 209–217.
- Braunschweig, H., Rian, D.D., Kai, H., Jan M., Krzysztof, R., and A. Vargas. 2012. "Ambient-temperature Isolation of a Compound with a Boron-boron Triple Bond." *Science* 336 (6087): 1420–1422.
- Brazhkin, V.V., Taniguichi, T., Akaishi, M., and S.V. Popova. 2004a. "Fabrication of  $\beta$ -boron by Chemical-reaction and Melt-quenching Methods at High Pressures." *J. Mat. Res.* 19 (06): 1643–1648.
- Bullett, D W. 1982. "Structure and Bonding in Crystalline Boron and B<sub>12</sub>C<sub>3</sub>." *J. Phys. C Solid State* 15 (3): 415–426.
- Callmer, B. 1977. "An Accurate Refinement of the  $\beta$ -Rhombohedral Boron Structure" *Acta Crystallogr. B.* 32449 (1973): 1951–1954.
- Clark, H. K., and J.L. Hoard. 1943. "The Crystal Structure of Boron Carbide." *J. Am. Chem. Soc.* 65 (11): 2115–2119.
- Cueilleron, J., and J.C. Viala. 1979. "The Chemical and Pyrometallurgical Purification of  $\beta$  Rhombohedral Boron." *J. Less Com. Met.* 67 (2): 333–337
- Decker, B. F., and J. S. Kasper. 1959. "The Crystal Structure of a Simple Rhombohedral Form of Boron." *Acta Crystallogr.* 12 (7): 503–506.
- Donohue, J. 1974. *Structures of the Elements*. Ed. Wiley. New York.
- Dubrovinskaia, N., and L. Dubrovinsky. 2003. "Whole-cell Heater for the Diamond Anvil Cell." *Rev. Sci. Instrum.* 74 (7): 3433.
- Dubrovinsky, L., Glazyrin, K., McCammon, C., Narygina, O., Greenberg, E., Ubelhack, S. Chumakov, A.I., Pascarelli, S., Prakapenka, V., Bock, J., and N. Dubrovinskaia. 2009.

- “Portable Laser-heating System for Diamond Anvil Cells.” *J. Synchrotron Radiat.* 16 (6): 737–41.
- Eremets, M.I, Struzhkin, V.V, Mao, H., and R.J. Hemley. 2001. “Superconductivity in Boron.” *Science* 293 (5528): 272–274.
- Frost, D.J, Poe, B.T, Trønnes, R.G, Liebske, C., Duba, A., and D.C Rubie. 2004. “A New Large-volume Multianvil System.” *Phys. Earth and Planet. In.* 143-144: 507–514.
- Garett, D.E. 1998. *Borates: Handbook of Deposits, Processing, Properties, and Use.* Academic Press.
- Greenwood, N.N. 1973. *Comprehensive Inorganic Chemistry.* Ed. Bailar., J.C. 1st ed. Oxford-New York: Pergamon Press.
- Greiner, E. S., and J. A. Gutowski. 1957. “Electrical Resistivity of Boron.” *J. App. Phys.* 28 (11): 1364-1366.
- Hammersley, A. P. 1998. “Two-Dimensional Detector Software: From Real Detector to Idealised Image or Two-Theta Scan.”
- Hayami, W., and S. Otani. 2007. “The Role of Surface Energy in the Growth of Boron Crystals.” *J. Phys. Chem. C* 111 (2): 688–692.
- Hayami, W., and S. Otani 2010. “First-principles Study of the Crystal and Electronic Structures of  $\alpha$ -tetragonal Boron.” *J. Solid State Chem.* 183 (7): 1521–1528.
- Hillert, M. 2007. *Phase Equilibria, Phase Diagrams and Phase Transformations: Their Thermodynamic Basis.* Cambridge Univ. Press.
- Hoard, J.L, and S. Geller. 1951. “On The Structure of Elementary Boron.” *J. Am. Chem. Soc.* 73 (4): 1982–1983.
- Hoard, J.L, Hughes, R.E., and D.E. Sands. 1958. “The Structure of Tetragonal Boron.” *J. Am. Chem. Soc.* 80 (17): 4507–4515.
- Hoard, J.L, Sullenger, D.B., Kennard, C.L., and R.E. Hughes. 1970. “The Structure Analysis of  $\beta$ -rhombohedral Boron.” *J. Solid State Chem.* 1 (2): 268–277.
- Holzmann, N., Stasch, A., Jones, C., and G. Frenking. 2011. “Structures and Stabilities of Group 13 Adducts [(NHC)(EX<sub>3</sub>)] and [(NHC)<sub>2</sub>(E<sub>2</sub>X<sub>(n)</sub>)] (E=B to In; X=H, Cl; N=4, 2, 0; NHC=N-heterocyclic Carbene) and the Search for Hydrogen Storage Systems: a Theoretical Study.” *Chemistry* 17 (48) 13517–13525.
- Horn, F.H. 1959. “On the Crystallization of Simple Rhombohedral Boron from Platinum.” *J. Electrochem. Soc.* 106: 905.
- Ito, E. 2012. “Development of the Kawai-type multi-anvil apparatus (KMA) and its application to high pressure earth science.” *J. Phys.: Conf. Ser* 377: 012001.

- Kaneshige, M., Hirayama, S., Yabuuchi, T., Matsuoka, T., Shimizu, K., Mita, Y., Hyoudo, H., and K. Kimura. 2007. "Measurement of Electrical Resistance and Raman Spectrum of Boron Under High Pressure." *J. Phys. Soc. Jpn. Supplement* 76: 19–20.
- Kawai, N., and S. Endo. 1970. "The Generation of Ultrahigh Hydrostatic Pressures by a Split Sphere Apparatus." *Rev. Sci. Instrum.* 41 (8): 1178–1181.
- Kawai, N., Togaya, M., and A. Onodera. 1973. "New Device for High Pressure-vessels." *P. Jpn. Acad.* 8: 623–626.
- Laubengayer, A.W., and D.T. Hurd. 1943. "Boron. I. Preparation and Properties of Pure Crystalline Boron." *J. Am. Chem. Soc.* 65: 1924–1931.
- Lee, S., Bylander, D.M., Kim, S.W., and L. Kleinman. 1992. "Computational Search for the Real Tetragonal B<sub>50</sub>." *Phys. Rev. B* 45 (7) 3248-3251.
- Lipscomb, W.N. 1966. "Framework Rearrangement in Boranes and Carboranes." *Science* 153 (3734): 373–378.
- Lipscomb W.N. 1973. "Three-center Bonds in Electron-deficient Compounds. Localized Molecular Orbital Approach." *Acc. Chem. Res.* 6 (8): 257–262.
- Lipscomb, W.N. 1981a. "Borides and Boranes." *J. Less-Common Met.* 82: 1–20.
- Lipscomb, W.N. 1981b. "Borides and Boranes." *J. Less-Common Met.* 82: 1–20.
- Liu, F., Liang, W.J., Su, Z.J., Xia, J.X., Deng, S.Z., Chen, J., She, J.C., Xu, N.S., Tian, J.F., Shen, C.M., and H.-J. Gao. 2009. "Fabrication and Field Emission Properties of Boron Nanowire Bundles." *Ultramicroscopy* 109: 447–450.
- Longuet-Higgins, H. C., and M. de V. Roberts. 1954. "The Electronic Structure of the Borides MB<sub>6</sub>." *P. Roy. Soc. A* 224 (1158): 336–347.
- Ma, Y., Prewitt, C., Zou, G., Mao, H., and R. Hemley. 2003. "High-pressure High-temperature X-ray Diffraction of  $\beta$ -boron to 30 GPa." *Phys. Rev. B* 67 (17): 174116.
- Mailhot, C., Grant, J., and A. McMahan. 1990. "High-pressure Metallic Phases of Boron." *Phys. Rev. B* (14): 9033–9039.
- Masago, A., and K. Shirai. 2006. "Crystal Stability of  $\alpha$ - and  $\beta$ - Boron." *Phys. Rev. B* 73: 104102.
- McCarty, L.V., Kasper, J.S., Horn, F.H., Decker, B.F., and A.E. Newkirk. 1958. "A New Crystalline Modification of Boron." *J. Am. Chem. Soc.* 80 (10): 2592–2592.
- Mitoraj, M.P., and A. Michalak. 2011. "Multiple Boron-boron Bonds in Neutral Molecules: An Insight from the Extended Transition State Method and the Natural Orbitals for Chemical Valence Scheme." *Inorg. Chem.* 50 (6): 2168–2174.
- Mondal S., van Smaalen, S., Schonleber, A., Filinchuk, Y., Chernyshov, D., Simak, S.I., Mikhaylushkin, A.S., Abrikosov, I.A., Zarechnaya, E., Dubrovinsky, L., and N.

- Dubrovinskaia. "Electron-deficient and Polycenter Bonds in the High-Pressure  $\gamma$ -B<sub>28</sub> Phase of Boron." *Phys. Rev. Lett.* 106: 215502.
- Morosin, B., Mullendore, A.W., Emin, D., and G. A. Slack. 1986 "Rhombohedral Crystal Structure of Compounds Containing Boron-rich Icosahedra." *AIP Conf. Proc.* 140: 70–86.
- Niemyski, T., and V. Zawadzki. 1962. "Some Properties of Pure Polycrystalline Boron." *Phys. Lett.* 2 (1): 30–31.
- Oganov, A.R. 2011. "Boron Under Pressure: Phase Diagram and Novel High-pressure Phase." Ed. Orlovskaya, N., and M. Lugovy. *Media*: 207–225.
- Oganov, A.R., Chen, J., Gatti, C., Ma, Y., Ma, Y., Glass, C.W., Liu, Z., Yu, T., Kurakevych, O.O., and V.L. Solozhenko. 2009. "Ionic High-pressure Form of Elemental Boron." *Nature* 457 (7231): 863–867.
- Ogitsu, T., Gygi, F., Reed, J., Motome, Y., Schwegler, E., and G. Galli. 2009. "Imperfect Crystal and Unusual Semiconductor: Boron, a Frustrated Element." *J. Am. Chem. Soc.* 131 (5): 1903–1909.
- Ohtani, E., Irifune, T., Hibberson, W.O., and A.E. Ringwood. 1987. "Modified Split-sphere Guide Block for Practical Operation of a Multiple-anvil Apparatus." *High Temp-High Press.* 19: 523–529.
- Parakhonskiy, G., Dubrovinskaia, N., Bykova, E., Wirth, R., and Dubrovinsky, L. 2011. "Experimental Pressure-temperature Phase Diagram of Boron: Resolving the Long-standing Enigma." *Sci. Rep.* 1: 1–7.
- Parakhonskiy, G., Dubrovinskaia, N., Dubrovinsky, L., Mondal, S., and S. van Smaalen. 2011. "High Pressure Synthesis of Single Crystals of  $\alpha$ -boron." *J. Cryst. Growth* 321 (1): 162–166.
- Perkins, G.L. 2011. *Boron: Compounds, Production and Application*. Noca Science Pub Inc.
- Polian, A., Chervin, J.C., Munsch, P., and M. Gauthier. 2008. " $\alpha$ -boron at Very High Pressure: structural and Vibrational Properties." *J. of Physics: Conf. Ser.* 121: 042017
- Polian A., Ovsyannikov, S., Gauthier, M., Munsch, P., Chervin, J.C., and E. Lemarchand. 2010. *High Pressure Crystallography: From Fundamental Phenomena to Technological Applications*. Ed. Boldyreva, E. Dordrecht: Springer Netherlands.
- Qin, J., Irifune, T., Dekura, H., Ohfuji, H., Nishiyama N., Ohhuji, H., Lei, L., and T. Shimei. 2012. "Phase Relations in Boron at Pressures up to 18 GPa and Temperatures up to 2200°C." *Phys. Rev. B* 85(1): 014107
- Richter, W., and K. Ploog. 1975. "Raman-Active Phonons in  $\alpha$ -boron." *Phys. Status Solidi B* 68: 201–205.
- Sands, D.E., and J.L. Hoard. 1957. "Rhombohedral Elemental Boron." *J. Am. Chem. Soc.* 79 (3): 5582–5583.

- van Setten, M.J., Uijtewaal, M., de Wijs, G., and R. de Groot. 2007. "Thermodynamic Stability of Boron: The Role of Defects and Zero Point Motion." *J. Am. Chem. Soc.* 129 (9): 2458–2465.
- Shalamberidze, S.O., Kalandadze, G.I., Khuelidze, D.E., and B.D. Tsurtsunia. 2000. "Production of  $\alpha$ -Rhombohedral Boron by Amorphous Boron Crystallization" *J. Solid State Chem.* 154: 199–203.
- Shang, S., Wang, Y., Arroyave, R., and Z. Liu. 2007. "Phase Stability in  $\alpha$ - and  $\beta$ -rhombohedral Boron." *Phys. Rev. B* 75 (9): 092101.
- Shirai, K., and H. Katayama-Yoshida. 1998. "The Narrow Raman Linewidth of a Librational Mode of  $\alpha$ -rhombohedral Boron and Its Anharmonic Effects." *J. Phys. Soc. Jpn.* 67 (11): 3801–3808.
- Shirai, K., Masago, A., and H. Katayama-Yoshida. 2007. "High-pressure Properties and Phase Diagram of Boron." *Phys. Status Solidi B* 244 (1): 303–308.
- Slack, G.A., Hejna, C.I., Garbaskas, M.F., and J.S. Kasper 1988. "The Crystal Structure and Density of  $\beta$ -rhombohedral Boron" *J. Solid State Chem.* 76: 52–63.
- Solozhenko, V.L., Kurakevych, O.O., and A.R. Oganov. 2009. "On the Hardness of a New Boron Phase, Orthorhombic  $\gamma$ -B28." *J. Superhard Mat.* 30 (6): 428–429..
- Spitzer, W., and W. Kaiser. 1958. "Optical Properties of Crystalline Boron." *Phys. Rev. Lett.* 1 (7): 230–232.
- Switendick, A.C., and B. Morosin. 1990. "Electronic Charge Density and Bonding in  $\alpha$ -boron: an Experimental - theoretical Comparison." *AIP Conf. Proc.* 231: 205–211.
- Syassen, K. 2008. "Ruby Under Pressure." *High Pressure Res.* 28 (2): 75–126.
- Talley, C.P., La Placa, S., and B. Post. 1960. "A New Polymorph of Boron." *Acta Crystallog.* 13 (3): 271–272.
- Terauchi, M., Kawamata, Y., Tanaka M., Takeda M., and K. Kimura. 1997. "Electron Energy-loss Spectroscopy Study of the Electronic Structure of  $\alpha$ -rhombohedral Boron". *J. Solid State Chem.* 133: 156-159.
- Tsagareishvili, G.V., and A.G. Khvedelidze. 1980. "Rhombohedral Boron in Wide Ranges of Temperature." *J. Less-Common Met.* 75: 141–145.
- Vast, N, Baroni, S., Zerah, G., Besson, J.M., Polian, A., Grimsditch, M., and J.C. Chervin. 1997. "Lattice Dynamics of Icosahedral  $\alpha$ -Boron Under Pressure." *Phys. Rev. Lett.* 78 (4): 693–696.
- Vast, N, Lazzari, R., Besson, J.M., Baroni, S., and A. Dal Corso. 2000. "Atomic Structure and Vibrational Properties of Icosahedral  $\alpha$ -boron and B<sub>4</sub>C Boron Carbide." *Comp. Mater. Sci.* 17 (2-4): 127–132.

- Vlasse, M., Naslain, R., Kasper, J.S., and K. Ploog 1979. "Crystal structure of tetragonal boron related to  $\alpha$ -AlB<sub>12</sub>." *J. Solid State Chem* 28 (3): 289-301.
- Wald, F. 1970. "Stability of the Red  $\alpha$ -rhombohedral B Modification" *Electron. Technol.* 3 (1-2): 103-108.
- Walker, D., Carpenter, M.A., and C.M. Hitch. 1990. "Some Simplifications to Multianvil Devices for High Pressure Experiments." *Am. Mineral.* 75: 273–286.
- Weintraub, E. 1909. "Preparation and properties of pure boron." *Trans. Amer. Electrochem. Soc.* 16: 165-184.
- Wentorf, R.H. 1965. "Boron: Another Form." *Science* 147 (3653): 49–50.
- Werheit, H., Filipov, V., Kuhlmann, U., Schwarz, U., Armbrüster, M., Leithe-Jasper, A., Tanaka, T., Higashi, I., Lundstrom, T., Gurlin, V.N., and M.M. Korsukova "Raman Effect in Icosahedral Boron-rich Solids." *Sci. Technol. Adv. Mat.* 11 (2): 023001.
- Widom, M., and M. Mihalkovič. 2008. "Symmetry-broken Crystal Structure of Elemental Boron at Low Temperature." *Phys. Rev. B* 77 (6): 064113.
- Will, G., and K.H. Kossobutzki. 1975. "On the Existence of Tetragonal Boron and the Crystal Structures of B<sub>50</sub>C<sub>2</sub> and B<sub>50</sub>N<sub>2</sub>: an X-ray Diffraction Analysis." *Z. Kristallogr.* 142 (5-6): 384–397.
- Will, G., and K. Ploog. 1974. "Crystal Structure of I-tetragonal Boron." *Nature* 251: 406–408.
- Will, G., and B. Kiefer. 2001. "Electron Deformation Density in Rhombohedral  $\alpha$ -Boron." *Z. Anorg. Allg. Chem* 627: 2100–2104.
- Wirth, R. 2004. "Focused Ion Beam (FIB): A Novel Technology for Advanced Application of Micro- and Nanoanalysis in Geosciences and Applied Mineralogy." *Eur. J. Mineral.* 16 (6): 863–876.
- Xu, T.T., Zheng, J., Nicholls, A.W., Roth, J.R., Dikin, D.A., and R.S. Ruoff. 2004. "Crystalline Boron Nanoribbons: Synthesis and Characterization." *Nano Lett.* 4 (5): 963–968.
- Zarechnaya, E., Dubrovinsky, L., Dubrovinskaia, N., Filinchuk, Y., Chernyshov, D., Dmitriev, V., Miyajima, El Goresy, A., Braun, H.F., Van Smaalen, S., Kantor, I., Kantor, A.M. Prakapenka, V., Hanfland, M., Mikhaylushkin, A.S., Abrikosov, I.A., and S.I. Simak. "Superhard Semiconducting Optically Transparent High Pressure Phase of Boron." *Phys. Rev. Lett.* 102 (18):185501.
- Zarechnaya, E., Dubrovinskaia, N., Caracas, R., Merlini, M., Hanfland, M., Filinchuk, Y., Chernyshov, D., Dmitriev, V., and L. Dubrovinsky. 2010. "Pressure-induced Isostructural Phase Transformation in  $\gamma$ -B<sub>28</sub>." *Phys. Rev. B* 82 (18): 184111.
- Zarechnaya, E., Dubrovinsky, L., Dubrovinskaia, N., Miyajima, N., Filinchuk, Y., Chernyshov, D., and V. Dmitriev. 2008. "Synthesis of an Orthorhombic High Pressure Boron Phase." *Sci. Tech. Adv. Mat.* 9 (4): 044209.

Zhou, W., Sun, H., and C. Chen. 2010. "Soft Bond-Deformation Paths in Superhard  $\gamma$ -Boron." *Phys. Rev. Lett.* 105 (21): 215503.

## 6 ACKNOWLEDGMENTS

Hereby on my behalf, I would like to express my gratitude to Natalia Dubrovinskaia and Leonid Dubrovinsky for the patient, warm and productive supervision. I would like to thank Yochi Nakajima, Scheka Svyatoslav, Elena Bykova, Geeth Manthilake and Swastik Mondal for the practical help and useful advices during my PhD work. As well I would like to thank Hubert Schulzte, Uwe Dittman, Gerti Gollner, Heinz Fischer, Sven Linhardt, Franz Fischer and Alfred Suttner for technical assistance.

I highly appreciate Hans Keppler, Andreas Schönleber for the very interesting lectures, which added a lot of sense to the work I did.

I am grateful to Florian Heidelberg and Stefan Keysnerr for helping me with translation, and to Denis Kelk-Huth, Petra Buchert and Lydia Kison-Herzing for helping with administrative issues.

Special thanks to all my collaborators and co-authors.

At last I would like to thank my wife Svetlana Zemskova for her help and support.

# ERKLÄRUNG

Hiermit erkläre ich, dass ich die vorliegende Arbeit selbständig verfasst und keine anderen als die von mir angegebenen Quellen und Hilfsmittel verwendet habe. Ferner erkläre ich, dass ich nicht anderweitig mit oder ohne Erfolg versucht habe, eine Dissertation einzureichen. Ich habe keine gleichartige Doktorprüfung an einer anderen Hochschule endgültig nicht bestanden.

Bayreuth, den 22. August 2012

Gleb Parakhonskiy